Asynchronous Instabilities of Crime Hotspots for a 1-D Reaction-Diffusion Model of Urban Crime with Focused Police Patrol

Wang Hung Tse* , Michael J. Ward†

December 10, 2017

Abstract

To be written

Key Words: Urban crime, hotspot patterns, nonlocal eigenvalue problem (NLEP), Hopf bifurcation, asynchronous oscillatory instability, cops-on-the-dots.

1 Introduction

The development of mathematical approaches to quantify and predict spatial patterns of urban crime originates from the pioneering studies in [25–27]. A primary motivation for this effort is the increased availability of residential burglary data, which clearly show that spatial patterns of urban crime are often concentrated in certain spatial regions, known as hotspots [4]. It is believed that these hotspots are due to a repeat or near-repeat victimization effect, which suggests that crime in a certain region induces more crime in that and nearby regions (cf. [10], [32]).

Need a small paragraph here about police and general goal: Refer to [11], [21], [33], [22], [5] (agent-based) for different police models.

Following [22], our simple police interaction model on the one-dimensional domain $0 \leq x \leq S$ is formulated as

$$A_t = \epsilon^2 A_{xx} - A + \rho A + \alpha \,, \tag{1.1a}$$

$$\rho_t = D \left(\rho_x - 2\rho A_x / A \right)_x - \rho A + \gamma - \alpha - U \,, \tag{1.1b}$$

$$\tau_u U_t = D \left(U_x - qU A_x / A \right)_x \,, \tag{1.1c}$$

where $A_x = \rho_x = U_x = 0$ at $x = 0, S$. Here A is the attractiveness field, while ρ and U are the density of criminals and police, respectively. The constants α and $\gamma - \alpha$ are the baseline attractiveness and the rate at which new criminals are introduced, respectively. From (1.1c), we obtain that the total level U_0 of police deployment is conserved in time, so that

$$U_0 \equiv \int_0^S U(x, t) \, dx \,. \tag{1.2}$$

In (1.1c), the parameter $q > 0$ measures the degree of focus in the police patrol toward maxima of the attractiveness field A. We will assume in our analysis below that $q > 1$. The choice $q = 2$ models a "cops-on-the-dots" strategy (cf. [11], [22], [33]) whereby the police have the same degree of focus as do the criminals towards maxima of A. When q is above or below

---

*Dept. of Mathematics, UBC, Vancouver, Canada
†Dept. of Mathematics, UBC, Vancouver, Canada. (corresponding author `ward@math.ubc.ca`)

2, the police force drift in a less or more focused manner, respectively, as compared to that of the criminals. In (1.1) the constant diffusivities of the criminals and the police is D and $D_p \equiv D/\tau_u$, respectively. The police are more mobile than the criminals when $\tau_u < 1$, while when $\tau_u > 1$ the police are comparatively more "sluggish" in their movements.

The corresponding two-component system, where $U_0 = 0$ and (1.1c) is omitted, which we refer to as the *basic crime model*, was derived in [25] and [27] from the continuum limit of an agent-based model that accounts for the effect of repeat or near-repeat victimization. This two-component RD system has been well-studied. When $D = \mathcal{O}(1)$, a formal weakly nonlinear analysis was developed in [26] to study the development of small amplitude spatial patterns of crime near a Turing bifurcation point associated with a spatially homogeneous steady-state solution. In [6] this local branching behavior near the Turing point was characterized rigorously (see also [8]). In [23] the local existence of solutions to the basic crime model in multi-dimensional domains was established. On the infinite line, and with $D = 1$, an intricate snaking-type bifurcation structure of hotspot equilibria was computed numerically in [16] in the singular limit $\epsilon \to 0$, for the subcritical regime $\alpha < \gamma < \gamma_c \sim 3\alpha/2$. On a finite domain with $D = \mathcal{O}(1)$, and for $\gamma > 3\alpha/2$, in [28] the slow dynamics of hotspot quasi-equilibria, together with a nucleation process through which new hotspots can be created, was revealed. For the parameter regime $D \gg 1$, hotspot equilibria and their linear stability properties were analyzed in [12]. The existence of these hotspot equilibria for the regime $D \gg 1$ was established rigorously in [1] by using a Lyapunov-Schmidt reduction.

Following [12] for the basic crime model, we will analyze the three-component system (1.1) for $\epsilon \to 0$ when $D = \mathcal{O}(\epsilon^{-2})$. On the $D = \mathcal{O}(\epsilon^{-2})$ regime, steady-state hotspot patterns for the basic crime model have a stability threshold [12]. Since $A = \mathcal{O}(\epsilon^{-1})$ in a hotspot region, it is convenient, as in [12], to introduce the new variables v and u by

$$\rho = \epsilon^2 v A^2 \,, \qquad U = u A^q \,, \qquad D = \epsilon^{-2} \mathcal{D}_0 \,. \tag{1.3}$$

In terms of v, u, and $\mathcal{D}_0 = \mathcal{O}(1)$, (1.1) becomes

$$A_t = \epsilon^2 A_{xx} - A + \epsilon^2 v A^3 + \alpha \,, \tag{1.4a}$$

$$\epsilon^2 \left(A^2 v \right)_t = \mathcal{D}_0 \left(A^2 v_x \right)_x - \epsilon^2 v A^3 + \gamma - \alpha - u A^q \,, \tag{1.4b}$$

$$\tau_u \epsilon^2 \left(A^q u \right)_t = \mathcal{D}_0 \left(A^q u_x \right)_x \,. \tag{1.4c}$$

In the limit $\epsilon \to 0$, we will analyze the existence and linear stability of hotspot steady-state solutions to (1.4), in which the attractiveness field is spatially localized. We will construct phase diagrams in parameter space where such patterns are linearly stable, and show these regions of stability depend on the parameters q, U_0, and D_p (or equivalently τ_u).

For $\epsilon \ll 1$, in §2 we use the method of matched asymptotic expansions to construct hotspot steady-state solutions to (1.4) that have a common hotspot amplitude. In Proposition 2.1 below, we show that such patterns exist for (1.1) only when $U_0 < U_{0,\max} \equiv S(\gamma - \alpha)$ For $q > 1$, Proposition 2.1 also shows that the total police deployment U_0 has an indirect effect on crime, in that it reduces the maxima, referred to here as "amplitudes", of the attractiveness field A.

To analyze the linear stability of a K-hotspot steady-state solution, in §3 we use asymptotic analysis to derive the nonlocal eigenvalue problem (NLEP), characterizing $\mathcal{O}(1)$ time-scale instabilities of the pattern. The methodology to derive this NLEP involves using a reference domain $|x| \leq \ell$ containing a single hotspot centered at $x = 0$, and then imposing Floquet-type boundary conditions at $x = \pm\ell$. In terms of this reference problem, the NLEP for the finite-domain problem $0 < x < S$ with Neumann conditions at $x = 0, S$ can then readily be extracted, as similar to that done in [12] for the basic two-component crime model. Such a Floquet-based approach to study the linear stability of multi-spike steady-states was first introduced in [20] in the context of 1-D spatially-periodic spike patterns for a class of two-component reaction-diffusion

systems. It has subsequently been extended to study the linear stability of 1-D mesa patterns [13], of 1-D spikes for a competition model with cross-diffusion effects [15], and 1-D hotspot patterns for the basic crime model [12].

There are two novel features in the derivation of the NLEP for our three-component RD system. Firstly, in our asymptotic analysis, we must carefully derive rather intricate jump conditions across the hotspot region. Secondly, the resulting NLEP that we obtain has two nonlocal terms, instead of the usual one. As a result, its analysis is seemingly beyond the general NLEP stability theory with a single nonlocal term, as surveyed in [31]. However, by using a key identity that is specific to our three-component RD crime model, we show how to reformulate the NLEP more conveniently in terms of a single nonlocal term, which can then be more readily analyzed.

Our NLEP linear stability analysis reveals that a steady-state with a single hotspot is always linearly stable, and that a steady-state with $K \geq 2$ hotspots is always linearly stable to synchronous perturbations of the amplitudes of the hotspots. For $K \geq 2$ hotspots, and for a given $U_0 > 0$ and fixed $q > 1$, our NLEP analysis provides phase diagrams in the D_p versus $\mathcal{D}_0$ parameter plane characterizing the linear stability of the hotspot steady-states to asynchronous perturbations in the hotspot amplitudes. For the special case $q = 3$, and for $K \geq 2$, for which the discrete spectrum of the NLEP can be reduced to the study of a family of $K-1$ quadratic equations in the eigenvalue parameter, these phase diagrams can be constructed explicitly. Such "explicitly solvable" NLEPs have been analyzed in other contexts [12, 17, 18]. For general $q > 1$, in §6 the phase diagrams are determined by combining some rigorous spectral results obtained from the argument principle together with numerical results obtained from a parameterization of the Hopf bifurcation threshold, as derived from the NLEP. This analysis shows that steady-state multiple hotspot patterns are unconditionally unstable if $\mathcal{D}_0 > \mathcal{D}_{0,c}$, and are always linearly stable if $0 < \mathcal{D}_0 < \mathcal{D}_{0,c}/(1 + qU_0/\omega)$, where $\omega = S(\gamma - \alpha) - U_0$ and $\mathcal{D}_{0,c}$ is the competition instability threshold given below in (4.9). Some technical results required for the analysis of the NLEP, together with a qualitative discussion on how the competition threshold $\mathcal{D}_{0,c}$ depends on the patrol focus q and the police deployment are given in §4.
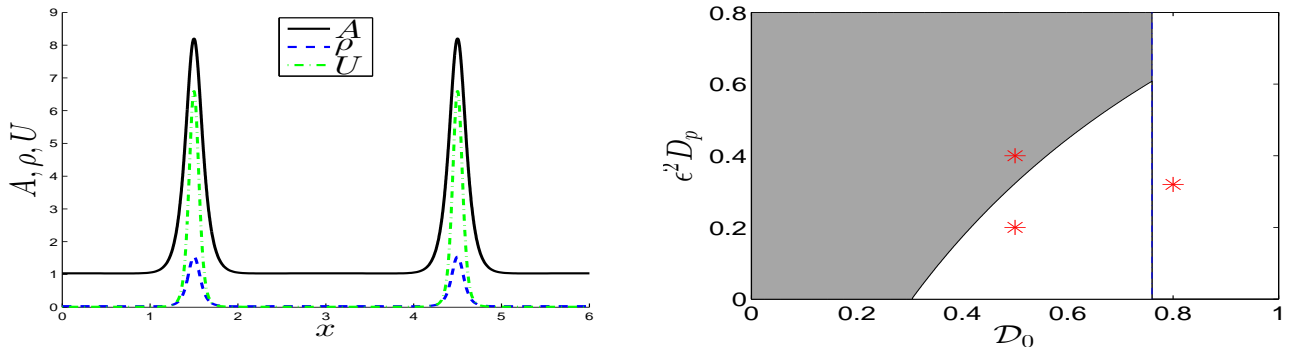

Figure 1: Left panel: The steady-state two-hotspot solution for $S = 6$, $\gamma = 2$, $\alpha = 1$, $U_0 = 2$, $\mathcal{D}_0 = 0.5$, $\epsilon = 0.075$, and $q = 3$. Right panel: the shaded region of linear stability in the (scaled) police diffusivity $\epsilon^2 D_p \equiv \mathcal{D}_0/\tau_u$ versus $\mathcal{D}_0$ parameter plane. The thin vertical line is the competition stability threshold $\mathcal{D}_{0,c}$ given in Proposition 5.2, while the leftmost edge of the instability region (at $D_p = 0$) is $\mathcal{D}_{0,c}/(1 + 3U_0/\omega)$ where $\omega = S(\gamma - \alpha) - U_0$. For $\mathcal{D}_0 > \mathcal{D}_{0c}$ the hotspot solution is unstable due to a competition instability, while in the unshaded region for $\mathcal{D}_0 < \mathcal{D}_{0c}$, the hotspot steady-state is unstable to an asynchronous oscillatory instability of the hotspot amplitudes. The full PDE simulations in Fig. 2 are done at the marked points.

On the intermediate range $\mathcal{D}_{0,c}/(1 + qU_0/\omega) < \mathcal{D}_0 < \mathcal{D}_{0,c}$, one of our main results is that when the police diffusivity D_p dips below a $\mathcal{D}_0$-dependent threshold, an asynchronous temporal oscillatory instability in the hotspot amplitudes will occur from a Hopf bifurcation of the NLEP. These asynchronous, anti-phase, oscillations of the hotspot amplitudes have the qualitative interpretation that, at least for short time, the police intervention has the effect of only displacing crime between different spatial regions. Qualitatively, this result is consistent with observations in [3] that a "cops-on-the-dots" policing

3

strategy will sometimes not eliminate crime, but instead will only displace it to surrounding areas. Our full numerical computations of the PDE system (1.4) suggest that these asynchronous oscillations arising from the Hopf bifurcation are subcritical, and that over a longer time-scale they trigger a nonlinear process whereby hotspots are annihilated.
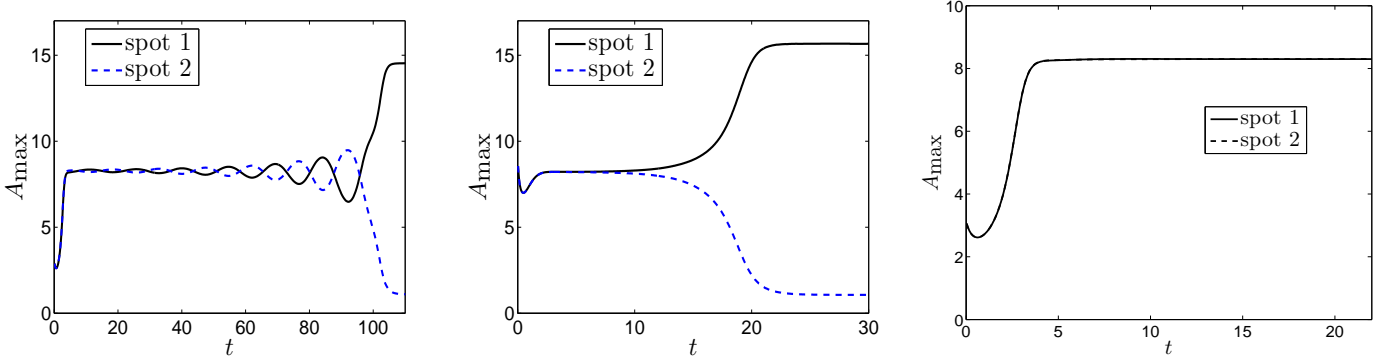

Figure 2: *Plot of the spot amplitudes computed numerically from the full PDE system (1.4) for a two-spot pattern with $S = 6$, $\gamma = 2$, $\alpha = 1$, $U_0 = 2$, $\epsilon = 0.075$, and $q = 3$, at the marked points in the right panel of Fig. 1. Left panel: $\hat{\tau}_u = 2.5$ and $\mathcal{D}_0 = 0.5$, so that $\epsilon^2 D_p = 0.2$. Spot amplitudes are unstable to asynchronous oscillations, which leads to the collapse of one hotspot. Middle panel: $\hat{\tau}_u = 2.5$ and $\mathcal{D}_0 = 0.8$, so that $\epsilon^2 D_p = 0.32$. Spot amplitudes are unstable to a competition instability. Right panel: $\hat{\tau}_u = 1.25$ and $\mathcal{D}_0 = 0.5$, so that $\epsilon^2 D_p = 0.4$. Spot amplitudes are stable to asynchronous oscillations and there is no competition instability. These results are consistent with the linear stability predictions in the right panel of Fig. 1 (see also the left panel of Fig. 7 below).*

To illustrate our results, we take $S = 6$, $\gamma = 2$, $\alpha = 1$, $q = 3$, $U_0 = 2$, and $\epsilon = 0.075$, and we consider a steady-state with exactly two hotspots, as shown in the left panel of Fig. 1. For this two-hotspot steady-state the linear stability phase diagram in the $\epsilon^2 D_p$ versus $\mathcal{D}_0$ parameter plane is shown in the right panel of Fig. 1. For the three marked points in the phase diagram in Fig. 1, where qualitative distinct solution behavior occurs, in Fig. 2 we validate our linear stability predictions by showing full numerical results for the maxima, or amplitudes, of A, as computed from the PDE system (1.4). The numerical methodology and initial conditions used in the simulations are discussed in §5.2. Observe from the left panel in Fig. 2 that the asynchronous oscillation of the hotspot amplitudes eventually leads to the annihilation of one of the two hotspots. Further detailed validations of our linear stability phase diagrams with full PDE simulations of (1.4) are given in §5.2 for $q = 3$ and in §6.3 for the "cops-on-the-dots" policing strategy $q = 2$.

We emphasize that the interval in $\mathcal{D}_0$ for the existence of asynchronous oscillations vanishes when $U_0 = 0$. In other words, it is the third component of the PDE system (1.4), modeling the police interaction, that is essential for the existence of these oscillations, with the basic two-component RD crime model [12] being incapable of supporting such oscillations. Robust asynchronous oscillations of localized spikes in 1-D does not occur for many classical two-component RD systems in the large diffusivity ratio limit, such as the Gray-Scott and Gierer-Meinhardt models (cf. [7], [9], [20], [30], [14]). For these two-component systems, the stability threshold for spike amplitude oscillations arising from a Hopf bifurcation in the NLEP is set by the synchronous mode. It is only for more non-traditional RD systems, such as the 1-D Brusselator model with influx boundary conditions [29] or the Gierer-Meinhardt model with anomalous diffusion [19], that asynchronous oscillations have been shown to be the dominant oscillatory instability in rather small parameter regimes.

Finally, in §8 we discuss a few open problems motivated by our study.

2 Asymptotic Construction of a Multiple Hotspot Steady-State

In this section we construct a steady-state solution to (1.4) on $0 \leq x \leq S$ with $K \geq 1$ interior hotspots.

To construct a steady-state with K interior hotspots to (1.4) on $0 < x < S$, where the hotspots have a common amplitude, we will first construct a one-hotspot solution to (1.4) on $|x| \leq l$ centered at $x = 0$. Then, by using the translation-invariance property of (1.4), we obtain a K interior hotspot steady-state solution on the original domain of length $S = (2\ell)K$. In terms of this reference domain $|x| \leq \ell$, (1.2) yields that

$$U_0 = K \int_{-\ell}^{\ell} U \, dx \,. \tag{2.1}$$

In this way, we need only construct a one-hotspot steady-state solution to (1.4) centered at $x = 0$ and impose $A_x = v_x = u_x = 0$ at $x = \pm\ell$. We refer to this as the *canonical* hotspot problem.

From the steady-state of (1.4c), together with $U = uA^q$ and (2.1), it follows that u is spatially constant and given by

$$u = \frac{U_0}{K \int_{-\ell}^{\ell} A^q \, dx} \,. \tag{2.2}$$

By using (2.2) in (1.4), the three-component steady-state system reduces to the nonlocal BVP problem

$$\epsilon^2 A_{xx} - A + \epsilon^2 v A^3 + \alpha = 0, \qquad |x| \leq \ell; \qquad A_x = 0 \quad x = \pm\ell, \tag{2.3a}$$

$$\mathcal{D}_0 \left(A^2 v_x \right)_x - \epsilon^2 v A^3 + \gamma - \alpha - \frac{U_0}{K} \frac{A^q}{\int_{-\ell}^{\ell} A^q \, dx} = 0, \qquad |x| \leq \ell; \qquad v_x = 0 \quad x = \pm\ell. \tag{2.3b}$$

We now construct the solution to (2.3) with a single hotspot centered at $x = 0$. In the outer region we have $A \sim \alpha + \mathcal{O}(\epsilon^2)$, while in the inner region we put $y = \epsilon^{-1} x$ and $A \sim A_0/\epsilon$ to obtain on $-\infty < y < \infty$ that

$$A_{0yy} - A_0 + v A_0^3 + \epsilon \alpha = 0, \qquad \mathcal{D}_0 \epsilon^{-4} \left(A_0^2 v_y \right)_y + \mathcal{O}(\epsilon^{-1}) = 0 \,.$$

Therefore, to leading order it follows that $v \sim v_0$ is a constant, and that

$$A_0 \sim \frac{w(y)}{\sqrt{v_0}} \,, \tag{2.4}$$

where $w(y) = \sqrt{2} \operatorname{sech} y$ is the homoclinic solution of

$$w'' - w + w^3 = 0, \qquad -\infty < y < \infty; \qquad w(0) > 0, \quad w'(0) = 0, \quad w \to 0 \quad \text{as} \quad y \to \pm\infty \,. \tag{2.5}$$

The integrals of $w(y)$ that are need beelow are

$$\int_{-\infty}^{\infty} w \, dy = \int_{-\infty}^{\infty} w^3 \, dy = \sqrt{2}\pi \,, \quad \int_{-\infty}^{\infty} w^2 \, dy = 4 \,, \quad \int_{-\infty}^{\infty} w^4 \, dy = \frac{16}{3} \,, \quad \frac{\int_{-\infty}^{\infty} w^5 \, dy}{\int_{-\infty}^{\infty} w^3 \, dy} = \frac{3}{2} \,. \tag{2.6}$$

More generally, we can readily calculate in terms of the usual Gamma function $\Gamma(z)$ that

$$I_q \equiv \int_{-\infty}^{\infty} w^q \, dy = 2^{3q/2 - 1} \frac{[\Gamma(q/2)]^2}{\Gamma(q)} \,. \tag{2.7}$$

We return to (2.2), and for $q > 1$ we estimate the key integral

$$\int_{-\ell}^{\ell} A^q \, dx \sim 2\ell\alpha + \epsilon^{1-q} v_0^{-q/2} \int_{-\infty}^{\infty} w^q \, dy = \mathcal{O}(\epsilon^{1-q}) \gg 1 \,.$$

From (2.2), we have $u = \mathcal{O}(\epsilon^{q-1}) \ll 1$ since $q > 1$. With our assumption $q > 1$, the integral $\int_{-\ell}^{\ell} A^q \, dx$, and thus u, depend to leading-order only on the inner region contribution from A^q. For $q > 1$, we obtain to leading-order from (2.2) that

$$u \sim \epsilon^{q-1} \tilde{u}_e \,, \qquad \text{where} \qquad \tilde{u}_e \equiv \frac{U_0 v_0^{q/2}}{K I_q} \,. \tag{2.8}$$

Next, we determine v_0 by integrating (2.3b) on $-\ell < x < \ell$ and then imposing $v_x(\pm\ell) = 0$. This yields that

$$\epsilon^2 \int_{-\ell}^{\ell} vA^3 \, dx = 2\ell \left(\gamma - \alpha \right) - U_0/K \, .$$

Therefore, since $A \sim \alpha = \mathcal{O}(1)$ in the outer region, while $A = \mathcal{O}(\epsilon^{-1})$ in the inner region, it follows that, when $q > 1$, the dominant contribution to the integral arises from the inner region where $v \sim v_0$. In this way, we estimate

$$\frac{\int_{-\infty}^{\infty} w^3 \, dy}{\sqrt{v_0}} = 2\ell \left(\gamma - \alpha \right) - U_0/K \, . \tag{2.9}$$

From (2.9), a steady-state hotspot solution exists only when the total level U_0 of police deployment is below the threshold

$$U_0 < U_{0,max} \equiv 2\ell K \left(\gamma - \alpha \right) = S(\gamma - \alpha) \, . \tag{2.10}$$

Here $S = 2\ell K$ is the original domain length. We will assume that (2.10) holds, so that a K-hotspot steady-state exists.

Upon solving (2.9) for v_0, and using (2.6) for $\int_{-\infty}^{\infty} w^3 \, dy$, we get

$$v_0 = 2\pi^2 \left[2\ell \left(\gamma - \alpha \right) - U_0/K \right]^{-2} = 2\pi^2 K^2 \left[S(\gamma - \alpha) - U_0 \right]^{-2} \, . \tag{2.11}$$

Since v_0 increases when either K increases or the total level U_0 of police increases, it follows from (2.4) that the maximum $A_{max} \equiv A(0) \gg 1$ of the attractiveness field, given by

$$A_{max} \equiv A(0) \sim \epsilon^{-1} A_0(0) = \frac{\epsilon^{-1}}{\pi K} \left[S(\gamma - \alpha) - U_0 \right] \, , \tag{2.12}$$

decreases with increasing K or increasing policing level U_0. However, A_{max} is independent of the patrol focus parameter q.

To complete the asymptotic construction of the hotspot, we must determine v. In the outer region, we expand $v \sim v_e(x) + \ldots$ and recall that $A \sim \alpha + \mathcal{O}(\epsilon^2)$ so that $A^q / \int_{-\ell}^{\ell} A^q \, dx = \mathcal{O}(\varepsilon^{q-1}) \ll 1$ since $q > 1$. In this way, from (2.3b), we obtain to leading order that $v_e(x)$ satisfies

$$\mathcal{D}_0 v_{exx} = -\frac{(\gamma - \alpha)}{\alpha^2} \, , \quad -\ell < x < \ell \, ; \qquad v_e(0) = v_0 \, , \qquad v_{ex}(\pm\ell) = 0 \, . \tag{2.13}$$

The solution to (2.13) is

$$v_e(x) = \frac{\zeta}{2} \left[(\ell - |x|)^2 - \ell^2 \right] + v_0 \, , \qquad 0 < |x| \le \ell \, ; \qquad \zeta \equiv -\frac{(\gamma - \alpha)}{\mathcal{D}_0 \alpha^2} \, , \tag{2.14}$$

where v_0 is given in (2.11). This is a uniformly valid leading order solution for v on $|x| \le \ell$.

We summarize the results for our leading-order construction of a steady-state K-hotspot pattern as follows:

Proposition 2.1 *Let $\epsilon \to 0$, $q > 1$, and $0 < U_0 < U_{0,max}$, as in (2.10). Then, (1.4) admits a steady-state solution on $(0, S)$ with K interior hotspots of a common amplitude. On each sub-domain of length $2\ell = S/K$, and translated to $(-\ell, \ell)$ to contain exactly one hotspot at $x = 0$, the steady-state solution, to leading order, is given by*

$$A \sim \frac{w(x/\epsilon)}{\epsilon\sqrt{v_0}} \, , \quad \text{if} \quad x = \mathcal{O}(\epsilon) \, ; \qquad A \sim \alpha \, , \quad \text{if} \quad x = \mathcal{O}(1) \, , \tag{2.15a}$$

$$v \sim v_e = \frac{\zeta}{2} \left[(\ell - |x|)^2 - \ell^2 \right] + v_0 \, , \qquad \text{where} \quad v_0 = 2\pi^2 K^2 \left[S(\gamma - \alpha) - U_0 \right]^{-2} \, , \tag{2.15b}$$

$$u \sim \epsilon^{q-1} \tilde{u}_e \, , \qquad \text{where} \quad \tilde{u}_e \equiv \frac{U_0 v_0^{q/2}}{K I_q} \, , \qquad I_q \equiv \int_{-\infty}^{\infty} w^q \, dy = 2^{3q/2 - 1} \frac{[\Gamma(q/2)]^2}{\Gamma(q)} \, . \tag{2.15c}$$

Here $w(y) = \sqrt{2}\,\text{sech}\,y$ is the homoclinic of (2.5).

6

In terms of the criminal and police densities, given by $\rho = \epsilon^2 v A^2$ and $U = uA^q$ from (1.3), we have the following:

Corollary 2.2 *Under the same conditions as in Proposition 2.1, (2.15) yields to leading-order that*

$$A \sim \frac{w(x/\epsilon)}{\epsilon\sqrt{v_0}}, \quad if \quad x = \mathcal{O}(\epsilon); \qquad A \sim \alpha, \quad if \quad \mathcal{O}(\epsilon) \ll |x| < \ell, \tag{2.16a}$$

$$\rho \sim [w(x/\epsilon)]^2, \quad if \quad x = \mathcal{O}(\epsilon); \qquad \rho \sim \epsilon^2 v_e \alpha^2, \quad if \quad \mathcal{O}(\epsilon) \ll |x| < \ell, \tag{2.16b}$$

$$U \sim \frac{U_0}{\epsilon K I_q} [w(x/\epsilon)]^q, \quad if \quad x = \mathcal{O}(\epsilon); \qquad U \sim \epsilon^{q-1} \alpha^q \frac{U_0 v_0^{q/2}}{K I_q}, \quad if \quad \mathcal{O}(\epsilon) \ll |x| < \ell, \tag{2.16c}$$

where v_e and v_0 are given in (2.15) and $w(y) = \sqrt{2}\,\mathrm{sech}\,y$.

From (2.16), we observe that the criminal density near a hotspot is independent of the police deployment U_0 and patrol focus q. However, the maximum of the attractiveness field is decreased by increasing U_0.

3   Derivation of the NLEP for a K-Hotspot Steady-State Pattern

To analyze the linear stability of a K-hotspot steady-state solution, we must use asymptotic analysis to derive the corresponding nonlocal eigenvalue problem (NLEP). To do so, we first follow the methodology in [12] by deriving the NLEP for a one-hotspot solution on the reference domain $|x| \leq \ell$, with Floquet-type boundary conditions imposed at $x = \pm \ell$. In terms of this reference problem, the NLEP for the finite-domain problem $0 < x < S$ with Neumann conditions at $x = 0, S$ is then readily recovered, as similar to that done in [12] for the basic crime model.

3.1   Linearization with Floquet Boundary Conditions

To study the linear stability of a K-hotspot steady-state we introduce the perturbation

$$A = A_e + e^{\lambda t} \phi, \qquad v = v_e + e^{\lambda t} \epsilon \psi, \qquad u = u_e + e^{\lambda t} \epsilon^q \eta, \tag{3.1}$$

where (A_e, v_e, u_e) is the steady-state with a single hotspot centered at the origin in $|x| \leq \ell$. The orders of the perturbations ($\mathcal{O}(1)$, $\mathcal{O}(\epsilon)$ and $\mathcal{O}(\epsilon^q)$ for the A, v and u components, respectively) are chosen so that ϕ, ψ, and η are all $\mathcal{O}(1)$ in the inner region. Upon substituting (3.1) into (1.4) and linearizing, we obtain that

$$\epsilon^2 \phi_{xx} - \phi + 3\epsilon^2 v_e A_e^2 \phi + \epsilon^3 A_e^3 \psi = \lambda \phi, \tag{3.2a}$$

$$\mathcal{D}_0 \left(2 A_e v_{ex} \phi + \epsilon A_e^2 \psi_x\right)_x - 3\epsilon^2 A_e^2 v_e \phi - \epsilon^3 A_e^3 \psi - q u_e A_e^{q-1} \phi - \epsilon^q \eta A_e^q = \lambda \epsilon^2 \left(2 A_e v_e \phi + \epsilon A_e^2 \psi\right), \tag{3.2b}$$

$$\mathcal{D}_0 \left(q A_e^{q-1} \phi u_{ex} + \epsilon^q A_e^q \eta_x\right)_x = \epsilon^2 \tau_u \lambda \left(q A_e^{q-1} u_e \phi + \epsilon^q A_e^q \eta\right). \tag{3.2c}$$

For $K \geq 2$, we will impose for the long-range components ψ and η in (3.2b) and (3.2c) the following Floquet-type boundary conditions at $x = \pm \ell$:

$$\begin{pmatrix} \eta(\ell) \\ \psi(\ell) \end{pmatrix} = z \begin{pmatrix} \eta(-\ell) \\ \psi(-\ell) \end{pmatrix}, \qquad \begin{pmatrix} \eta_x(\ell) \\ \psi_x(\ell) \end{pmatrix} = z \begin{pmatrix} \eta_x(-\ell) \\ \psi_x(-\ell) \end{pmatrix}, \tag{3.3}$$

where z is a complex-valued parameter. For the $K = 1$ case, considered separately in §3.3 below, we need only impose Neumann conditions at $x = \pm l$ for the perturbations. Here we treat the $K \geq 2$ case.

For $K \geq 2$, the NLEP associated with a K-hotspot pattern on $[-l, (2K-1)l]$ with *periodic boundary conditions*, on a domain of length $2Kl$, is obtained by setting $z^K = 1$, which yields

$$z_j = e^{2\pi i j/K}, \qquad j = 0, \ldots, K-1. \tag{3.4}$$

By using these values of z_j in (3.3) we obtain the spectral problem for the linear stability of a K-hotspot solution on a domain of length $2Kl$ subject to periodic boundary conditions. The next step is then to relate the spectra of the periodic problem to the Neumann problem in such a way that the Neumann problem is still posed on a domain of length S (cf. [12]). As discussed in §3 of [12] for $K \geq 2$, this involves simply replacing $2K$ with K in (3.4). As such, our Floquet parameter in (3.3) for a hotspot steady-state on a domain of length $S = 2lK$, having $K \geq 2$ interior hotspots and Neumann boundary conditions at $x = 0$ and $x = S$ is $z = e^{\pi i j/K}$. For $z = e^{\pi i j/K}$, we calculate the following identity, which is needed below:

$$\frac{(z-1)^2}{2z} = \mathrm{Re}(z) - 1 = \cos\left(\frac{\pi j}{K}\right) - 1\,, \quad j = 0, \ldots, K-1\,. \tag{3.5}$$

We now begin our derivation of the NLEP. For (3.2a), in the inner region where $A_e \sim \epsilon^{-1} w/\sqrt{v_0}$, $v_e \sim v_0$, and $\psi \sim \psi(0) \equiv \psi_0$, we obtain that the leading-order term $\Phi(y) = \phi(\epsilon y)$ in the inner expansion of ϕ satisfies

$$\Phi'' - \Phi + 3w^2\Phi + \frac{\psi(0)}{v_0^{3/2}} w^3 = \lambda\Phi\,. \tag{3.6}$$

In contrast, in the outer region, we obtain to leading order from (3.2) that

$$\phi \sim \epsilon^3 \alpha^3 \psi / [\lambda + 1 - 3\epsilon^2 \alpha^2 v_e] = \mathcal{O}(\epsilon^3)\,, \qquad \psi_{xx} \approx 0\,, \qquad \eta_{xx} \approx 0\,. \tag{3.7}$$

To determine $\psi(0)$, which from (3.6) will yield the NLEP, we must first carefully derive appropriate jump conditions for ψ_x and η_x across the hotspot region centered at $x = 0$. This is done in the next sub-section.

3.2 Jump Conditions and the Derivation of the NLEP for $K \geq 2$

To derive the appropriate jump condition for ψ_x across the hotspot region, we integrate (3.2b) over an intermediate domain $-\delta < x < \delta$ with $\epsilon \ll \delta \ll 1$. We use the facts that $A_e \sim \epsilon^{-1} w/\sqrt{v_0}$, $\phi \sim \Phi(y)$, $A_e(\pm\delta) \sim \alpha$, and $u_e = \epsilon^{q-1}\tilde{u}_e$ as given in (2.15), to obtain, upon letting $\delta/\epsilon \to +\infty$, that

$$\begin{aligned}
\epsilon\mathcal{D}_0\alpha^2\left[\psi_x\right]_0 + 2\mathcal{D}_0\alpha\left[v_{ex}\phi\right]_0 \;=\;& 3\epsilon\int_{-\infty}^{\infty} w^2\Phi\,dy + \frac{\epsilon\psi(0)}{v_0^{3/2}}\int_{-\infty}^{\infty} w^3\,dy \\
& + \frac{\epsilon q\tilde{u}_e}{v_0^{(q-1)/2}}\int_{-\infty}^{\infty} w^{q-1}\Phi\,dy + \frac{\epsilon\eta(0)}{v_0^{q/2}}\int_{-\infty}^{\infty} w^q\,dy + \mathcal{O}(\epsilon^2\lambda)\,,
\end{aligned}$$

where we have introduced the notation $[a]_0 \equiv a(0^+) - a(0^-)$ to indicate that the evaluation is to be done with the outer solution. In addition, below we will use the convenient shorthand notation that $\int(\ldots) \equiv \int_{-\infty}^{\infty}(\ldots)\,dy$. Since $\phi = \mathcal{O}(\epsilon^3)$ in the outer region from (3.7), we can neglect the second term on the left-hand side of the expression above. For eigenvalues for which $\lambda \ll \mathcal{O}(\epsilon^{-1})$, we obtain that

$$\mathcal{D}_0\alpha^2[\psi_x]_0 = 3\int w^2\Phi + \frac{\psi(0)}{v_0^{3/2}}\int w^3 + \frac{q\tilde{u}_e}{v_0^{(q-1)/2}}\int w^{q-1}\Phi + \frac{\eta(0)}{v_0^{q/2}}\int w^q\,. \tag{3.8}$$

Now from (3.2b), we use $\phi = \mathcal{O}(\epsilon^3)$ in the outer region, together the fact $\epsilon^q\eta A_e^q \ll \mathcal{O}(\epsilon)$ since $q > 1$. In this way, from (3.2b) and (3.8), we obtain the following leading-order BVP problem for ψ with a jump condition for ψ_x across $x = 0$:

$$\psi_{xx} = 0\,, \quad |x| \leq \ell\,; \qquad e_0[\psi_x]_0 = e_1\psi(0) + e_2\eta(0) + e_3\,, \quad \psi(\ell) = z\psi(-\ell)\,, \quad \psi_x(\ell) = z\psi_x(-\ell)\,, \tag{3.9a}$$

where we have defined e_j, for $j = 0, \ldots, 3$, by

$$e_0 \equiv \mathcal{D}_0\alpha^2\,, \qquad e_1 \equiv \frac{1}{v_0^{3/2}}\int w^3\,, \qquad e_2 \equiv \frac{1}{v_0^{q/2}}\int w^q\,, \qquad e_3 \equiv 3\int w^2\Phi + \frac{q\tilde{u}_e}{v_0^{(q-1)/2}}\int w^{q-1}\Phi\,. \tag{3.9b}$$

8

This BVP is defined in terms of $\eta(0)$, which itself must be calculated from a separate BVP. To formulate this additional BVP, we integrate (3.2c) over $-\delta < x < \delta$, with $\epsilon \ll \delta \ll 1$, and let $\delta/\epsilon \to \infty$ to obtain

$$\mathcal{D}_0\epsilon^q\alpha^q\left[\eta_x\right]_0 + \mathcal{D}_0 q\alpha^{q-1}\mathcal{O}(\epsilon^{q+2}) = \epsilon^3\tau_u\lambda\left[\frac{q\tilde{u}_\epsilon}{v_0^{(q-1)/2}}\int w^{q-1}\Phi + \frac{\eta(0)}{v_0^{q/2}}\int w^q\right].\tag{3.10}$$

To achieve a distinguished balance in (3.10), we introduce $\hat{\tau}_u$ defined by

$$\hat{\tau}_u \equiv \epsilon^{3-q}\tau_u.\tag{3.11}$$

With this scaling, the police diffusivity $D_p \equiv \epsilon^{-2}\mathcal{D}_0/\tau_u$, is simply

$$D_p \equiv \epsilon^{1-q}\mathcal{D}_0/\hat{\tau}_u.\tag{3.12}$$

In this way, (3.10) yields the following jump condition for the outer solution:

$$\mathcal{D}_0\alpha^q\left[\eta_x\right]_0 = \hat{\tau}_u\lambda\left[\frac{q\tilde{u}_e}{v_0^{(q-1)/2}}\int w^{q-1}\Phi + \frac{\eta(0)}{v_0^{q/2}}\int w^q\right].\tag{3.13}$$

Now in the outer region we obtain from (3.2c) that

$$\mathcal{D}_0\epsilon^q\alpha^q\eta_{xx} + \mathcal{O}(\epsilon^{q+2}) = \epsilon^2\tau_u\lambda\left[\mathcal{O}(\epsilon^{q+2}) + \epsilon^q\alpha^q\eta\right].\tag{3.14}$$

We will consider the range of τ_u, and consequently $\hat{\tau}_u$, where

$$\tau_u \ll \mathcal{O}(\epsilon^{-2}), \qquad \text{for which} \qquad \hat{\tau}_u \ll \mathcal{O}(\epsilon^{1-q}).\tag{3.15}$$

We will assume in our theory below that $\hat{\tau}_u = \mathcal{O}(1)$, so that (3.15) for $\hat{\tau}_u$ holds for all $q > 1$.

For this range, (3.14) reduces to $\eta_{xx} \approx 0$ to leading order. In this way, we obtain using (3.13), the following BVP for the leading-order outer solution for η with a jump condition for η_x across $x = 0$:

$$\eta_{xx} = 0, \quad |x| \leq \ell; \qquad d_0\left[\eta_x\right]_0 = d_1\eta(0) + d_2, \quad \eta(\ell) = z\eta(-\ell), \quad \eta_x(\ell) = z\eta_x(-\ell).\tag{3.16a}$$

Here the constants d_0, d_1, and d_2, are defined by

$$d_0 \equiv \mathcal{D}_0\alpha^q, \qquad d_1 \equiv \frac{\hat{\tau}_u\lambda}{v_0^{q/2}}\int w^q, \qquad d_2 \equiv \frac{\hat{\tau}_u\lambda q\tilde{u}_e}{v_0^{(q-1)/2}}\int w^{q-1}\Phi.\tag{3.16b}$$

To solve the BVPs (3.16) and (3.9), and in this way determine $\psi(0)$ and $\eta(0)$, we need to establish a simple lemma.

Lemma 3.1 *Consider the BVP for $y = y(x)$ on $-\ell < x < \ell$ given by*

$$y_{xx} = 0, \quad -\ell < x < \ell; \qquad f_0\left[y_x\right]_0 = f_1 y(0) + f_2; \qquad y(\ell) = zy(-\ell), \quad y_x(\ell) = zy_x(-\ell),\tag{3.17}$$

where f_0, f_1 and f_2, are nonzero constants, and let z satisfy (3.5). Then, $y(0)$ is given by

$$y(0) = f_2\left[\frac{f_0}{\ell}\frac{(z-1)^2}{2z} - f_1\right]^{-1} = -\frac{f_2}{f_0(1 - \cos(\pi j/K))/\ell + f_1}.\tag{3.18}$$

9

Proof: Let $y_0 = y(0)$. The solution of this BVP is continuous but not differentiable at $x = 0$, and has the form

$$y(x) = \begin{cases} y_0 + A_+ x & \text{if } 0 < x < \ell, \\ y_0 + A_- x & \text{if } -\ell < x < 0, \end{cases}$$

where $y_0 \equiv y(0)$. Upon imposing the Floquet boundary conditions we obtain $A_+ = z A_-$ and $y_0 + A_+ \ell = z(y_0 - A_- \ell) = z y_0 - A_+ \ell$, which yields that $A_+ = (z-1)y_0/(2\ell)$. Then, upon imposing the jump condition across $x = 0$ we get

$$f_1 y_0 + f_2 = f_0 [y_x]_0 = f_0 (A_+ - A_-) = \frac{f_0 y_0}{2\ell}(z-1)\left(1 - \frac{1}{z}\right).$$

Upon solving for $y(0)$, and recalling the identify (3.5), we obtain (3.18) for $y(0)$. ∎

Upon using Lemma 3.1 with $f_0 = e_0$, $f_1 = e_1$, and $f_2 = e_2 \eta(0) + e_3$, we can determine $\psi(0)$ from (3.9). Similarly, we obtain $\eta(0)$ from (3.16) by applying Lemma 3.1 with $f_0 = d_0$, $f_1 = d_1$, and $f_2 = d_2$. This yields that

$$\psi(0) = -\frac{e_2 \eta(0) + e_3}{e_0(1 - \cos(\pi j/K))/\ell + e_1}, \qquad \text{and} \qquad \eta(0) = -\frac{d_2}{d_0(1 - \cos(\pi j/K))/\ell + d_1}. \tag{3.19}$$

The final step in the derivation of the NLEP is to combine the expressions in (3.19) so as to isolate $\psi(0)$. This will yield the key coefficient $\psi(0)/v_0^{3/2}$ in (3.6) in terms of the original parameters.

To do so, we first define D_j by

$$D_j \equiv \frac{\mathcal{D}_0}{\ell}\left(1 - \cos\left(\frac{\pi j}{K}\right)\right), \qquad j = 0, \ldots, K-1, \quad \text{where} \quad l = S/(2K), \tag{3.20}$$

so that $D_j < D_{j+1}$ for any $j = 0, 1, 2, \ldots, K-2$. Then, by calculating e_0 and d_0 from (3.9b) and (3.16b), we substitute (3.19) into (3.19) to obtain

$$\psi(0) = -\frac{1}{D_j \alpha^2 + e_1}\left[e_3 - \frac{e_2 d_2}{D_j \alpha^q + d_1}\right]. \tag{3.21}$$

Then, by using (2.8) for $\tilde{u}_e$, we rewrite the expressions for e_1, e_2, e_3, d_1, and d_2 in (3.9b) and (3.16b), as

$$e_1 = \frac{\int w^3}{v_0^{3/2}}, \qquad e_2 = \frac{\int w^q}{v_0^{q/2}}, \qquad e_3 = 3\int w^2 \Phi + \frac{U_0 \sqrt{v_0}}{K}\frac{q \int w^{q-1}\Phi}{\int w^q}, \tag{3.22a}$$

$$d_1 = \hat{\tau}_u \lambda \frac{\int w^q}{v_0^{q/2}}, \qquad d_2 = \hat{\tau}_u \lambda \left(\frac{U_0 \sqrt{v_0}}{K}\frac{q \int w^{q-1}\Phi}{\int w^q}\right). \tag{3.22b}$$

Upon substituting (3.22) into (3.21), we obtain, after some algebra, that

$$\mathcal{B}(\lambda) \equiv -\frac{\psi(0)}{v_0^{3/2}} = \frac{1}{\left(1 + v_0^{3/2}D_j\alpha^2/\int w^3\right)}\left[\frac{3\int w^2\Phi}{\int w^3} + \frac{v_0^{q/2}D_j\alpha^q}{v_0^{q/2}D_j\alpha^q + \hat{\tau}_u\lambda\int w^q}\left(\frac{U_0\sqrt{v_0}}{K\int w^3}\right)\left(\frac{q\int w^{q-1}\Phi}{\int w^q}\right)\right]. \tag{3.23}$$

We first consider the synchronous mode for which $j = 0$, and $\mathcal{D}_0 = 0$ from (3.20). In this case, upon substituting (3.23) into (3.6) we obtain the following NLEP for the synchronous mode $j = 0$:

$$L_0 \Phi - 3w^3 \frac{\int w^2 \Phi}{\int w^3} = \lambda \Phi, \qquad \Phi \to 0 \quad \text{as} \quad |y| \to \infty. \tag{3.24}$$

From Lemma 3.2 of [12], any nonzero eigenvalue of (3.24) must satisfy $\text{Re}(\lambda) < 0$. We summarize this result as follows:

Proposition 3.2 *For $\epsilon \to 0$, $K \geq 2$, $q > 1$, $0 < U_0 < U_{0,\max}$, $\mathcal{D}_0 = \epsilon^2 D = \mathcal{O}(1)$, and $\tau_u \ll \mathcal{O}(\varepsilon^{-2})$, a K-hotspot steady-state for (1.4) is linearly stable on an $\mathcal{O}(1)$ time-scale to synchronous perturbations of the hotspot amplitudes.*

Remark 3.3 *In the large diffusivity ratio limit, for the two-component Gierer-Meinhardt and Gray-Scott RD systems in 1-D, the synchronous mode is always the dominant oscillatory temporal instability for the spike amplitudes (cf. [30], [14]). However, for our three-component system (1.4), Proposition 3.2 shows that the synchronous mode is always linearly stable.*

Therefore, in our linear stability analysis we need only consider the asynchronous modes $j = 1, \ldots, K - 1$, for which $D_j \neq 0$. For these modes, (3.23) motivates the introduction of new quantities $\chi_{0,j}$, $\chi_{1,j}$ and $\mathcal{C}_q(\lambda)$, defined by

$$\chi_{0,j} \equiv \frac{1}{1 + v_0^{3/2} D_j \alpha^2 / \int w^3}, \qquad \chi_{1,j} \equiv \left(\frac{U_0 \sqrt{v_0}}{K \int w^3}\right) \frac{\chi_{0,j}}{\mathcal{C}_q(\lambda)}, \qquad \mathcal{C}_q(\lambda) \equiv 1 + \frac{\hat{\tau}_u \lambda \int w^q}{v_0^{q/2} D_j \alpha^q}. \tag{3.25}$$

Then, $\mathcal{B}(\lambda)$ in (3.23) can be written compactly as

$$\mathcal{B}(\lambda) \equiv -\frac{\psi(0)}{v_0^{3/2}} = \chi_{0,j} \frac{3 \int w^2 \Phi}{\int w^3} + \chi_{1,j} \frac{q \int w^{q-1} \Phi}{\int w^q}. \tag{3.26}$$

In this way, from (3.6) and (3.26), we obtain an NLEP with two nonlocal terms. The result is summarized as follows:

Proposition 3.4 *For $\epsilon \to 0$, $K \geq 2$, $q > 1$, $0 < U_0 < U_{0,\max}$, $\mathcal{D}_0 = \epsilon^2 D = \mathcal{O}(1)$, and $\tau_u \ll \mathcal{O}(\varepsilon^{-2})$, the linear stability on an $\mathcal{O}(1)$ time-scale of a K-hotspot steady-state solution for (1.4), for the asynchronous modes $j = 1, \ldots, K - 1$, is characterized by the spectrum of the following NLEP for $\Phi(y)$ with two nonlocal terms:*

$$L_0 \Phi - \chi_{0,j} w^3 \frac{3 \int w^2 \Phi}{\int w^3} - \chi_{1,j} w^3 \frac{q \int w^{q-1} \Phi}{\int w^q} = \lambda \Phi, \qquad where \qquad L_0 \Phi \equiv \Phi'' - \Phi + 3w^2 \Phi. \tag{3.27}$$

Here $\chi_{0,j}$ and $\chi_{1,j}$ are defined in (3.25), and $w(y) = \sqrt{2} \operatorname{sech} y$.

Next, we express $\chi_{0,j}$ and $\chi_{1,j}$ in the NLEP (3.27) in terms of the original parameters. To do so, we first substitute (2.11) for v_0 into (3.25) for $\chi_{0,j}$ and $\chi_{1,j}$. It is then convenient to introduce two new quantities κ_q and ω defined by

$$\kappa_q \equiv \left(\int w^q\right)^{-1} \left(\frac{\sqrt{2}\pi \alpha K}{\omega}\right)^q, \qquad where \qquad \omega \equiv S(\gamma - \alpha) - U_0. \tag{3.28}$$

In terms of these new variables, (3.25) becomes

$$\chi_{0,j} = \left(1 + \frac{\kappa_3 D_j}{\alpha}\right)^{-1}, \qquad \chi_{1,j} = \frac{U_0}{\omega \mathcal{C}_q(\lambda)} \chi_{0,j}, \qquad \mathcal{C}_q(\lambda) \equiv 1 + \frac{\hat{\tau}_u \lambda}{D_j \kappa_q}. \tag{3.29}$$

Next, we proceed to reformulate (3.27) as an NLEP with a single nonlocal term. To do so, we use the special property of the local operator L_0 that $L_0 w^2 = 3w^2$ (cf. [12]). Owing to the decay of Φ and w as $|y| \to \infty$, and since L_0 is self-adjoint, we obtain from Green's identity that $\int \left(w^2 L_0 \Phi - \Phi L_0 w^2\right) = 0$. By using (3.27) for $L_0 \Phi$, together with $L_0 w^2 = 3w^2$ and the integral ratio $\int w^5 / \int w^3 = 3/2$ from (2.6), we conclude from this Green's identity that

$$\left(\frac{\int w^2 \Phi}{\int w^3}\right) \left[\frac{9\chi_{0,j}}{2} + (\lambda - 3)\right] = -\frac{3q\chi_{1,j}}{2} \left(\frac{\int w^{q-1} \Phi}{\int w^q}\right). \tag{3.30}$$

There are several interesting limiting cases of the key identity (3.30) for any eigenpair of the NLEP (3.27) with two nonlocal terms. Since $\chi_{1,j}$ is proportional to U_0 from (3.29), we first observe from (3.30) that for any eigenpair for which $\int w^m \Phi \neq 0$ for any $m > 0$, we must have $\lambda = 3 - 9\chi_{0,j}/2$ if and only if $U_0 = 0$. We remark that this recovers the result in equation (3.17) of [12] that the unique discrete eigenvalue of the linearization of a K-hotspot steady-state of the two-component "basic" crime model with no police is

$$\lambda = 3 - \frac{9\chi_{0,j}}{2}, \tag{3.31}$$

11

where $\chi_{0,j}$ is defined in (3.29). By setting $\lambda = 0$ in this expression, the stability threshold in equation (3.19) of [12] is recovered. This is discussed in more detail in §4.3 below.

A second special case of (3.30), which is examined in detail in §5, is when $q = 3$, for which (3.30) becomes

$$\left(\frac{\int w^2 \Phi}{\int w^3}\right)\left[\frac{9}{2}\left(\chi_{0,j} + \chi_{1,j}\right) + \lambda - 3\right] = 0. \tag{3.32}$$

Therefore, when $q = 3$, and for any eigenpair Φ and λ of (3.27) with $\int w^2 \Phi \neq 0$, we have that λ must satisfy

$$\frac{9}{2}\left(\chi_{0,j} + \chi_{1,j}\right) + \lambda - 3 = 0. \tag{3.33}$$

By using (3.29) for $\chi_{1,j}$, we obtain that (3.33) reduces to a family of quadratic equations for λ of the form

$$c_2 \lambda^2 + c_1 \lambda + c_0 = 0, \tag{3.34a}$$

where c_0, c_1, and c_2, are defined for $j = 1, \ldots, K-1$ by

$$c_2 = \frac{\hat{\tau}_u}{3\chi_{0,j}D_j\kappa_3}, \qquad c_1 = \frac{\hat{\tau}_u}{D_j\kappa_3}\left(\frac{3}{2} - \frac{1}{\chi_{0,j}}\right) + \frac{1}{3\chi_{0,j}}, \qquad c_0 = \frac{3U_0}{2\omega} + \frac{3}{2} - \frac{1}{\chi_{0,j}}. \tag{3.34b}$$

In §5 we will analyze the implications of (3.34) for the possibility of Hopf bifurcations.

Since $U_0 > 0$, and since we only consider eigenfunctions for which $\int w^m \Phi \neq 0$ for any $m > 0$, we have $\lambda \neq 3 - 9\chi_{0,j}/2$. Therefore, in (3.30) we can isolate $\int w^2 \Phi$ as

$$\frac{3 \int w^2 \Phi}{\int w^3} = \frac{-9}{9\chi_{0,j} + 2(\lambda - 3)}\left(\chi_{1,j}\frac{q \int w^{q-1}\Phi}{\int w^q}\right).$$

Upon substituting this expression back into (3.26) for $\beta(\lambda)$ we eliminate the nonlocal term $\int w^2 \Phi$, and obtain that

$$\beta(\lambda) = \chi(\lambda)\frac{\int w^{q-1}\Phi}{\int w^q}, \qquad \text{where} \qquad \chi(\lambda) \equiv q\chi_{1,j}\left(\frac{2(\lambda - 3)}{9\chi_{0,j} + 2(\lambda - 3)}\right). \tag{3.35}$$

Finally, by substituting (3.29) for $\chi_{0,j}$ and $\chi_{1,j}$ into (3.35) we obtain an NLEP with one nonlocal term:

Proposition 3.5 *For $\epsilon \to 0$, $K \geq 2$, $q > 1$, $0 < U_0 < U_{0,\max}$, $\mathcal{D}_0 = \epsilon^2 D = \mathcal{O}(1)$, and $\tau_u \ll \mathcal{O}(\varepsilon^{-2})$, the linear stability on an $\mathcal{O}(1)$ time-scale of a K-hotspot steady-state solution for (1.4), for the asynchronous modes $j = 1, \ldots, K-1$, is characterized by the spectrum of the NLEP for $\Phi(y)$ given by*

$$L_0\Phi - \chi(\lambda)w^3\frac{\int w^{q-1}\Phi}{\int w^q} = \lambda\Phi, \qquad \Phi \to 0 \quad as \quad |y| \to \infty, \tag{3.36a}$$

where $L_0\Phi \equiv \Phi'' - \Phi + 3w^2\Phi$. Here the multiplier $\chi(\lambda)$ of the NLEP is defined by

$$\chi(\lambda) \equiv \frac{qU_0}{\omega\mathcal{C}_q(\lambda)}\left(\frac{(\lambda - 3)\chi_{0,j}}{(\lambda - 3) + 9\chi_{0,j}/2}\right), \qquad \text{where} \quad \frac{1}{\chi_{0,j}} = 1 + \frac{\kappa_3 D_j}{\alpha}, \quad \text{and} \quad \mathcal{C}_q(\lambda) = 1 + \frac{\hat{\tau}_u\lambda}{D_j\kappa_q}. \tag{3.36b}$$

Here κ_q and ω are defined in (3.28), D_j is defined in (3.20), and $\hat{\tau}_u$ is related to τ_u by (3.11).

Remark 3.6 *We observe that our NLEP (3.36) has the general form*

$$L_0\Phi - \left(\frac{a_0 + a_1\lambda}{b_0 + b_1\lambda + b_2\lambda^2}\right)w^3\frac{\int w^{q-1}\Phi}{\int w^q} = \lambda\Phi,$$

where the coefficients a_0, a_1, b_0, b_1 and b_2 are independent of λ. To our knowledge there have been no previous studies of NLEPs in 1-D where the multiplier χ of the NLEP is a proper rational function of degree two. Some results of this type are given in [24] for the linear stability analysis of spot patterns on the sphere for the Brusselator RD system.

The key model parameters we will use to analyze the NLEP are $\hat{\tau}_u$, q, U_0, $\mathcal{D}_0$, and ω. We remark that $\omega = U_{0,\max} - U_0$ where $U_{0,\max} = S(\gamma - \alpha)$ is the maximum police deployment for which a hotspot steady-state can exist.

3.3 Derivation of the NLEP for a Single Hotspot: $K = 1$ case

For $K \geq 2$, the NLEP (3.36) was derived by imposing Floquet boundary conditions at $x = \pm \ell$. For the case of a single hotspot, we can impose the Neumann boundary conditions directly at $x = \pm \ell$, as the Floquet analysis is not needed. With the same procedure as that leading to (3.9) and (3.16) above, we now obtain for ψ and η that

$$\psi_{xx} = 0, \quad |x| \leq \ell; \qquad e_0 [\psi_x]_0 = e_1 \psi(0) + e_2 \eta(0) + e_3, \qquad \psi_x(\pm \ell) = 0, \tag{3.37a}$$

$$\eta_{xx} = 0, \quad |x| \leq \ell; \qquad d_0 [\eta_x]_0 = d_1 \eta(0) + d_2, \qquad \eta_x(\pm \ell) = 0. \tag{3.37b}$$

Here the coefficients e_0, e_1, e_2, e_3 and d_0, d_1 and d_2, are as defined in (3.9b) and (3.16b), respectively.

From (3.37) we obtain that $\eta(x) = \eta(0)$ and $\psi(x) = \psi(0)$ on $|x| \leq \ell$, where $\eta(0) = -d_2/d_1$ and

$$\psi(0) = -\frac{1}{e_1} (e_2 \eta(0) + e_3) = -\frac{1}{e_1} \left(e_3 - \frac{e_2 d_2}{d_1} \right).$$

This is precisely the formula given in (3.21) with D_j set to zero.

Therefore, by proceeding in the same way as was done in the Floquet analysis performed earlier for the $K \geq 2$ case, we simply set D_j to zero in the expression (3.23), and in this way determine $\beta(\lambda)$ as

$$\beta \equiv -\frac{\psi(0)}{v_0^{3/2}} = \frac{3 \int w^2 \Phi}{\int w^3}. \tag{3.38}$$

By substituting (3.38) into (3.6) we obtain that the NLEP for a single hotspot solution is given by (3.24). For this NLEP, Lemma 3.2 of [12] proves that $\mathrm{Re}(\lambda) < 0$ for eigenfunctions for which $\int w^2 \Phi \neq 0$. Therefore, we conclude that a single hotspot steady-state solution is unconditionally stable for any $\mathcal{D}_0$ when $\tau_u \ll \mathcal{O}(\epsilon^{-2})$.

3.4 Reformulation of the NLEP as Zeros of a Meromorphic Function

We now reformulate our NLEP (3.36) for a $K \geq 2$ hotspot steady-state so that its unstable discrete eigenvalues are the zeros of a meromorphic function $\zeta(\lambda)$ in the right-half $\mathrm{Re}(\lambda) \geq 0$ of the complex plane. To do so, we first write (3.36) as

$$(L_0 - \lambda) \Phi = \chi(\lambda) w^3 \frac{\int w^{q-1} \Phi}{\int w^q}, \qquad \text{so that} \qquad \Phi = \chi(\lambda) \frac{\int w^{q-1} \Phi}{\int w^q} (L_0 - \lambda)^{-1} w^3.$$

We then multiply both sides of this expression by w^{q-1} and integrate to get

$$\left(\int w^{q-1} \Phi \right) \left[1 - \chi(\lambda) \frac{\int w^{q-1} (L_0 - \lambda)^{-1} w^3}{\int w^q} \right] = 0. \tag{3.39}$$

For eigenfunctions that satisfy $\int w^{q-1} \Phi \neq 0$, it follows that an eigenvalue λ of the NLEP (3.36) must be a root of

$$\zeta(\lambda) \equiv \mathcal{C}(\lambda) - \mathcal{F}(\lambda) = 0, \qquad \text{where} \qquad \mathcal{F}(\lambda) \equiv \frac{\int w^{q-1} (L_0 - \lambda)^{-1} w^3}{\int w^q}. \tag{3.40a}$$

Here $\mathcal{C}(\lambda) \equiv [\chi(\lambda)]^{-1}$, and in terms of $\chi_{0,j}$ and $\mathcal{C}_q(\lambda)$, as defined in (3.36b), we have

$$\mathcal{C}(\lambda) = \frac{\omega \mathcal{C}_q(\lambda)}{q U_0} \left(\frac{1}{\chi_{0,j}} + \frac{9}{2(\lambda - 3)} \right). \tag{3.40b}$$

We will proceed to analyze the zeros of the meromorphic function $\zeta(\lambda) \equiv \mathcal{C}(\lambda) - \mathcal{F}(\lambda)$ in two cases: $q = 3$ and $q > 1$, with the former being explicitly solvable, and the latter requiring the Nyquist criterion to count the number of zeros in

the unstable right half-plane $\text{Re}(\lambda) > 0$. Moreover, we will also investigate the possibility of a Hopf bifurcation, by seeking a pure imaginary root of the form $\lambda = \pm i\lambda_I$ to (3.40) with $\lambda_I > 0$. Since $j = 1, \ldots, K - 1$, such a Hopf bifurcation will correspond to an asynchronous temporal oscillation of the hotspot amplitudes.

Remark 3.7 *When $\int w^{q-1}\Phi = 0$, the NLEP (3.36) reduces to the local eigenvalue problem $L_0\Phi = \lambda\Phi$ with the extra condition $\int w^{q-1}\Phi = 0$. From Proposition 5.6 of [7], L_0 has exactly two discrete eigenvalues. One is $\Phi = w^2$ with $\lambda = 3$, arising from the identity $L_0 w^2 = 3w^2$, for which $\int w^{q-1}\Phi \neq 0$, while the other is the odd eigenfunction $\Phi = w'$ for which $\lambda = 0$ and $\int w^{q-1}\Phi = 0$. Therefore, since there are no instabilities associated with modes for which $\int w^{q-1}\Phi = 0$, the zeroes of $\zeta(\lambda)$, as defined in (3.40), in $\text{Re}(\lambda) > 0$ will determine any instability of the K-hotspot steady-state with $K \geq 2$.*

4   Analysis of the NLEP: Competition Instability

In order to analyze zero-eigenvalue crossings for the NLEP (3.36), as well as the possibility of Hopf bifurcations, in §4.1 we need to provide some global properties of $\mathcal{F}(\lambda)$, as defined in (3.40a), on both the non-negative real axis $\lambda \geq 0$ and on the non-negative imaginary axis $\lambda = i\lambda_I$ with $\lambda_I \geq 0$. In §4.2 we apply the winding number criterion of complex analysis to count the number of zeroes of $\zeta(\lambda)$, defined in (3.40), in the unstable right half-plane $\text{Re}(\lambda) > 0$. With these properties, in §4.3 we study the competition stability threshold characterized by zero-eigenvalue crossings of the NLEP (3.36). Oscillatory instabilities for $q = 3$ and for general $q > 1$ due to a Hopf bifurcation are studied in detail in §5 and §6, respectively.

Before summarizing the global properties of $\mathcal{F}(\lambda)$, we first show that $\mathcal{F}(\lambda)$ can be found explicitly when $q = 3$ by using the identity $L_0 w^2 = 3w^2$. When $q = 3$, we calculate the integral I in the numerator for $\mathcal{F}(\lambda)$, given in (3.40a), as

$$I \equiv \int w^2 \left(L_0 - \lambda\right)^{-1} w^3 = \frac{1}{3} \int \left(L_0 w^2\right) \left(L_0 - \lambda\right)^{-1} w^3 = \int \left[(L_0 - \lambda)w^2 + \lambda w^2\right] \left(L_0 - \lambda\right)^{-1} w^3 \,.$$

Upon integrating this last expression by parts, we get the algebraic equation $I = \left(\int w^5 + \lambda I\right)/3$, so that $I = \int w^5/(3 - \lambda)$. Then, since $\mathcal{F} = I/\int w^3$ and $\int w^5/\int w^3 = 3/2$ from (2.6), we conclude that

$$\mathcal{F}(\lambda) = \frac{3}{2(3 - \lambda)}\,, \qquad \text{when} \quad q = 3\,. \tag{4.1}$$

4.1   Key Global and Asymptotic Properties of $\mathcal{F}(\lambda)$

We first recall some key properties of $\mathcal{F}(\lambda)$, defined in (3.40a), on the non-negative real axis $\lambda \geq 0$.

Proposition 4.1 *On the non-negative real axis $\lambda \geq 0$, $\mathcal{F}(\lambda)$ given in (3.40a) satisfies*

(i) $\mathcal{F}(\lambda) \sim \frac{1}{2} + \frac{\lambda}{4}\left(1 - \frac{1}{q}\right) + \mathcal{O}(\lambda^2) \quad as \quad \lambda \to 0\,.$

(ii) $\mathcal{F}(\lambda) \to +\infty \quad as \quad \lambda \to 3^-\,.$

(iii) $\mathcal{F}'(\lambda) > 0\,, \quad for \quad 0 < \lambda < 3\,, \quad when \ q = 2, 3, 4\,.$

(iv) $\mathcal{F}(\lambda) < 0\,, \quad for \quad \lambda > 3\,.$

Proof: The statements in (i), (ii), and (iv), as well as in (iii) for $q = 2$ and $q = 4$, were proved in Proposition 3.5 of [30]. For $q = 3$, the monotonicity result in (iii) is seen to hold by using the explicit form for $\mathcal{F}(\lambda)$ given in (4.1). ∎

In addition to the results (i), (ii), and (iv), which hold for all $q > 1$, we conjecture that the monotonicity result in (iii) holds not just for $q = 2, 3, 4$ but for all $q > 1$. As additional support of this conjecture, in Fig. 3 we plot the numerically computed function $\mathcal{F}(\lambda)$ on $0 < \lambda < 3$ for $q = 2, 3, 4, 5$.
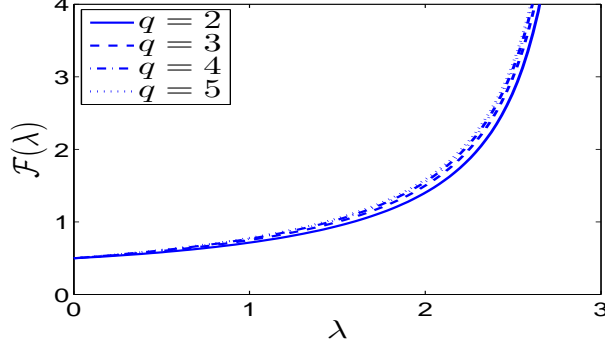
Figure 3: Plot of $\mathcal{F}(\lambda)$ on $0 < \lambda < 3$ for $q = 2, 3, 4, 5$. Note that $\mathcal{F}(0) = 1/2$ and that $\mathcal{F}(\lambda) \to +\infty$ as $\lambda \to 3$ from below. We observe that $\mathcal{F}(\lambda)$ is rather insensitive to changes in q.

Conjecture 4.2 *The monotonocity property (iii) of Proposition 4.1 that $\mathcal{F}'(\lambda) > 0$ on $0 < \lambda < 3$ holds for all $q > 1$.*

Next, in order to count the number of eigenvalues of the NLEP (3.36) in $\text{Re}(\lambda) > 0$ below, we need some properties of $\mathcal{F}(\lambda)$, as defined in (3.40a), as restricted to the non-negative imaginary axis. By rewriting the operator as

$$(L_0 - i\lambda_I)^{-1} = (L_0 + i\lambda_I)\left[(L_0 + i\lambda_I)^{-1}(L_0 - i\lambda_I)^{-1}\right] = L_0\left[L_0^2 + \lambda_I^2\right]^{-1} + i\lambda_I\left[L_0^2 + \lambda_I^2\right]^{-1},$$

we readily obtain upon upon separating $\mathcal{F}(i\lambda_I) = \int w^{q-1}(L_0 - i\lambda_I)^{-1}w^3 / \int w^q$ into real and imaginary parts that

$$\mathcal{F}(i\lambda_I) = \mathcal{F}_R(\lambda_I) + i\mathcal{F}_I(\lambda_I); \qquad \mathcal{F}_R(\lambda_I) = \frac{\int w^{q-1}L_0\left[L_0^2 + \lambda_I^2\right]^{-1}w^3}{\int w^q}, \qquad \mathcal{F}_I(\lambda_I) = \frac{\lambda_I \int w^{q-1}\left[L_0^2 + \lambda_I^2\right]^{-1}w^3}{\int w^q}. \quad (4.2)$$

We then recall some rigorous results of [30] for $\mathcal{F}_R(\lambda_I)$ and $\mathcal{F}_I(\lambda_I)$ on $\lambda_I \geq 0$.

Proposition 4.3 *For $\lambda = i\lambda_I$ with $\lambda_I > 0$, we have that $\mathcal{F}_R(\lambda_I)$ and $\mathcal{F}_I(\lambda_I)$ satisfy*

(i) $\mathcal{F}_R(\lambda_I) = \mathcal{O}(\lambda_I^{-2})$ *as* $\lambda_I \to +\infty$, $\mathcal{F}_R(0) = 1/2$.

(ii) $\mathcal{F}_R'(\lambda_I) < 0$, *when* $q = 2, 3$.

(iii) $\mathcal{F}_I(\lambda_I) = \mathcal{O}(\lambda_I^{-1})$ *as* $\lambda_I \to +\infty$.

(iv) $\mathcal{F}_I(\lambda_I) \sim \frac{\lambda_I}{4}\left(1 - \frac{1}{q}\right) > 0$ *as* $\lambda_I \to 0^+$.

(v) $\mathcal{F}_I(\lambda_I) > 0$, *when* $q = 2, 3, 4$.

<u>Proof:</u> The statement in (i), and in (ii) for $q = 2$, were proved in Proposition 3.1 of [30]; Statements (iii), (iv), and (v) for $q = 2, 4$, were proved in Proposition 3.2 of [30]. The results in (ii) and (v) for $q = 3$ follow by using the explicit formula in (4.1). For $q = 3$, we have $\mathcal{F}(i\lambda_I) = 3/\left[2(3 - i\lambda_I)\right]$, so that

$$\mathcal{F}_R(\lambda_I) = \frac{9}{2(9 + \lambda_I^2)}, \quad \mathcal{F}_R'(\lambda_I) = -\frac{9\lambda_I}{(9 + \lambda_I^2)^2}, \quad \mathcal{F}_I(\lambda_I) = \frac{3\lambda_I}{2(9 + \lambda_I^2)}, \quad \mathcal{F}_I'(\lambda_I) = \frac{3(9 - \lambda_I^2)}{2(9 + \lambda_I^2)^2}, \quad \text{for} \quad q = 3. \quad (4.3)$$

This clearly shows that properties (ii) and (v) also hold for $q = 3$. $\blacksquare$

Although we only have a rigorous proof that $\mathcal{F}_R'(\lambda_I) < 0$ when $q = 2, 3$ and that $\mathcal{F}_I(\lambda_I) > 0$ when $q = 2, 3, 4$, we now conjecture that these key properties hold for all $q > 1$. In Fig. 4 we plot the numerically computed functions $\mathcal{F}_R(\lambda_I)$ and $\mathcal{F}_I(\lambda_I)$ for various values of q, which give numerical evidence for this conjecture. From this figure we observe that $\mathcal{F}_R(\lambda_I)$ is rather insensitive to changes in q.

Conjecture 4.4 *Properties (ii) and (v) in Proposition 4.3 that $\mathcal{F}'_R(\lambda_I) < 0$ and $\mathcal{F}_I(\lambda_I) > 0$ on $\lambda_I > 0$ hold for all $q > 1$.*
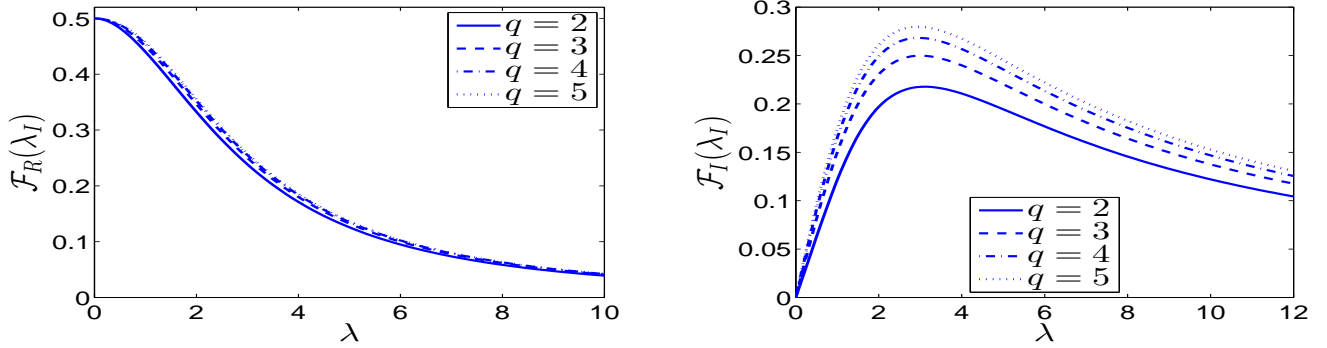

Figure 4: Plots of $\mathcal{F}_R(\lambda_I)$ (left panel) and $\mathcal{F}_I(\lambda_I)$ (right panel) for $q = 2, 3, 4, 5$. Note that $\mathcal{F}_R(0) = 1/2$ and $\mathcal{F}_I(0) = 0$, and that the maximum of $\mathcal{F}_I$ occurs near $\lambda_I = 3$. In fact, the maximum does occur exactly at $\lambda_I = 3$ when $q = 3$.

4.2 A Winding Number Criterion for the Number of Unstable Eigenvalues of the NLEP

We now use the argument principle of complex analysis to count the number N of eigenvalues of the NLEP (3.36) in $\mathrm{Re}(\lambda) > 0$. For each $j = 1, \ldots, K-1$, these discrete eigenvalues are the complex zeroes of the function $\zeta(\lambda) \equiv \mathcal{C}(\lambda) - \mathcal{F}(\lambda)$, as defined in (3.40). Here $\mathcal{F}(\lambda)$ is defined in (3.40a) and from (3.40b) we have that $\mathcal{C}(\lambda)$ has the explicit form

$$\mathcal{C}(\lambda) = a(1 + \tilde{\tau}_j \lambda)\left(1 - \frac{b}{3 - \lambda}\right), \tag{4.4a}$$

where a, b, and $\tilde{\tau}_j$, are defined for $j = 1, \ldots, K-1$ by

$$a \equiv \frac{\omega}{qU_0\chi_{0,j}}, \qquad b \equiv \frac{9}{2}\chi_{0,j}, \qquad \tilde{\tau}_j \equiv \frac{\hat{\tau}_u}{D_j\kappa_q}, \qquad \frac{1}{\chi_{0,j}} = 1 + \frac{\kappa_3 D_j}{\alpha}. \tag{4.4b}$$

Here ω and κ_q are given in (3.28), while D_j and $\hat{\tau}_u$ are defined in (3.20) and 3.11, respectively.

From (4.4a), $\mathcal{C}(\lambda)$ is a meromorphic function with a simple pole at $\lambda = 3$. Moreover, $\mathcal{F}(\lambda)$ is analytic in $\mathrm{Re}(\lambda) \geq 0$ except at the simple pole at $\lambda = 3$. The simple poles of $\mathcal{C}(\lambda)$ and $\mathcal{F}(\lambda)$ do not cancel as $\lambda \to 3^-$, since when restricted to the real line we get $\mathcal{F}(\lambda) \to +\infty$ while $\mathcal{C}(\lambda) \to -\infty$ as $\lambda \to 3^-$. Thus, $\zeta(\lambda) = \mathcal{C}(\lambda) - \mathcal{F}(\lambda)$ has a simple pole at $\lambda = 3$.

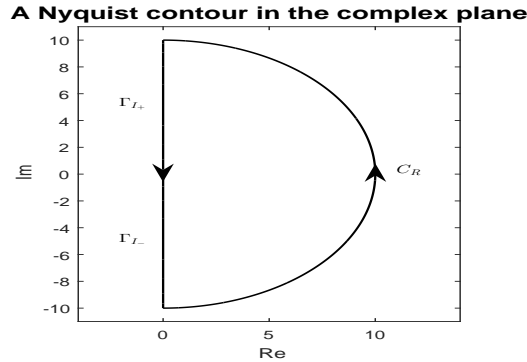*Figure 5: Schematic plot of the Nyquist contour Γ used for determining the number N of unstable eigenvalues of the NLEP (3.36).*

To determine a formula for N, we calculate the winding of $\zeta(\lambda)$ over the Nyquist contour Γ traversed in the counterclockwise direction that consists of the following segments in the complex λ-plane (see the schematic in Fig. 5): Γ_I^+ ($0 < \mathrm{Im}(\lambda) < iR$, $\mathrm{Re}(\lambda) = 0$), Γ_I^- ($-iR < \mathrm{Im}(\lambda) < 0$, $\mathrm{Re}(\lambda) = 0$), and C_R defined by $|\lambda| = R > 0$ for $|\arg(\lambda)| < \pi/2$.

For each $j = 1, \ldots, K - 1$, $\zeta(\lambda)$ is analytic in $\mathrm{Re}(\lambda) \geq 0$ except at the simple pole $\lambda = 3$ corresponding to the unique positive eigenvalue of the local operator L_0. Therefore, for each $j = 1, \ldots, N - 1$, and assuming that $\zeta(\lambda)$ has no zeroes on the imaginary axis, we have by the argument principle that $N = 1 + (2\pi)^{-1} \lim_{R \to \infty} [\arg \zeta]_\Gamma$, where $[\arg \zeta]_\Gamma$ denotes the change in the argument of ζ over Γ. Since $\mathcal{F}(\lambda) = \mathcal{O}(|\lambda|^{-1})$ on the semi-circle C_R as $R = |\lambda| \to \infty$, we have that $\lim_{R \to \infty} [\arg \zeta]_{C_R} = \lim_{R \to \infty} [\arg \mathcal{C}]_{C_R}$. From (4.4a) we calculate that $\lim_{R \to \infty} [\arg \mathcal{C}]_{C_R} = \pi$ when $\hat{\tau}_u > 0$, and $\lim_{R \to \infty} [\arg \mathcal{C}]_{C_R} = 0$ when $\hat{\tau}_u = 0$. For the contour Γ_I^-, we use that $\zeta(\overline{\lambda}) = \overline{\zeta(\lambda)}$ so that $[\arg \zeta]_{\Gamma_I^-} = [\arg \zeta]_{\Gamma_I^+}$. In this way, for each $j = 1, \ldots, K - 1$, we conclude that

$$N = \frac{3}{2} + \frac{1}{\pi} [\arg \zeta]_{\Gamma_I^+}, \quad \text{for} \quad \hat{\tau}_u > 0; \qquad N = 1 + \frac{1}{\pi} [\arg \zeta]_{\Gamma_I^+}, \quad \text{for} \quad \hat{\tau}_u = 0. \tag{4.5}$$

Here $[\arg \zeta]_{\Gamma_I^+}$ denotes the change in the argument of ζ as the imaginary axis $\lambda = i\lambda_I$ is traversed from $\lambda_I = +\infty$ to $\lambda_I = 0$.

We remark that (4.5) determines the number of unstable eigenvalues of the NLEP (3.36) for any *specific* asynchronous mode $j = 1, \ldots, K - 1$. The total number of such unstable eigenvalues, for all asynchronous modes, is simply the union of (4.5) over $j = 1, \ldots, K - 1$. In this way, the problem of determining N for a particular mode j is reduced to calculating the change of argument of $\zeta(\lambda) = \mathcal{C}(\lambda) - \mathcal{F}(\lambda)$ as we traverse down the positive imaginary axis. To do so, we will need the properties of $\mathcal{F}(i\lambda_I)$ given in Proposition 4.3, together with results for $\mathcal{C}(i\lambda)$ to be obtained from (4.4).

4.3 The Competition Instability Threshold

We now determine the competition instability threshold value of the diffusivity $\mathcal{D}_0$, which is characterized by a zero-eigenvalue crossing of the NLEP (3.36). Since $\mathcal{F}(0) = 1/2$ (see (i) of Proposition 4.1), we conclude that $\zeta(0) = 0$ when $\mathcal{C}(0) = 1/2$. From using (3.40b), or equivalently (4.4), for $\mathcal{C}(\lambda)$ we conclude that $\lambda = 0$ when

$$\frac{\omega}{qU_0} \left(\frac{1}{\chi_{0,j}} - \frac{3}{2} \right) = \frac{1}{2}, \qquad j = 1, \ldots, K - 1. \tag{4.6}$$

By using (4.4b) for $\chi_{0,j}$, together with (3.28) for κ_3, (4.6) yields that $\lambda = 0$ when

$$D_j = \frac{\omega^3}{4\pi^2 K^3 \alpha^2} \left(1 + \frac{qU_0}{\omega} \right), \qquad j = 1, \ldots, K - 1. \tag{4.7}$$

Finally, by using $D_j = 2K\mathcal{D}_0 (1 - \cos(\pi j/K))/S$, as obtained from (3.20), we conclude that the NLEP has a zero-eigenvalue crossing at the $K - 1$ distinct values $\mathcal{D}_{0,j}$ of $\mathcal{D}_0$ given by

$$\mathcal{D}_{0,j} = \frac{\omega^3 S}{8\pi^2 \alpha^2 K^4 (1 - \cos(\pi j/K))} \left(1 + \frac{qU_0}{\omega} \right), \qquad j = 1, \ldots, K - 1. \tag{4.8}$$

As we show in Proposition 4.6 below, the competition instability threshold $\mathcal{D}_{0,c}$ corresponds to the smallest such $\mathcal{D}_{0,j}$, which occurs when $j = K - 1$. This yields that

$$\mathcal{D}_{0,c} \equiv \mathcal{D}_{0,K-1} = \frac{\omega^3 S}{8\pi^2 \alpha^2 K^4 (1 + \cos(\pi/K))} \left(1 + \frac{qU_0}{\omega} \right). \tag{4.9}$$

In terms of the unscaled diffusivity $D = \epsilon^{-2} \mathcal{D}_0$, the competition stability threshold occurs at $D_c \equiv \epsilon^{-2} \mathcal{D}_{0,c}$.

Remark 4.5 *The zero-eigenvalue crossing condition (4.6) can also be obtained from the NLEP (3.27) with two nonlocal terms by setting $\Phi = w$ and $\lambda = 0$ in (3.27). By using the identity $L_0 w = 2w^3$, this substitution yields $2 - 3\chi_{0,j} - q\chi_{1,j} = 0$, where from (3.29) we have $\chi_{1,j} = U_0 \chi_{0,j}/\omega$ at $\lambda = 0$. Some simple algebra then recovers (4.6).*

We now prove an instability result related to zero-eigenvalue crossings:

Proposition 4.6 *For $\epsilon \to 0$, $K \geq 2$, $q > 1$, $0 < U_0 < U_{0,\max}$, $\mathcal{D}_0 = \epsilon^2 D = \mathcal{O}(1)$, a K-hotspot steady-state solution for (1.4) is unstable for all $\hat{\tau}_u \geq 0$ when $\mathcal{D}_0 > \mathcal{D}_{0,c}$, where $\mathcal{D}_{0,c}$ is the competition stability threshold defined in (4.9). For $\mathcal{D}_0 < \mathcal{D}_{0,c}$, a K-hotspot steady-state is linearly stable when $\hat{\tau}_u = 0$ and $q = 2, 3, 4$.*

<u>Proof:</u> We first prove that when $\mathcal{D}_0 > \mathcal{D}_{0,c}$, then $\zeta(\lambda) = 0$ in (3.40) has a positive real root in $0 < \lambda < 3$ for each $j = 1, \ldots, K - 1$. This readily follows from the fact that $\mathcal{C}(0) > 1/2$ for each $j = 1, \ldots, K - 1$, that $\mathcal{C}(\lambda) \to -\infty$ as $\lambda \to 3^-$, and from Proposition 4.1 where we have $\mathcal{F}(0) = 1/2$ and $\mathcal{F}(\lambda) \to +\infty$ as $\lambda \to 3^-$. Thus, by continuity, there is at least one positive real root to $\zeta(\lambda) = 0$ on $0 < \lambda < 3$ for each $j = 1, \ldots, K - 1$ and for any $\hat{\tau}_u \geq 0$. Next, for $\mathcal{D}_0 < \mathcal{D}_{0,c}$, we show that $N = 0$ by using the winding number criterion (4.5) and calculating $[\arg \zeta]_{\Gamma_I^+}$ explicitly. From (4.4a), we decompose $\mathcal{C}(i\lambda_I) = \mathcal{C}_R(\lambda_I) + i\mathcal{C}_I(\lambda_I)$, and for $\hat{\tau}_u = 0$ calculate that

$$\mathcal{C}_I(\lambda_I) = -\frac{ab\lambda_I}{9 + \lambda_I^2} < 0 \qquad \text{for} \quad \lambda_I > 0 \,.$$

Since $\mathcal{F}_I(\lambda_I) > 0$ for $\lambda_I > 0$ for $q = 2, 3, 4$ from property (v) of Proposition 4.3, we conclude that $\text{Im}\,[\zeta(i\lambda_I)] < 0$ for $\lambda_I > 0$. Then, since $\mathcal{C}(0) > 1/2$ when $\mathcal{D}_0 < \mathcal{D}_{0,c}$, and $\mathcal{F}(0) = 1/2$ from (i) of Proposition 4.1, we have $\zeta(0) > 0$ for each $j = 1, \ldots, K - 1$, and $\zeta(i\lambda_I) \to \omega/(qU_0\chi_{0,j}) > 0$ as $\lambda_I \to +\infty$. It follows that $[\arg \zeta]_{\Gamma_I^+} = -\pi$, and consequently $N = 0$ from the second statement in (4.5) for $\hat{\tau}_u = 0$. ■

We remark that if Conjecture 4.4 holds, then a K-hotspot steady-state is linearly stable when $\mathcal{D}_0 < \mathcal{D}_{0,c}$ and $\hat{\tau}_u = 0$ for any $q > 1$. Moreover, by continuity of eigenvalue paths in $\hat{\tau}_u$, the stability result in Proposition 4.6 should hold for all $\hat{\tau}_u > 0$ but sufficiently small. The possibility of Hopf bifurcations values of $\hat{\tau}_u$ for the range $\mathcal{D}_0 < \mathcal{D}_{0,c}$ is examined for $q = 3$ in §5 and for general $q > 1$ in §6.

4.4 Qualitative Interpretation of the Competition Instability Threshold

Next, we discuss the qualitative behavior of the competition instability threshold $\mathcal{D}_{0,c}$ with respect to the degree q of patrol focus and the total level U_0 of police patrol deployment. From (2.12), the maximum $A_{\max}$ of the steady-state attractiveness field is $A_{\max} \sim \epsilon^{-1}\omega/(K\pi)$, which decreases as either ω decreases or K increases. However, from Corollary 2.2, the amplitude of the steady-state criminal density ρ at the hotspot locations is $\rho_{\max} = [w(0)]^2 = 2$, which is independent of all model parameters, while away from the maxima of A the criminal density is $\mathcal{O}(\epsilon^2) \ll 1$. Therefore, it is the reduction of the number of stable steady-state hotspots on a given domain length that is the primary factor in reducing the total crime in the domain. As such, we seek to tune the police parameters q and U_0 so that the range of diffusivity $\mathcal{D}_0$ for which a K-hotspot steady-state is unconditionally unstable, i.e. unstable for all $\hat{\tau}_u > 0$, is as large as possible. This corresponds to minimizing the competition stability threshold $\mathcal{D}_{0,c}$ in (4.9).

From (4.9), we observe that $\mathcal{D}_{0,c}$ increases with q in a linear fashion. Within the context of our RD model (1.4), this predicts that if the police become increasingly focused on patrolling the more crime-attractive areas, then paradoxically the range of $\mathcal{D}_0$ where a K-hotspot steady-state is unstable decreases. Therefore, for the goal of reducing the number of stable crime hotspots, a police deployment with intense focus on crime-attractive areas does not offer an advantage over that of a less focused patrol (assuming that $q > 1$ for our analysis to hold). At a fixed level U_0 of police deployment, and for integer values of q with $q > 1$, the best patrol strategy is to take $q = 2$, which corresponds to the "cops-on-the-dots" strategy (cf. [11], [22], [33]) where the police mimic the movement of the criminals.

For a fixed $q > 1$, we next examine how the competition stability threshold for a K-hotspot steady-state changes with

the total police deployment U_0. To this end, we substitute $U_0 = S(\gamma - \alpha) - \omega$ into (4.9), and write $\mathcal{D}_{0,c}$ as

$$\mathcal{D}_{0,c} = \frac{S}{8\pi^2\alpha^2 K^4\left(1 + \cos\left(\pi/K\right)\right)}\, g(U_0)\,, \qquad g(U_0) \equiv \omega^3(1-q) + qS(\gamma-\alpha)\omega^2\,; \qquad \omega \equiv S(\gamma-\alpha) - U_0\,. \tag{4.10}$$

To analyze the critical points of $g(U_0)$, we first observe that $d\omega/dU_0 = -1$ and that $U_0 \to U_{0,\max} = S(\gamma - \alpha)$ as $\omega \to 0$. We then calculate that

$$\frac{dg}{dU_0} = -3(1-q)\omega\left(\omega - \omega_c\right)\,, \qquad \text{where} \qquad \omega_c \equiv \frac{2qS(\gamma-\alpha)}{3(q-1)}\,.$$

We conclude that $\omega_c < S(\gamma - \alpha)$, so that $0 < U_0 < U_{0,\max}$, iff $q > 3$. Therefore, $g(U_0)$ has a unique maximum point on $0 < U_0 < U_{0,\max}$ iff $q > 3$. Alternatively, for $q \leq 3$ we have $dg/dU_0 < 0$ for $0 < U_0 < U_{0,\max}$.

Therefore, $\mathcal{D}_{0,c}$ is monotonically decreasing in U_0 when the patrol focus satisfies $q \leq 3$. For $q \leq 3$, increasing the level U_0 of police deployment leads to a larger range of $\mathcal{D}_0$ where the K-hotspot steady-state is unconditionally unstable. However, if $q > 3$, then initially as U_0 is increased from zero, the range of $\mathcal{D}_0$ where the steady-state hotspot pattern is unstable is decreased, until the critical value $U_{0,c} \equiv S(\gamma - \alpha) - \omega_c = S(\gamma - \alpha)(q-3)/[3(q-1)]$ is reached. For $U_0 > U_{0,c}$, the hotspot pattern becomes less stable when the policing level is increased. These qualitative results are displayed in Fig. 6.

Finally, we can interpret our competition stability threshold in terms of a critical threshold K_c for which a steady-state pattern of $K \geq 2$ hotspots is unconditionally unstable when $K > K_c$. This instability, which develops on an $\mathcal{O}(1)$ time scale as $\varepsilon \to 0$, is due to a real positive eigenvalue of the NLEP, and as we show from full numerical simulations in §5.2 and in §6.3 it triggers the collapse of some of the hotspots in the pattern. By writing (4.10) in terms of K, this critical threshold $K_c > 0$ when $D = \mathcal{D}_0/\epsilon^2$, and where $g(U_0)$ is defined in (4.10), is the unique root of

$$K\left[1 + \cos\left(\pi/K\right)\right]^{1/4} = \frac{(S/D)^{1/4}}{2^{3/4}\sqrt{\pi\epsilon\alpha}}\left[g(U_0)\right]^{1/4}\,. \tag{4.11}$$
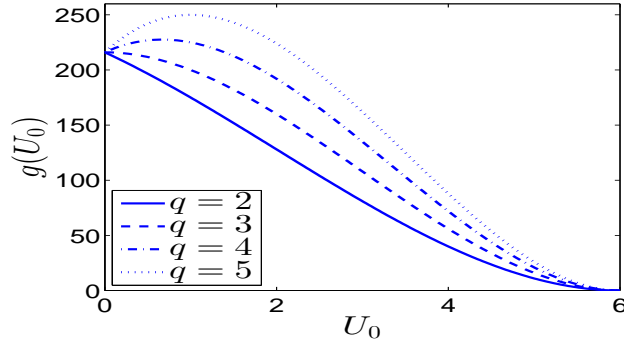

Figure 6: *Competition instability threshold nonlinearity $g(U_0)$, as defined in (4.10), versus total police deployment U_0 for patrol focus parameters $q = 2, 3, 4, 5$. Other model parameters are $S = 6$, $\gamma = 2$, $\alpha = 1$, so that $U_{0,\max} = 6$ as shown in the right-most tick of the figure. The competition instability threshold $\mathcal{D}_{0,c}$ is simply a positive scaling of $g(U_0)$ according to (4.10).*

5 Explicitly Solvable Case $q = 3$: Asynchronous Hotspot Oscillations

For each $j = 1, \ldots, K - 1$, we now analyze the quadratic equation (3.34) in the eigenvalue parameter λ characterizing the discrete spectrum of the NLEP (3.36) for the special case where $q = 3$. In terms of the coefficients of the quadratic (3.34a), for each $j = 1, \ldots, K$ the eigenvalues λ_1 and λ_2 satisfy

$$\lambda_1\lambda_2 = \frac{c_0}{c_2}\,, \qquad \lambda_1 + \lambda_2 = -\frac{c_1}{c_2}\,, \tag{5.1}$$

where c_0, c_1, and $c_2 > 0$, are given in (3.34b). For the j-th mode, we conclude that $\text{Re}(\lambda) < 0$ when $c_0 > 0$ and $c_1 > 0$. We have instability of the j-th mode if either $c_0 < 0$, or if $c_0 > 0$ and $c_1 < 0$. We have purely complex eigenvalues, corresponding to a Hopf bifurcation point, when $c_0 > 0$ and $c_1 = 0$.

We first determine the signs of c_0 and c_1 in terms of D_j and $\hat{\tau}_u$. From (3.34b) we observe that $c_0 = 0$ when the zero-eigenvalue crossing condition (4.6) holds, which yields (4.7) for D_j, which we relabel as

$$D_j = D_{\text{up}}^\star \equiv \frac{\omega^3}{4\pi^2 K^3 \alpha^2} \left(1 + \frac{3U_0}{\omega}\right) . \tag{5.2}$$

Next, we set $c_1 = 0$ in (3.34b) to get, using (3.29) for $\chi_{0,j}^{-1}$, that

$$\frac{\hat{\tau}_u}{D_j \kappa_3} = \frac{2\chi_{0,j}^{-1}}{3\left(2\chi_{0,j}^{-1} - 3\right)} = \frac{1}{3} \frac{(D_j + \alpha/\kappa_3)}{(D_j - \alpha/(2\kappa_3))} . \tag{5.3}$$

The denominator of this expression motivates introducing $D_{\text{low}}^\star$, defined by

$$D_{\text{low}}^\star \equiv \frac{\alpha}{2\kappa_3} = \frac{\omega^3}{4\pi^2 K^3 \alpha^2} , \tag{5.4}$$

where we have used the expression (3.28) for κ_3. Upon using (5.4) in (5.3), we obtain that $c_1 = 0$ when $\hat{\tau}_u$ satisfies

$$\hat{\tau}_u = \hat{\tau}_{uH,j} \equiv \mathcal{H}\left(D_j/D_{\text{low}}^\star\right) , \qquad j = 1, \dots, K - 1 , \tag{5.5a}$$

where the function $\mathcal{H}(\beta)$ is defined by

$$\mathcal{H}(\beta) \equiv \frac{\alpha\beta}{2} \left(\frac{1}{3} + \frac{1}{\beta - 1}\right) . \tag{5.5b}$$

Notice that $\hat{\tau}_{uH,j} > 0$ only when $D_j > D_{\text{low}}^\star$. Some simple algebra then shows that we can write c_1 in (3.34b) as

$$c_1 = \frac{1}{\alpha} \left(\frac{D_{\text{low}}^\star}{D_j} - 1\right) (\hat{\tau}_u - \hat{\tau}_{uH,j}) . \tag{5.6}$$

For the j-th mode, we have $c_1 < 0$ if $D_j > D_{\text{low}}^\star$ and $\hat{\tau}_u > \hat{\tau}_{uH,j}$, while $c_1 > 0$ if either $D_j < D_{\text{low}}^\star$, or $D_j > D_{\text{low}}^\star$ and $\hat{\tau}_u < \hat{\tau}_{uH,j}$. With these signs for c_0 and c_1, we summarize our stability result for the j-th mode so far as follows:

- For $D_j > D_{\text{up}}^\star$ ($c_0 < 0$), we have $\text{Re}(\lambda) > 0$, and instability is due to a positive real eigenvalue.

- For $D_j < D_{\text{low}}^\star$ ($c_0 > 0$ and $c_1 > 0$), we have stability $\text{Re}(\lambda) < 0$.

- On the range $D_{\text{low}}^\star < D_j < D_{\text{up}}^\star$ ($c_0 > 0$), we have instability if $\hat{\tau}_u > \hat{\tau}_{uH,j}$ ($c_1 < 0$) and stability if $\hat{\tau}_u < \hat{\tau}_{uH,j}$ ($c_1 > 0$). On this range of D_j, the Hopf bifurcation threshold, $\hat{\tau}_{uH,j} > 0$, is given in (5.5).

Next, we must reformulate this result in terms of $\mathcal{D}_0$ rather than D_j, by using $D_j = \mathcal{D}_0 \left(2K/S\right) \left(1 - \cos\left(\pi j/K\right)\right)$. The interval $D_{\text{low}}^\star < D_1 < D_{\text{up}}^\star$, where a Hopf bifurcation value of $\hat{\tau}_u$ exists, becomes

$$\frac{S D_{\text{low}}^\star}{2K\left(1 - \cos\left(\pi j/K\right)\right)} \leq \mathcal{D}_0 \leq \frac{S D_{\text{up}}^\star}{2K\left(1 - \cos\left(\pi j/K\right)\right)} , \tag{5.7}$$

where $D_{\text{up}}^\star/D_{\text{low}}^\star = 1 + 3U_0/\omega$ from (5.2) and (5.4). It is convenient to write (5.7) in terms of the competition stability threshold $\mathcal{D}_{0,c}$ defined by setting $q = 3$ in (4.9). In this way, the interval in (5.7) becomes

$$D_{0,j}^- < \mathcal{D}_0 < D_{0,j}^+ ; \qquad D_{0,j}^+ \equiv \mathcal{D}_{0,c} \left(\frac{1 + \cos\left(\pi/K\right)}{1 - \cos\left(\pi j/K\right)}\right) , \qquad D_{0,j}^- \equiv \frac{\mathcal{D}_{0,c}}{(1 + 3U_0/\omega)} \left(\frac{1 + \cos\left(\pi/K\right)}{1 - \cos\left(\pi j/K\right)}\right) , \tag{5.8a}$$

20

where $\mathcal{D}_{0,c}$ is given by

$$\mathcal{D}_{0,c} \equiv \frac{\omega^3 S}{8\pi^2 \alpha^2 K^4 \left(1 + \cos\left(\pi/K\right)\right)} \left(1 + \frac{3U_0}{\omega}\right). \tag{5.8b}$$

We observe that when $j = K - 1$, we have $D_{0,K-1}^+ = \mathcal{D}_{0,c}$. Now since $D_j/D_{\text{low}}^\star = \mathcal{D}_0/D_{0,j}^-$, the Hopf bifurcation threshold in (5.5) becomes

$$\hat{\tau}_{uH,j} = \mathcal{H}\left(\mathcal{D}_0/D_{0,j}^-\right), \qquad \text{on} \quad D_{0,j}^- < \mathcal{D}_0 < D_{0,j}^+. \tag{5.9}$$

From this expression, we readily derive the following limiting behavior for $\hat{\tau}_{uH,j}$ at the two ends of the interval:

$$\hat{\tau}_{uH,j} \sim \frac{\alpha}{2} \left[\frac{\mathcal{D}_0}{D_{0,j}^-} - 1\right]^{-1}, \quad \text{as} \quad \mathcal{D}_0 \to D_{0,j}^-; \qquad \hat{\tau}_{uH_j} \sim \frac{\omega\alpha}{6U_0}\left(\frac{U_0}{\omega} + 1\right)\left(\frac{3U_0}{\omega} + 1\right), \quad \text{as} \quad \mathcal{D}_0 \to D_{0,j}^+. \tag{5.10}$$

For each fixed $j = 1, \ldots, K - 1$, we summarize the behavior of the roots of the quadratic (3.34), corresponding to the discrete eigenvalues of the NLEP (3.36) as follows:

Proposition 5.1 *For each fixed $j = 1, \ldots, K - 1$, let λ_+ and λ_-, with $\text{Re}(\lambda_+) \geq \text{Re}(\lambda_-)$, denote the two solutions of the quadratic equation (3.34). Then, their location in the complex plane depends on $\mathcal{D}_0$ and $\hat{\tau}_u$ as follows:*

- *For $\mathcal{D}_0 > D_{0,j}^+$, we have $\lambda_+ > 0$ and $\lambda_- < 0$ for all $\hat{\tau}_u \geq 0$.*

- *For $\mathcal{D}_0 < D_{0,j}^-$, we have $\text{Re}(\lambda_\pm) < 0$ for all $\hat{\tau}_u \geq 0$.*

- *For $D_{0,j}^- < \mathcal{D}_0 < D_{0,j}^+$ we have $\text{Re}(\lambda_\pm) > 0$ when $\hat{\tau}_u > \hat{\tau}_{uH,j}$ and $\text{Re}(\lambda_\pm) < 0$ when $0 \leq \hat{\tau}_{uH,j} < \hat{\tau}_u$.*

Here $D_{0,j}^-$ and $D_{0,j}^+$ are defined in (5.8a). The Hopf bifurcation threshold $\hat{\tau}_{uH,j}$, which is defined on the interval $D_{0,j}^- < \mathcal{D}_0 < D_{0,j}^+$, is given in (5.9).

Since $D_{0,j}^+/D_{0,j}^- = 1 + 3U_0/\omega$, we observe that the width of the interval $D_{0,j}^- < \mathcal{D}_0 < D_{0,j}^+$ where an asynchronous oscillatory instability in the hotspot amplitudes occurs is nonzero only as a result of the simple coupling term $-U$ in our three-component RD system (1.1). In the absence of police, this interval disappears and the basic crime model does not support oscillatory instabilities in this parameter regime.

Next, we examine the monotonicity properties of the universal function $\mathcal{H}(\beta)$ characterizing Hopf bifurcations, as defined in (5.5b), on the interval $1 < \beta < D_{0,j}^+/D_{0,j}^- = 1 + 3U_0/\omega$. We calculate $\mathcal{H}'(\beta)$ to get

$$\mathcal{H}'(\beta) = \frac{\alpha}{6(\beta - 1)^2} \left[(\beta - 1)^2 - 3\right],$$

so that $\mathcal{H}'(\beta) < 0$ if $1 < \beta < 1 + \sqrt{3}$ and $\mathcal{H}'(\beta) > 0$ if $\beta > 1 + \sqrt{3}$. We conclude that $\mathcal{H}'(\beta) < 0$ on $1 < \beta < 1 + 3U_0/\omega$ only when $\omega > \sqrt{3}U_0$. Since $\omega = S(\gamma - \alpha) - U_0$ we conclude that

$$\mathcal{H}'(\beta) < 0 \quad \text{on} \quad 1 < \beta < 3U_0/\omega, \quad \text{iff} \quad U_0 < \frac{S(\gamma - \alpha)}{1 + \sqrt{3}}. \tag{5.11}$$

If $\frac{S(\gamma - \alpha)}{1 + \sqrt{3}} < U_0 < U_{0,\text{max}}$, then $\mathcal{H}(\beta)$ increases on $1 + \sqrt{3} < \beta < 1 + 3U_0/\omega$.

Next, we rewrite the coefficients c_0, c_1, and c_2, in the quadratic (3.34) so as to readily calculate the Hopf bifurcation eigenvalue $\lambda = i\lambda_{IH}$. After some algebra we obtain that

$$c_0 = -\frac{1}{2}\left(1 + \frac{3U_0}{\omega}\right)\left(\frac{\mathcal{D}_0}{D_{0,j}^+} - 1\right), \qquad c_1 = \frac{\hat{\tau}_{uH,j}}{\alpha}\left(\frac{D_{0,j}^-}{\mathcal{D}_0} - 1\right)\left(\frac{\hat{\tau}_u}{\hat{\tau}_{uH,j}} - 1\right), \qquad c_2 = \frac{\hat{\tau}_{uH,j}}{3\alpha}\left(\frac{2D_{0,j}^-}{\mathcal{D}_0} + 1\right), \tag{5.12}$$

where $\hat{\tau}_{uH,j}$ is defined in (5.9). The Hopf bifurcation eigenvalue $\lambda = i\lambda_{IH}$ with $\lambda_{IH} > 0$ is $\lambda_{IH} = \sqrt{c_0/c_2}$, which yields

$$\lambda_{IH} = \frac{3}{\left(2 + \mathcal{D}_0/D_{0,j}^-\right)}\sqrt{\left(1 + \frac{3U_0}{\omega}\right)\left(1 - \frac{\mathcal{D}_0}{D_{0,j}^+}\right)\left(\frac{\mathcal{D}_0}{D_{0,j}^-} - 1\right)}, \quad \text{on} \quad D_{0,j}^- < \mathcal{D}_0 < D_{0,j}^+. \tag{5.13}$$

This shows that λ_{IH} vanishes at both endpoints. We use the asymptotic behaviors $\mathcal{D}_0/D_{0,j}^+ \to (1 + 3U_0/\omega)^{-1}$ as $\mathcal{D}_0 \to D_{0,j}^-$ and $\mathcal{D}_0/D_{0,j}^- \to (1 + 3U_0/\omega)$ as $\mathcal{D}_0 \to D_{0,j}^+$, so that from (5.13) we obtain the limiting asymptotic behavior

$$\lambda_{IH} \sim \frac{1}{(1 + U_0/\omega)}\sqrt{\frac{3U_0}{\omega}\left(1 + \frac{3U_0}{\omega}\right)\left(1 - \frac{\mathcal{D}_0}{D_{0,j}^+}\right)} \quad \text{as} \quad \mathcal{D}_0 \to D_{0,j}^+; \qquad \lambda_{IH} \sim \sqrt{\frac{3U_0}{\omega}\left(\frac{\mathcal{D}_0}{D_{0,j}^-} - 1\right)} \quad \text{as} \quad \mathcal{D}_0 \to D_{0,j}^-. \tag{5.14}$$

For the special case $K = 2$, we now state our main result stability result related to Hopf bifurcations.

Proposition 5.2 *For $\epsilon \to 0$, $q = 3$, $0 < U_0 < U_{0,\max}$, $\hat{\tau}_u \ll \mathcal{O}(\epsilon^{-2})$, and $\mathcal{D}_0 = \epsilon^2 D = \mathcal{O}(1)$, the linear stability properties of a two-hotspot steady-state solution of (1.4) are as follows:*

- *For $\mathcal{D}_0 > D_{0,1}^+ \equiv \mathcal{D}_{0,c}$, the NLEP (3.36) has a positive real eigenvalue for all $\hat{\tau}_u \geq 0$ and so the two-hotspot steady-state is unstable. Here $\mathcal{D}_{0,c} = S\omega^3\left(1 + 3U_0/\omega\right)/[128\pi^2\alpha^2]$ is the competition stability threshold with $\omega \equiv S(\gamma - \alpha) - U_0$.*

- *On the range $D_{0,1}^- \equiv \mathcal{D}_{0,c}/\left(1 + 3U_0/\omega\right) < \mathcal{D}_0 < \mathcal{D}_{0,c}$, there is a Hopf bifurcation corresponding to an asynchronous oscillatory instability of the hotspot amplitudes when*

$$\hat{\tau}_u \equiv \hat{\tau}_{uH,1} = \mathcal{H}\left(\mathcal{D}_0/D_{0,1}^-\right), \quad \text{on} \quad D_{0,1}^- < \mathcal{D}_0 < \mathcal{D}_{0,c}, \tag{5.15}$$

  where $\mathcal{H}(\beta)$ is defined in (5.5b). When $\hat{\tau}_u > \hat{\tau}_{uH,1}$, the two-hotspot steady-state is unstable, while if $\hat{\tau}_u < \hat{\tau}_{uH,1}$ the two-hotspot pattern is linearly stable.

- *On the range $0 < \mathcal{D}_0 < D_{0,1}^- \equiv \mathcal{D}_{0,c}/\left(1 + 3U_0/\omega\right)$, the two-hotspot steady-state is linearly stable for all $\hat{\tau}_u \geq 0$.*

In terms of a scaled police diffusivity defined by $\epsilon^2 D_p \equiv \mathcal{D}_0/\hat{\tau}_u$, Proposition 5.2 implies the following:
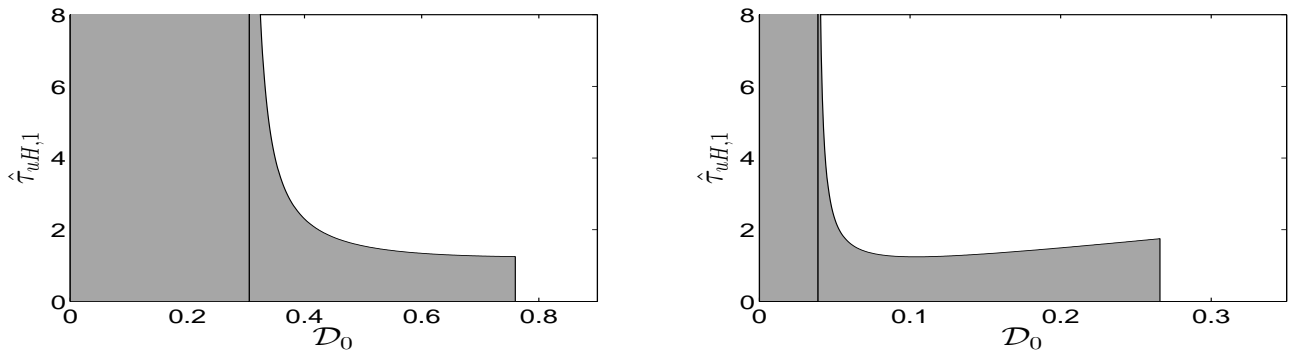

Figure 7: *The Hopf bifurcation threshold $\hat{\tau}_{uH_1}$ versus $\mathcal{D}_0$ on the range $\mathcal{D}_{0,c}/(1 + 3U_0/\omega) < \mathcal{D}_0 < \mathcal{D}_{0c}$ for $K = 2$, $q = 3$, $S = 6$, $\gamma = 2$, $\alpha = 1$, for $U_0 = 2$ (left panel) and $U_0 = 4$ (right panel). The two-hotspot pattern is linearly stable in the shaded region. The thin vertical line in each figure is the lower boundary $\mathcal{D}_{0,c}/(1 + 3U_0/\omega)$, while the right edge of the shaded region is the competition stability threshold. The Hopf bifurcation curve in the right panel is not monotonic since $U_0 > S(\gamma - \alpha)/(1 + \sqrt{3})$ when $U_0 = 4$.*

Corollary 5.3 *Under the conditions of Proposition 5.2 we have the following:*

- For $\mathcal{D}_0 > \mathcal{D}_{0,c} \equiv S\omega^3 \left(1 + 3U_0/\omega\right)/[128\pi^2\alpha^2]$, the two-hotspot steady-state is unstable for all scaled police diffusivities $\epsilon^2 D_p > 0$.

- On the range $\mathcal{D}_{0,c}/\left(1 + 3U_0/\omega\right) < \mathcal{D}_0 < \mathcal{D}_{0,c}$, the two hotspot steady-state is unstable to an asynchronous oscillatory instability of the hotspot amplitudes if $\epsilon^2 D_p < \mathcal{D}_0/\hat{\tau}_{uH,1}$, while the steady-state is linearly stable when $\epsilon^2 D_p > \mathcal{D}_0/\hat{\tau}_{uH,1}$. Here $\hat{\tau}_{uH,1}$ is the Hopf bifurcation threshold in (5.15).

- On the range $0 < \mathcal{D}_0 < \mathcal{D}_{0,c}/\left(1 + 3U_0/\omega\right)$, the two-hotspot steady-state is linearly stable for all $\epsilon^2 D_p \geq 0$.

We now illustrate our main stability results for $K = 2$, $S = 6$, $\gamma = 2$, and $\alpha = 1$. In Fig. 7 we plot the region of linear stability in the $\hat{\tau}_u$ versus $\mathcal{D}_0$ parameter plane for $U_0 = 2$ (left panel) and $U_0 = 4$ (right panel). For $U_0 = 4$, we have $\omega < \sqrt{3}U_0$, and so the Hopf bifurcation threshold $\hat{\tau}_{uH,1}$ is not monotone in $\mathcal{D}_0$, as seen in the right panel of Fig. 7. From this figure, we observe that as U_0 increases the region where the two-hotspot steady-state is linearly stable is smaller, as expected. With regards to the scaled police diffusivity $\epsilon^2 D_p \equiv \mathcal{D}_0/\hat{\tau}_u$, in the right panels of Fig. 1 and Fig. 8 we plot the corresponding region of linear stability in the $\epsilon^2 D_p$ versus $\mathcal{D}_0$ plane for $U_0 = 2$ and $U_0 = 4$, respectively. For $U_0 = 2$ and $U_0 = 4$, the corresponding steady-state two-hotspot solution is shown in the left panels of Fig. 1 and Fig. 8. For $U_0 = 2$, the predicted linear stability results were validated in Fig. 2 by performing full numerical solutions of the PDE system (1.4).
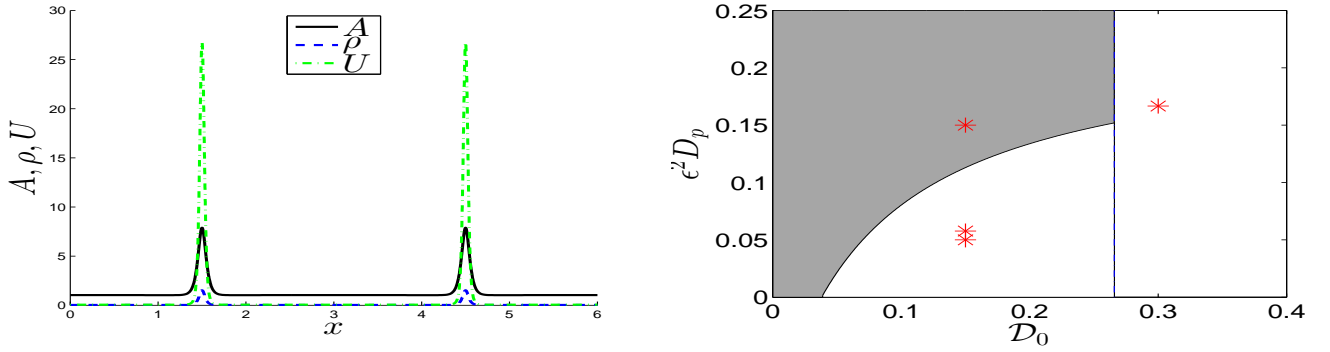

Figure 8: Left panel: the steady-state two-hotspot solution for $S = 6$, $\gamma = 2$, $\alpha = 1$, $U_0 = 4$, $\mathcal{D}_0 = 0.15$, $\epsilon = 0.035$, and $q = 3$. Right panel: Plot of the Hopf bifurcation threshold for the scaled police diffusivity $\epsilon^2 D_p \equiv \mathcal{D}_0/\hat{\tau}_{uH_1}$ versus $\mathcal{D}_0$ on the range $\mathcal{D}_{0,c}/(1 + 3U_0/\omega) < \mathcal{D}_0 < \mathcal{D}_{0c}$. The thin vertical line is the competition stability threshold $\mathcal{D}_{0,c}$ given in Proposition 5.2. The shaded region is where the steady-state two-hotspot pattern is linearly stable. For $\mathcal{D}_0 > \mathcal{D}_{0c}$ the hotspot solution is unstable due to a competition instability, whereas in the small unshaded region for $\mathcal{D}_0 < \mathcal{D}_{0c}$, the hotspot steady-state is unstable to an asynchronous oscillatory instability of the hotspot amplitudes. The full PDE simulations in Fig. 14 and in Fig. 15 are done at the marked points.

5.1 The Stability Phase Diagram for $q = 3$: $K \geq 3$ Hotspots

Next, we determine the parameter range of $\mathcal{D}_0$ and $\hat{\tau}_u$ for which a K-hotspot steady-state solution, with $K \geq 3$, is linearly stable. To do so, we need to guarantee that $\text{Re}(\lambda) < 0$ for each of the quadratics in (3.34), i.e. for each $j = 1, \ldots, K - 1$. In this way, we will ensure that any discrete eigenvalue of the NLEP (3.36) satisfies $\text{Re}(\lambda) \leq 0$.

By using (5.8a), we readily obtain the ordering principle that

$$D_{0,j+1}^{\pm} < D_{0,j}^{\pm}, \quad \text{and} \quad D_{0,j}^{-} < D_{0,j}^{+}, \qquad \text{for} \quad j = 1, \ldots, K - 2. \tag{5.16}$$

We conclude that

$$D_{0,K-1}^{+} = \min_{j=1,\ldots,K-1}\{D_{0,j}^{+}\}, \qquad D_{0,K-1}^{-} = \min_{j=1,\ldots,K-1}\{D_{0,j}^{-}\}. \tag{5.17}$$

23

From Proposition 5.1, we conclude for each of the quadratics (3.34), i.e. for each $j = 1, \ldots, K - 1$, that $\text{Re}(\lambda) < 0$ for any $\hat{\tau}_u \geq 0$ when $\mathcal{D}_0 < D_{0,K-1}^-$. Therefore, a K-hotspot steady-state pattern is linearly stable for all $\hat{\tau}_u \geq 0$ on the range $0 < \mathcal{D}_0 < D_{0,K-1}^-$. For the range $\mathcal{D}_0 > D_{0,K-1}^-$, we conclude from Proposition 5.1 that the $K-1$ mode must be unstable due to a positive real eigenvalue for any $\hat{\tau}_u \geq 0$. Therefore, for $\mathcal{D}_0 > D_{0,K-1}^+$, a K-hotspot steady-state solution is unstable for all $\hat{\tau}_u \geq 0$. Additional unstable eigenvalues due to Hopf bifurcations associated with the remaining modes $j = 1, \ldots, K - 2$ are possible depending on the value of $\hat{\tau}_u$.

To complete the stability phase diagram in the $\hat{\tau}_u$ versus $\mathcal{D}_0$ parameter plane, we need only focus on the interval $D_{0,K-1}^- < \mathcal{D}_0 < D_{0,K-1}^+$ where the sign-alternating $K - 1$ mode undergoes a Hopf bifurcation at $\hat{\tau}_u = \hat{\tau}_{uH,K-1}$, given from (5.9) by

$$\hat{\tau}_{uH,K-1} \equiv \mathcal{H}(\beta), \qquad \text{on} \quad 1 \leq \beta \leq \frac{D_{0,K-1}^+}{D_{0,K-1}^-} = 1 + \frac{3U_0}{\omega}, \qquad \text{where} \quad \beta \equiv \frac{\mathcal{D}_0}{D_{0,K-1}^-}. \tag{5.18}$$

Here $\mathcal{H}(\beta)$ is defined in (5.5b). The $K - 1$ mode is linearly stable if and only if $\hat{\tau}_u < \hat{\tau}_{uH,K-1}$.

We now seek to determine conditions for which the Hopf bifurcation threshold for the $K - 1$ mode is smaller than any of the other $K - 2$ possible Hopf bifurcation values $\hat{\tau}_{uH,j}$ for $j = 1, \ldots, K - 2$ when restricted to the interval $D_{0,K-1}^- < \mathcal{D}_0 < D_{0,K-1}^+$. From (5.9), these other Hopf bifurcation thresholds, for $j = 1, \ldots, K - 2$, can be written in terms of β, as defined in (5.18), by

$$\hat{\tau}_{uH,j} = \mathcal{H}(\xi_j \beta), \qquad \text{on} \quad \frac{1}{\xi_j} \leq \beta \leq \frac{1}{\xi_j}\left(1 + \frac{3U_0}{\omega}\right), \tag{5.19a}$$

where, from (5.8), we define

$$\xi_j \equiv \frac{D_{0,K-1}^-}{D_{0,j}^-} = \frac{1 - \cos(\pi j/K)}{1 + \cos(\pi/K)}, \qquad j = 1, \ldots, K - 2. \tag{5.19b}$$

We observe from (5.19b) that the following ordering principle holds:

$$\xi_j < \xi_{j+1} < 1, \qquad j = 1, \ldots, K - 3, \qquad \xi_{K-2} = \max_{j=1,\ldots,K-2}\{\xi_j\}. \tag{5.19c}$$

Comparing the intervals in (5.19a) and (5.18), we want to determine a specific parameter range of the total police deployment U_0 for which, for any $j = 1, \ldots, K - 2$, we have that $\hat{\tau}_{uH,K-1} < \hat{\tau}_{uH,j}$ on the overlap domain $\xi_j^{-1} \leq \beta \leq 1 + 3U_0/\omega$. If the overlap domain is the null-set for the j-th mode, i.e. if $\xi_j < 1/(1 + 3U_0/\omega)$, then we can simply ignore the j-th mode on $D_{0,K-1}^- < \mathcal{D}_0 < D_{0,K-1}^+$. As such, we need only consider values of j (if any) for which $\xi_j^{-1} < 1 + 3U_0/\omega$, so that an overlap domain exists. Since $\mathcal{H}(\beta)$ is monotone decreasing on $1 < \beta < 1 + \sqrt{3}$, we readily obtain that $\mathcal{H}(\beta) - \mathcal{H}(\xi_j \beta) \equiv \int_{\xi_j \beta}^{\beta} \mathcal{H}'(y)\, dy < 0$ on the interval $\xi_j^{-1} < \beta < 1 + \sqrt{3}$. In this way, we conclude that

$$\mathcal{H}(\xi_j \beta) < \mathcal{H}(\beta), \qquad \text{on} \quad \xi_j^{-1} \leq \beta \leq 1 + \frac{3U_0}{\omega}, \qquad \text{when} \quad \omega > \sqrt{3}U_0. \tag{5.20}$$

Therefore, on the range for which $\mathcal{H}(\beta)$ is monotonically decreasing, it follows that the Hopf bifurcation threshold of $\hat{\tau}_u$ for any mode $j = 1, \ldots, K - 2$ cannot be smaller than that for the $K - 1$ mode. Although the monotonicity of $\mathcal{H}(\beta)$ on $\xi_j^{-1} \leq \beta \leq 1 + 3U_0/\omega$ for $\omega > \sqrt{3}U_0$ provides a sufficient condition for the ordering principle $\hat{\tau}_{uH,K-1} < \hat{\tau}_{uH,j}$ for $j = 1, \ldots, K - 2$ to hold, we now show explicitly that the monotonicity of $\mathcal{H}(\beta)$ is not strictly necessary.

We now determine a precise condition that ensures that $\hat{\tau}_{uH,K-1} < \hat{\tau}_{uH,K-2}$ on an assumed overlap domain $\xi_{K-2}^{-1} \leq \beta \leq 1 + 3U_0/\omega$. Owing to the ordering principle $\xi_j < \xi_{j+1}$ for $j = 1, \ldots, K - 3$ from (5.19c), the first Hopf threshold to potentially decrease below that of the $K - 1$ mode must be the $K - 2$ mode, and so we focus only on a comparison with

the $K-2$ mode. From (5.18) and (5.19a), and by using the explicit expression for $\mathcal{H}(\beta)$ in (5.5b), we calculate after some algebra that $\mathcal{H}(\xi_{K-2}\beta) \geq \mathcal{H}(\beta)$ on $\xi_{K-2}^{-1} \leq \beta \leq 1 + 3U_0/\omega$, if and only if

$$\mathcal{K}(\beta) \equiv (\xi_{K-2}\beta - 1)(\beta - 1) < 3, \qquad \text{on} \quad 1 < \xi_{K-2}^{-1} \leq \beta \leq 1 + 3U_0/\omega. \tag{5.21}$$

Since $\mathcal{K}'(\beta) > 0$ on this interval, this inequality holds if and only if $1 + 3U_0/\omega < \beta_{\max}$, where $\mathcal{K}(\beta_{\max}) = 3$. By setting $\mathcal{K}(\beta) = 3$, and solving the quadratic for $\beta = \beta_{\max}$, we obtain that (5.21) holds if and only if

$$\frac{\sqrt{3}U_0}{\omega} < \mathcal{Z}(\xi_{K-2}), \qquad \text{where} \quad \mathcal{Z}(\xi_{K-2}) \equiv \frac{1}{\sqrt{3}}\left(-\frac{1}{2} + \frac{1}{2\xi_{K-2}}\left[1 + \sqrt{\xi_{K-2}^2 + 10\xi_{K-2} + 1}\right]\right). \tag{5.22}$$

Here $\omega = S(\gamma - \alpha) - U_0$ and ξ_{K-2} can be found from (5.19b). On $0 < \xi < 1$, we have that $\mathcal{Z}(\xi)$ satisfies

$$\mathcal{Z}(\xi) \to +\infty \quad \text{as} \quad \xi \to 0^+, \qquad \mathcal{Z}(1) = 1, \qquad \mathcal{Z}'(\xi) < 0, \quad \text{on} \quad 0 < \xi < 1. \tag{5.23}$$

It follows that $\mathcal{Z}(\xi) > 1$ on $0 < \xi < 1$. The key inequality (5.22) implies that $\omega > \sqrt{3}U_0/\mathcal{Z}(\xi_{K-2})$, which yields a larger range of ω than the range $\omega > \sqrt{3}U_0$ where $\mathcal{H}(\beta)$ is monotonic. This inequality (5.22) can also be used to give a precise upper bound on U_0 for which the $K-1$ mode determines the Hopf bifurcation threshold for $\hat{\tau}_u$ on the entire range $D_{0,K-1}^- < \mathcal{D}_0 < D_{0,K-1}^+$. In this way, for $K \geq 3$, we summarize our main stability result for a K-hotspot steady-state solution as follows:

Proposition 5.4 *For $\epsilon \to 0$, $q = 3$, $K \geq 3$, $0 < U_0 < U_{0,\max}$, $\hat{\tau}_u \ll \mathcal{O}(\epsilon^{-2})$, and $\mathcal{D}_0 = \epsilon^2 D = \mathcal{O}(1)$, the linear stability properties of a K-hotspot steady-state solution of (1.4) are as follows:*

- *For $\mathcal{D}_0 > D_{0,K-1}^+ \equiv \mathcal{D}_{0,c}$, the NLEP (3.36) has at least one positive real eigenvalue for all $\hat{\tau}_u \geq 0$. Additional unstable eigenvalues as a result of Hopf bifurcations associated with the other modes $j = 1, \ldots, K-2$ are possible depending on the value of $\hat{\tau}_u$. Here $\mathcal{D}_{0,c}$ is the competition stability threshold given in (4.9) with $q = 3$.*

- *On the range $D_{0,K-1}^- \equiv \mathcal{D}_{0,c}/(1 + 3U_0/\omega) < \mathcal{D}_0 < \mathcal{D}_{0,c}$, and when U_0 satisfies*

$$U_0 < U_{0,swit} \equiv \left(\frac{\mathcal{Z}(\xi_{K-2})}{\sqrt{3} + \mathcal{Z}(\xi_{K-2})}\right) S(\gamma - \alpha), \qquad \text{where} \quad \xi_{K-2} \equiv \frac{1 - \cos(\pi(K-2)/K)}{1 + \cos(\pi/K)}, \tag{5.24}$$

  and where $\mathcal{Z}(\xi)$ is defined in (5.22), the $K-1$ sign-alternating mode sets the stability threshold on the entire range. For $\hat{\tau}_u > \hat{\tau}_{uH,K-1}$, the K-hotspot pattern is unstable, while if $\hat{\tau}_u < \hat{\tau}_{uH,K-1}$ the K-hotspot pattern is linearly stable. With $\mathcal{H}(\beta)$, as defined in (5.5b), the minimal Hopf bifurcation value of $\hat{\tau}_u$ is

$$\hat{\tau}_{uH,K-1} \equiv \mathcal{H}\left(\mathcal{D}_0/D_{0,K-1}^-\right), \qquad \text{on} \quad D_{0,K-1}^- \equiv \frac{\mathcal{D}_{0c}}{1 + 3U_0/\omega} < \mathcal{D}_0 < \mathcal{D}_{0,c}, \tag{5.25}$$

  where

- *On the range $0 < \mathcal{D}_0 < D_{0,K-1}^- \equiv \mathcal{D}_{0,c}/(1 + 3U_0/\omega)$, the K-hotspot steady-state is linearly stable for all $\hat{\tau}_u \geq 0$.*

In terms of a scaled police diffusivity defined by $\epsilon^2 D_p \equiv \mathcal{D}_0/\hat{\tau}_u$, Proposition 5.4 implies the following:

Corollary 5.5 *Under the conditions of Proposition 5.4, we have the following:*

- *For $\mathcal{D}_0 > \mathcal{D}_{0,c}$, the K-hotspot steady-state is unstable for all scaled police diffusivities $\epsilon^2 D_p > 0$. Here $\mathcal{D}_{0,c}$ is defined in (4.9) with $q = 3$.*

25

- *On the range $\mathcal{D}_{0,c}/\left(1 + 3U_0/\omega\right) < \mathcal{D}_0 < \mathcal{D}_{0,c}$, and when $U_0 < U_{0,swit}$, as defined in (5.24), the K-hotspot steady-state is unstable to a sign-alternating asynchronous oscillatory instability of the hotspot amplitudes if $\epsilon^2 D_p < \mathcal{D}_0/\hat{\tau}_{uH,K-1}$ where $\hat{\tau}_{uH,K-1}$ is defined in (5.25). Alternatively, this steady-state is linearly stable when $\epsilon^2 D_p > \mathcal{D}_0/\hat{\tau}_{uH,K-1}$.*

- *On the range $0 < \mathcal{D}_0 < \mathcal{D}_{0,c}/\left(1 + 3U_0/\omega\right)$, the K-hotspot steady-state is linearly stable for all $\epsilon^2 D_p \geq 0$.*

We remark that the upper bound $U_{0,\text{swit}}$ in (5.24) can be calculated explicitly when $K = 3$ and $K = 4$. When $K = 3$, we calculate $\xi_1 = 1/3$ and $\mathcal{Z}(\xi_1) = \left(1 + \sqrt{10}\right)/\sqrt{3}$. We then obtain from (5.24) that the sign-alternating $K - 1$ mode sets the Hopf bifurcation threshold when

$$U_0 < U_{0,\text{swit}} \equiv \frac{3S(\gamma - \alpha)}{2 + \sqrt{10}} \approx (0.58114)S(\gamma - \alpha), \qquad \text{for} \quad K = 3. \tag{5.26}$$

Similarly, for $K = 4$, we calculate $\xi_2 = 2 - \sqrt{2}$, and

$$\mathcal{Z}(\xi_2) = \frac{1}{\sqrt{3}}\left[\frac{\sqrt{2}}{4} + \left(\frac{1}{2} + \frac{\sqrt{2}}{4}\right)\sqrt{27 - 14\sqrt{2}}\right] \approx 1.5265.$$

From (5.24), the $K - 1$ mode sets the Hopf bifurcation threshold when

$$U_0 < U_{0,\text{swit}} \approx (0.46847)S(\gamma - \alpha), \qquad \text{for} \quad K = 4. \tag{5.27}$$
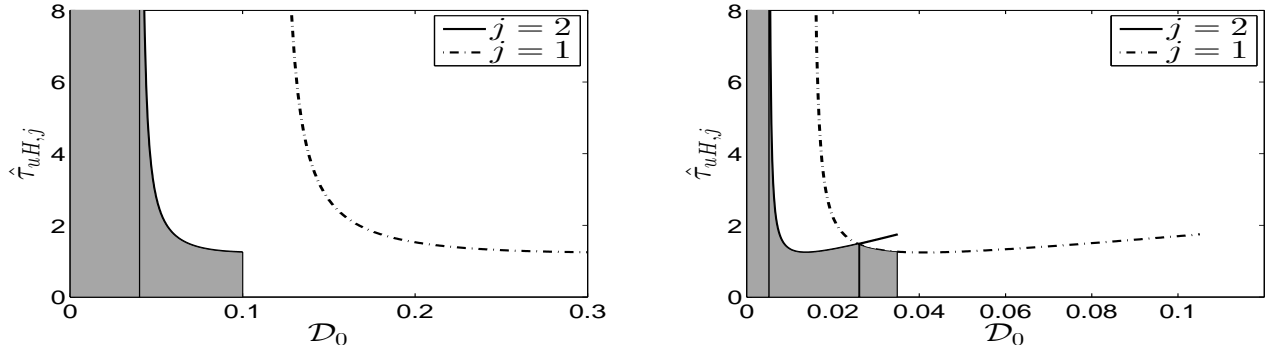
Figure 9: *Linear stability (shaded) region in the $\hat{\tau}_u$ versus $\mathcal{D}_0$ plane for $K = 3$ when $S = 6$, $\gamma = 2$, and $\alpha = 1$, and for $U_0 = 2$ (left panel) and $U_0 = 4$ (right panel), as characterized by Proposition 5.4. To the left of the thin vertical line the steady-state is unconditionally stable. The solid and dot-dashed curves are the Hopf bifurcation boundaries for the (sign-alternating) $j = 2$ mode and the $j = 1$ mode, respectively. For $U_0 = 2$ (left panel) the Hopf boundary is determined by the $j = 2$ mode. For $U_0 = 4 > U_{0,swit} \approx 3.478$ (right panel) the Hopf boundary consists of both the $j = 2$ and $j = 1$ mode. The three-hotspot steady-state is unstable to an oscillatory instability above the solid or dotted curves. At the ends of the Hopf bifurcation curves the Hopf eigenvalue tends to zero.*

We now illustrate our main stability results in Proposition 5.4 and Corollary 5.5 for $S = 6$, $\gamma = 2$, and $\alpha = 1$. We take $K = 3$ or $K = 4$, and either $U_0 = 2$ and $U_0 = 4$. For these parameters, (5.26) and (5.27) yield that $U_{0,\text{swit}} \approx 3.487$ for $K = 3$ and $U_{0,\text{swit}} \approx 2.811$ for $K = 4$. Therefore, for both $K = 3$ and $K = 4$ it is only for the smaller value $U_0 = 2$ that the sign-alternating mode sets the Hopf bifurcation threshold.

For $K = 3$, the shaded region in Fig. 9 is the theoretically predicted region of linear stability in the $\hat{\tau}_u$ versus $\mathcal{D}_0$ parameter plane for $U_0 = 2$ (left panel) and for $U_0 = 4$ (right panel). In this figure the dotted curve and solid curves are the Hopf bifurcation thresholds for the $j = 1$ mode and the sign-alternating $j = 2$ mode. When $U_0 = 2$ (left panel), the sign-alternating mode sets the boundary of the region of stability, whereas for $U_0 = 4$ (right panel) both the $j = 1$ and
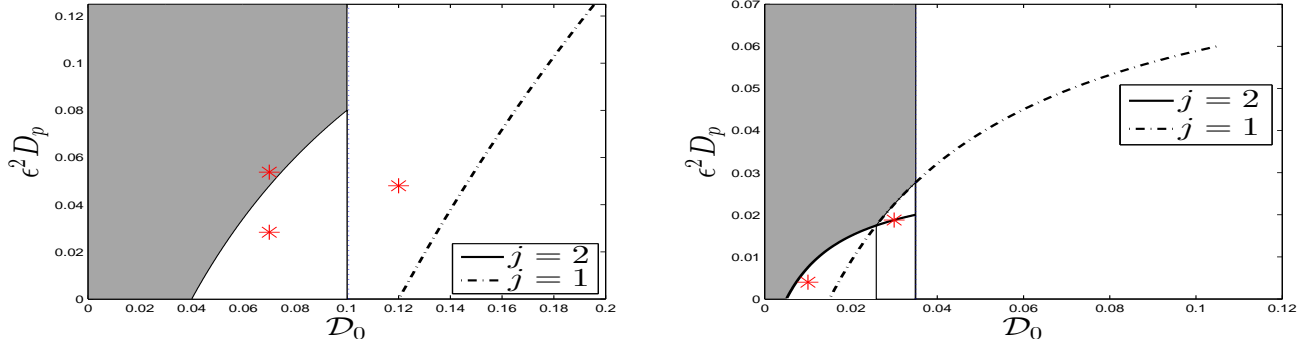
Figure 10: *Same plot as Fig. 9 except in the scaled police diffusivity $\epsilon^2 D_p = \mathcal{D}_0/\hat\tau_u$ versus $\mathcal{D}_0$ plane for $K = 3$, $S = 6$, $\gamma = 2$, and $\alpha = 1$, with $U_0 = 2$ (left panel) and $U_0 = 4$ (right panel) (see Corollary 5.5). The three-hotspot steady-state is linearly stable in the shaded region. This steady-state undergoes an oscillatory instability below the solid or dot-dashed curves. In the left panel the thin vertical line is the competition threshold $\mathcal{D}_{0,c}$. The additional thin vertical line in the right panel is where the Hopf boundary switches from $j = 2$ to $j = 1$. This switch occurs since $U_0 = 4 > U_{0,swit} \approx 3.478$ (see (5.26) and the second statement of Corollary 5.5). The full PDE simulations in Fig. 16 and in Fig. 17 are done at the marked points in the left and right panels, respectively.*

$j = 2$ Hopf bifurcation thresholds form the boundary of the region of stability. The corresponding region of stability in the scaled police diffusivity $\epsilon^2 D_p$ versus $\mathcal{D}_0$ parameter plane is shown in Fig. 10.

Similar results for $K = 4$ and for $U_0 = 2$ and $U_0 = 4$ are shown in Fig. 11 in the $\hat\tau_u$ versus $\mathcal{D}_0$ plane and in Fig. 12 in the $\epsilon^2 D_p$ versus $\mathcal{D}_0$ plane. From the left panels of Fig. 11 and Fig. 12, the $j = K - 1 = 3$ sign-alternating mode always sets the Hopf bifurcation boundary. However, as seen in the right panels of Fig. 11 and Fig. 12, where $U_0 = 4 > U_{0,swit} \approx 2.811$, we observe that both the $j = 3$ and $j = 2$ modes determine the Hopf bifurcation boundary when $\mathcal{D}_0 < \mathcal{D}_{0,c}$.
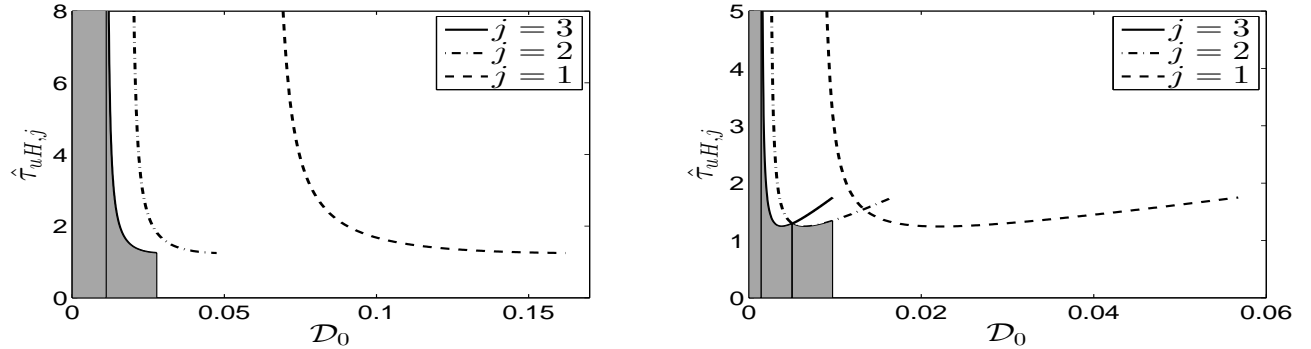

Figure 11: *Linear stability (shaded) region in the $\hat\tau_u$ versus $\mathcal{D}_0$ plane for $K = 4$ when $S = 6$, $\gamma = 2$, and $\alpha = 1$, and for $U_0 = 2$ (left panel) and $U_0 = 4$ (right panel). The solid, dot-dashed, and dashed curves are the Hopf bifurcation boundaries for the (sign-alternating) $j = 3$ mode and the other $j = 2$ and $j = 1$ modes. For $U_0 = 2$ (left panel) the Hopf boundary is determined by the sign-alternating $j = 3$ mode. For $U_0 = 4 > U_{0,swit} \approx 2.811$ (see (5.27)), the Hopf boundary consists of both the $j = 3$ and $j = 2$ mode. Asynchronous oscillatory instabilities of the hotspot amplitudes occur above any of the Hopf bifurcation curves.*

Remark 5.6 *More generally, for $K \geq 3$ there can be $K-2$ distinct mode switches for the minimal Hopf bifurcation threshold on the interval $D_{0,K-1}^- < \mathcal{D}_0 < D_{0,K-1}^+$ when U_0 increases beyond $U_{0,swit}$ towards $U_{0,\max}$. Although we do not work out precise conditions for this cascading behavior of the minimal Hopf bifurcation value here, we illustrate this phenomena in Fig. 13 for $K = 4$, $S = 6$, $\gamma = 2$, $\alpha = 1$, and $U_0 = 5$. From this figure, we observe two mode switches of the minimal Hopf bifurcation threshold. This suggests that as U_0 approaches the existence threshold $U_{0,\max}$, there is a window of $\mathcal{D}_0$ where $K - 2$ distinct modes of oscillatory instability of the hotspot amplitudes can occur if $\hat\tau_u$ is large enough, suggesting*

27

the possibility of intricate spatio-temporal dynamics in this parameter regime.
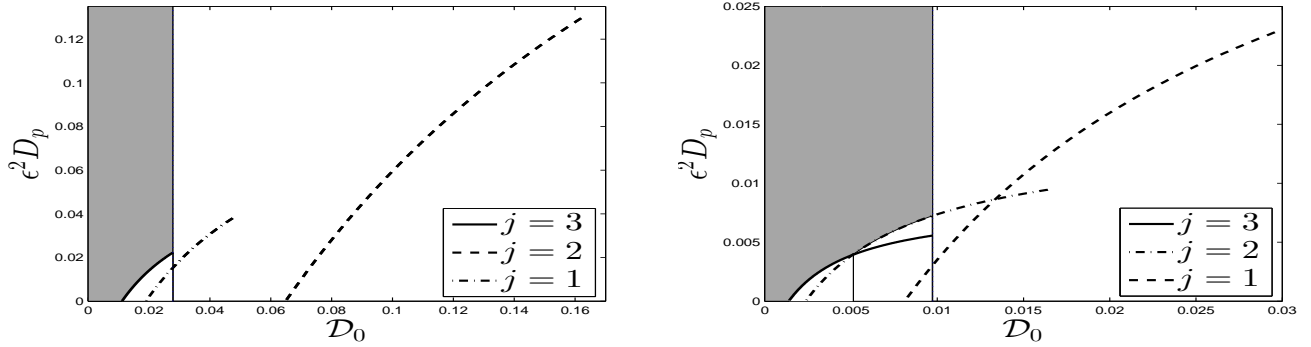

Figure 12: Plot corresponding to Fig. 11 in the scaled police diffusivity $\epsilon^2 D_p = \mathcal{D}_0/\hat{\tau}_u$ versus $\mathcal{D}_0$ plane for $K = 4$, $S = 6$, $\gamma = 2$, and $\alpha = 1$, with $U_0 = 2$ (left panel) and $U_0 = 4$ (right panel). The four-hotspot steady-state is linearly stable in the shaded region. This steady-state undergoes an asynchronous oscillatory instability below either of the three Hopf bifurcation curves. In the left panel the thin vertical line is the competition threshold $\mathcal{D}_{0,c}$. The additional thin vertical line in the right panel is where the Hopf boundary switches from $j = 3$ to $j = 2$. The Hopf eigenvalue tends to zero at the ends of each of the two curves.
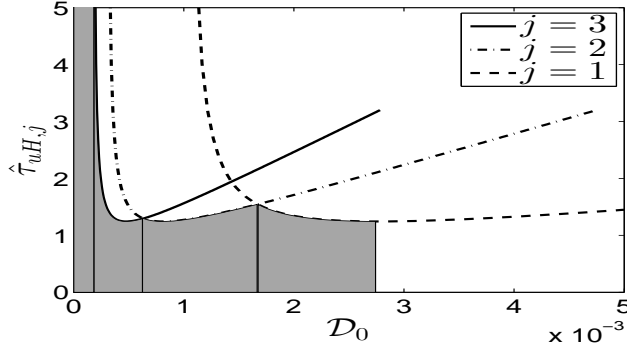
Figure 13: Linear stability (shaded) region in the $\hat{\tau}_u$ versus $\mathcal{D}_0$ plane for $K = 4$ when $S = 6$, $\gamma = 2$, and $\alpha = 1$, and for $U_0 = 5$. The solid, dot-dashed, and dashed curves are the Hopf bifurcation boundaries for the (sign-alternating) $j = 3$ mode, the $j = 2$ mode, and the $j = 1$ mode, respectively. Notice that the minimal Hopf bifurcation threshold on $D^-_{0,K-1} < \mathcal{D}_0 < D^+_{0,K-1}$ now consists of all three modes. Asynchronous oscillatory instabilities of the hotspot amplitudes occur above either of the three Hopf bifurcation curves.

5.2 Comparison of Linear Stability Theory with PDE Simulations: $q = 3$

For various points in the stability phase diagrams of $\epsilon^2 D_p$ versus $\mathcal{D}_0$, we now confirm our linear stability predictions by performing full numerical simulations of the RD system (1.4) using the collocation-based 1-D VLUGR [2] software, which uses adaptive meshing and error controlled time-stepping. For the initial condition for (1.4) we use a slightly smoothed approximation to a K-hotspot steady-state solution, as given in Corollary 2.2, with the explicit form

$$A(x, 0) = \frac{1}{\sigma\sqrt{v_0}} \sum_{j=1}^{K} (1 + 0.01 a_j)\, w\left[\sigma^{-1}(x - x_j)\right] + \alpha \left(1 - \sum_{j=1}^{K} e^{-(x - x_j)^2/\sigma^2}\right), \tag{5.28a}$$

$$\rho(x, 0) = \sum_{j=1}^{K} \left(w[\sigma^{-1}(x - x_j)]\right)^2, \qquad U(x, 0) = \frac{U_0}{\sigma K I_q} \sum_{j=1}^{K} \left(w[\sigma^{-1}(x - x_j)]\right)^q. \tag{5.28b}$$

28

Here $q = 3$ and the hotspot locations are at their steady-state values $x_j = S(2j-1)/(2K)$ for $j = 1, \ldots, K$. The last term in (5.28a) is used solely to subtract off the baseline attractiveness from the localized hotspot regions. In (5.28a), the random coefficient a_j of the 1% perturbation of the hotspot amplitudes is taken to be uniformly distributed in $[-1, 1]$. In addition, the smoothing parameter σ, taken as $\sigma = 1.2\epsilon$, was introduced so as to allow the time-stepper to converge in the PDE simulations with an initial uniformly-spaced of 1000 points on $0 < x < S$. For all of the full PDE simulations reported below, we will display the amplitudes of the maxima of A versus t for the baseline parameter set $S = 6$, $\gamma = 2$, and $\alpha = 1$.
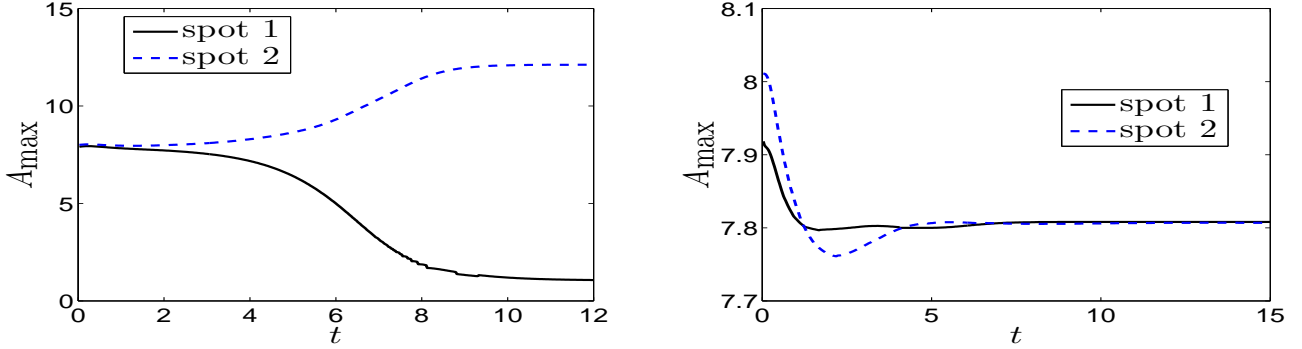
Figure 14: *The spot amplitudes computed numerically from the full PDE system (1.4) for a two-spot pattern with $S = 6$, $\gamma = 2$, $\alpha = 1$, $U_0 = 4$, $\epsilon = 0.035$, and $q = 3$, at two of the marked points in the right panel of Fig. 8. Left panel: $\hat{\tau}_u = 1.8$ and $\mathcal{D}_0 = 0.3$, so that $\epsilon^2 D_p \approx 0.1667$. Spot amplitudes are unstable to a competition instability. Right panel: $\hat{\tau}_u = 1.0$ and $\mathcal{D}_0 = 0.15$, so that $\epsilon^2 D_p = 0.15$. Spot amplitude asynchronous oscillations decay in time and there is no competition instability. These results are consistent with the linear stability predictions in the right panel of Fig. 8 (see also the right panel of Fig. 7).*

For a two-hotspot steady-state, in Fig. 2 of §1 we confirmed the predictions of the three marked points in the phase diagram in Fig. 1 for $U_0 = 2$ and $\epsilon = 0.075$. A similar validation of the linear stability phase diagram in the right panel of Fig. 8 for $U_0 = 4$, with the smaller value $\epsilon = 0.035$, is given in Fig. 14 and Fig. 15. Our choice of a smaller ϵ here is due to the fact that the steady-state hotspot amplitude is considerably smaller for $U_0 = 4$ than when $U_0 = 2$. Moreover, in Fig. 15 we show that for two nearby points in the phase diagram where an asynchronous oscillatory instability is predicted, the long-time dynamics can be rather different in that either one, or both, of the hotspots are ultimately annihilated.
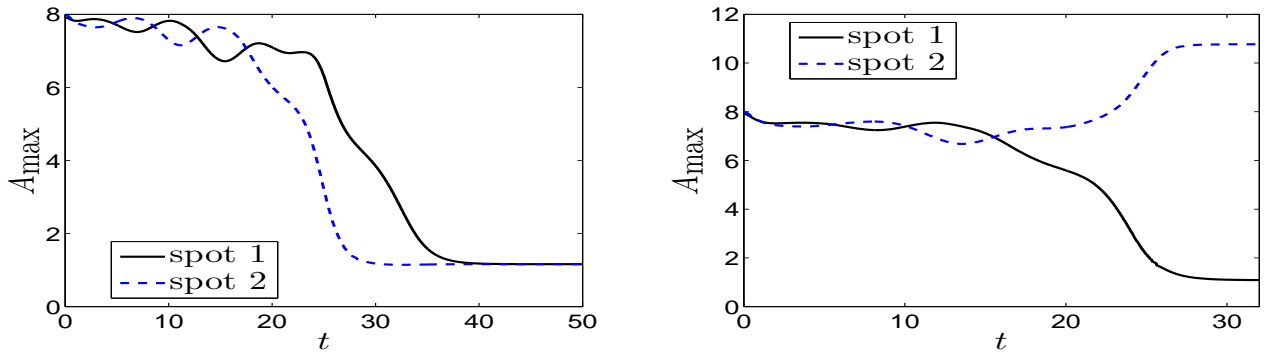

Figure 15: *The oscillatory instabilities of the spot amplitudes computed numerically from the full PDE system (1.4) for a two-spot pattern with $S = 6$, $\gamma = 2$, $\alpha = 1$, $U_0 = 4$, $\epsilon = 0.035$, and $q = 3$, at the marked points in the right panel of Fig. 8 where an oscillatory instability occurs. Left panel: $\hat{\tau}_u = 2.6$ and $\mathcal{D}_0 = 0.15$, so that $\epsilon^2 D_p \approx 0.0577$. Spot amplitudes are unstable to asynchronous oscillations, which leads to the collapse of both hotspots. Right panel: $\hat{\tau}_u = 3.0$ and $\mathcal{D}_0 = 0.15$, so that $\epsilon^2 D_p = 0.05$. Spot amplitudes are unstable to asynchronous oscillations, but now only one of the two hotspots is annihilated.*

For a three-hotspot pattern with $\epsilon = 0.05$ and $U_0 = 2$, in Fig. 16 we show full numerical results, as computed from (1.4),

for the hotspot amplitudes at the three marked points in the left panel of Fig. 10. These results are completely consistent with the prediction of our phase diagram. The middle panel of Fig. 16 shows that the asynchronous oscillation is due to the sign-altering mode, as predicted theoretically.
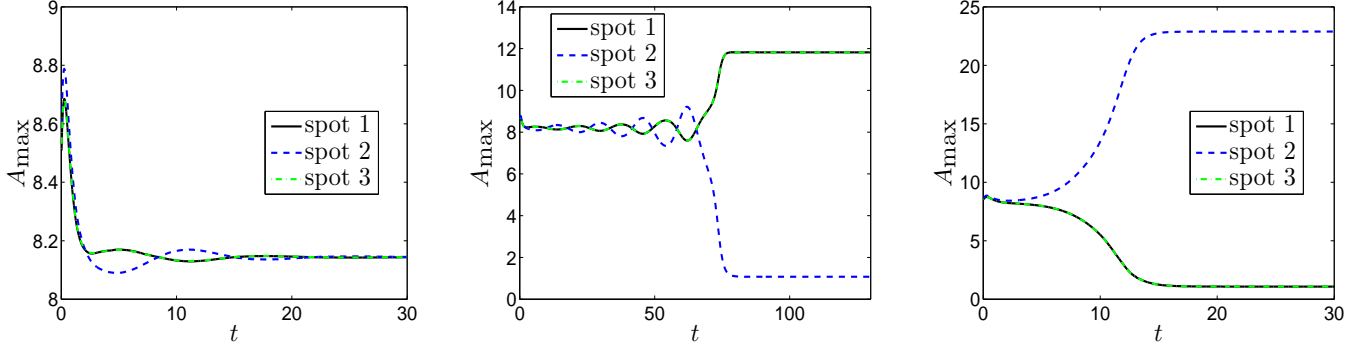

Figure 16: *The spot amplitudes computed numerically from the full PDE system (1.4) for a three-spot pattern with $S = 6$, $\gamma = 2$, $\alpha = 1$, $U_0 = 2$, $\epsilon = 0.05$, and $q = 3$. Left panel: $\hat{\tau}_u = 1.3$ and $\mathcal{D}_0 = 0.07$, so that $\epsilon^2 D_p \approx 0.0538$. Spot amplitudes are stable to asynchronous oscillations and to the competition instability. Middle panel: $\hat{\tau}_u = 2.5$ and $\mathcal{D}_0 = 0.07$, so that $\epsilon^2 D_p = 0.028$. Spot amplitudes are unstable to asynchronous oscillations due to the sign-altering mode, which leads to the collapse of middle hotspot. Right panel: $\hat{\tau}_u = 2.5$ and $\mathcal{D}_0 = 0.12$, so that $\epsilon^2 D_p = 0.048$. Spot amplitudes are unstable to a competition instability due to the sign-altering mode, which leads to the collapse of the first and third hotspots. These results are consistent with the linear stability predictions in the left panels of Fig. 9 and Fig. 10. The results correspond to the marked points in the left panel of Fig. 10.*
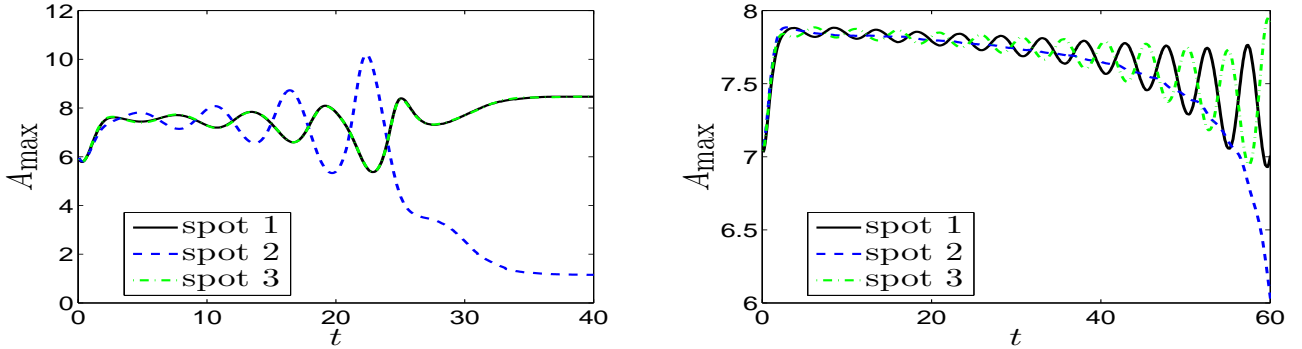

Figure 17: *The spot amplitudes computed numerically from the full PDE system (1.4) for a three-spot pattern with $S = 6$, $\gamma = 2$, $\alpha = 1$, $U_0 = 4$, $\epsilon = 0.025$, and $q = 3$, for the two marked points in the right panel of Fig. 10. Left panel: $\hat{\tau}_u = 2.5$ and $\mathcal{D}_0 = 0.01$, so that $\epsilon^2 D_p \approx 0.004$. Unstable asynchronous spot amplitude oscillations are of sign-altering type as predicted by the theory. Right panel: $\hat{\tau}_u = 1.6$ and $\mathcal{D}_0 = 0.03$, so that $\epsilon^2 D_p = 0.01875$. The unstable spot amplitude oscillations are no longer sign-altering. Here the first and third spots exhibit anti-phase oscillations as predicted by the right panel of Fig. 10.*

As a more refined test of our linear stability theory, we again consider a three-hotspot pattern but now take $U_0 = 4$ and $\epsilon = 0.025$. For $U_0 = 4$, the phase diagram shown in the right panel of Fig. 10 predicts that there will be a switch at some critical value of $\mathcal{D}_0$ between the dominant spatial mode for asynchronous temporal oscillations. The full numerical results for the spot amplitudes shown in Fig. 17 at the two marked points in the right panel of Fig. 10 validate this theoretical prediction. In particular, in the right panel of Fig. 17 we observe that it is the first and third hotspots, instead of the first and second hotspots as in the left panel of Fig. 17, that exhibit anti-phase temporal oscillations.

6 Oscillatory Instabilities of the Hotspot Amplitudes: $q \neq 3$ and $q > 1$

In this section we analyze the NLEP (3.36) for the general case where $q \neq 3$, by determining the roots of $\zeta(\lambda) = 0$ in $\operatorname{Re}(\lambda) > 0$. In (4.4a) we re-write $\mathcal{C}(\lambda)$ as

$$\mathcal{C}(\lambda) = \frac{\eta}{b}\left(1 + \tilde{\tau}_j \lambda\right)\left(1 - \frac{b}{3 - \lambda}\right), \qquad \text{where} \qquad \eta \equiv \frac{9\omega}{2qU_0}, \quad b \equiv \frac{9\chi_{0,j}}{2}, \quad \tilde{\tau}_j \equiv \frac{\hat{\tau}_u}{D_j \kappa_q}, \quad \frac{1}{\chi_{0,j}} = 1 + \frac{\kappa_3 D_j}{\alpha}. \tag{6.1}$$

To relate our key parameter b (which depends on j) to the diffusivity $\mathcal{D}_0$, we first use the expression for $\chi_{0,j}$ to write D_j in terms of b as $D_j = [\alpha/(2\kappa_3)]\,(9/b - 2)$. Then, upon using (5.4) for $\alpha/(2\kappa_3)$ and (3.20) to relate D_j to $\mathcal{D}_0$, we obtain that

$$\frac{\mathcal{D}_0}{D_{0,j}^-} = \frac{9}{b} - 2, \qquad \text{or} \qquad b = \frac{9}{2 + \mathcal{D}_0/D_{0,j}^-}. \tag{6.2}$$

Thus, $\mathcal{D}_0 > 0$ only when $b < 9/2$. Here $D_{0,j}^-$ is defined in terms of the competition threshold $\mathcal{D}_{0c}$ of (4.9) by

$$D_{0,j}^- \equiv \frac{\mathcal{D}_{0,c}}{(1 + qU_0/\omega)}\left(\frac{1 + \cos{(\pi/K)}}{1 - \cos{(\pi j/K)}}\right), \qquad D_{0,j}^+ \equiv \mathcal{D}_{0,c}\left(\frac{1 + \cos{(\pi/K)}}{1 - \cos{(\pi j/K)}}\right), \qquad \frac{D_{0,j}^+}{D_{0,j}^-} = 1 + \frac{qU_0}{\omega}, \tag{6.3}$$

where $D_{0,K-1}^+ = \mathcal{D}_{0,c}$. In our analysis below, the following ranges of b will play a prominent role:

$$(I): \quad 3 < b < 9/2 \quad \implies \quad D_{0,j}^- > \mathcal{D}_0 > 0 \quad \implies \quad \mathcal{C}(0) < 0, \tag{6.4a}$$

$$(II): \quad b_c \equiv 3\eta/\left(\eta + 3/2\right) < b < 3 \quad \implies \quad D_{0,j}^+ > \mathcal{D}_0 > D_{0,j}^- \quad \implies \quad 1/2 > \mathcal{C}(0) > 0, \tag{6.4b}$$

$$(III): \quad b < b_c \quad \implies \quad \mathcal{D}_0 > D_{0,j}^+ \quad \implies \quad \mathcal{C}(0) > 1/2. \tag{6.4c}$$

Since $\mathcal{F}(0) = 1/2$, and $\mathcal{C}(0) = 1/2$ when $b = b_c$, we conclude that $b = b_c$ corresponds to a zero-eigenvalue crossing.

6.1 Analytical Results Based on the Winding Number Criterion

Here we use the winding number criterion of §4.2 to determine some rigorous results for the number N of unstable eigenvalues in $\operatorname{Re}(\lambda) > 0$ for the ranges of b listed in (6.4). In our analysis we will assume that Conjecture 4.4 on $\mathcal{F}_R(\lambda_I)$ and $\mathcal{F}_I(\lambda_I)$ holds for $q > 1$. With $\zeta(\lambda)$ as defined in (3.40), (4.5) when $\hat{\tau}_u > 0$ yields that

$$N = \frac{3}{2} + \frac{1}{\pi}\left[\arg \zeta\right]_{\Gamma_I^+}. \tag{6.5}$$

To calculate $\left[\arg \zeta\right]_{\Gamma_I^+}$ we need the following properties of the real and imaginary parts of $\mathcal{C}(i\lambda_I)$:

Lemma 6.1 *Let $\mathcal{C}(i\lambda_I) = \mathcal{C}_R(\lambda_I) + i\mathcal{C}_I(\lambda_I)$. Then, from (6.1) we have*

$$\mathcal{C}_R(\lambda_I) = \frac{\eta}{b}\left(1 + \tilde{\tau}_j b - \frac{3b}{9 + \lambda_I^2}\left(1 + 3\tilde{\tau}_j\right)\right), \qquad \mathcal{C}_I(\lambda_I) = \frac{\eta\lambda_I}{b}\left[\tilde{\tau}_j - \frac{b(1 + 3\tilde{\tau}_j)}{(9 + \lambda_I^2)}\right]. \tag{6.6}$$

For the imaginary part we have:

(i) $\mathcal{C}_I(\lambda_I) \sim (9b)^{-1}\eta\lambda_I\left[3\tilde{\tau}_j(3 - b) - b\right]$ *as* $\lambda_I \to 0^+$,

(ii) $\mathcal{C}_I(\lambda_I) \sim b^{-1}\eta\tilde{\tau}_j\lambda_I$ *as* $\lambda_I \to +\infty$.

(iii) *If* $b < 3/(1 + \frac{1}{3\tilde{\tau}_j})$, *then* $\mathcal{C}_I(\lambda_I) > 0$ *for all* $\lambda_I > 0$.

(iv) *If* $b > 3/(1 + \frac{1}{3\tilde{\tau}_j})$, *then* $\mathcal{C}_I(\lambda_I) < 0$ *on* $0 < \lambda_I < \sqrt{3(b - 3) + \frac{b}{\tilde{\tau}_j}} \equiv \lambda_{I_I}$ *and* $\mathcal{C}_I(\lambda_I) > 0$ *on* $\lambda_I > \lambda_{I_I}$.

Alternatively, for the real part we have:

(v) $\mathcal{C}'_R(\lambda_I) > 0$ for $\lambda_I > 0$.

(vi) $\mathcal{C}_R(\lambda_I) \sim b^{-1}\eta(1 + \tilde{\tau}_j b)$ as $\lambda_I \to \infty$.

(vii) $\mathcal{C}_R(0) > 0$ if $b < 3$ and $\mathcal{C}_R(0) < 0$ if $b > 3$. When $b > 3$, then $\mathcal{C}_R(\lambda_I) < 0$ on $0 < \lambda_I < \sqrt{\frac{3(b-3)}{1+\tilde{\tau}_j b}} \equiv \lambda_{IR}$, and $\mathcal{C}_R(\lambda_I) > 0$ on $\lambda_I > \lambda_{IR}$.

(viii) $\mathcal{C}_R(0) > 1/2$ iff $b < b_c \equiv 3\eta/(\eta + 3/2)$, where b_c is the zero-eigenvalue crossing.

With properties (ii) and (vi) of Lemma 6.1, together with the decay of $\mathcal{F}_R(\lambda_I)$ and $\mathcal{F}_I(\lambda_I)$ as $\lambda_I \to +\infty$ (see Proposition 4.3), we conclude that

$$\zeta(i\lambda_I) \sim b^{-1}\eta\left(1 + \tilde{\tau}_j b\right) + ib^{-1}\eta\tilde{\tau}_j\lambda_I \quad \text{as} \quad \lambda_I \to +\infty.$$

Therefore, with respect to the origin, the path $\zeta(i\lambda_I) = \zeta_R(\lambda_I) + i\zeta_I(\lambda_I)$ begins (as $\lambda_I \to \infty$) asymptotically close to the positive infinity of the imaginary axis in the complex ζ plane.

Moreover, from property (v) of Lemma 6.1, and under Conjecture 4.4 that $\mathcal{F}'_R(\lambda_I) < 0$ for all $\lambda_I > 0$, we conclude that

$$\zeta'_R(\lambda_I) > 0 \quad \text{for all} \quad \lambda_I > 0. \tag{6.7}$$

With this key result, the path $\zeta(i\lambda_I)$ in the ζ-plane for $\lambda_I > 0$ can only intersect the imaginary ζ_I axis exactly one or zero times. In particular if $\zeta(0) \equiv \zeta_R(0) > 0$, then $\zeta_R(\lambda_I) > 0$ for all $\lambda_I > 0$ so that $[\arg\zeta]_{\Gamma_I^+} = -\pi/2$ and $N = 1$ from (6.5). In contrast, if $\zeta(0) \equiv \zeta_R(0) < 0$, then there is a unique $\lambda_I^\star > 0$ for which $\zeta_R(\lambda_I^\star) = 0$. In this case, (6.5) yields that

$$(I): \quad \zeta_I(\lambda_I^\star) > 0 \quad \Longrightarrow \quad [\arg\zeta]_{\Gamma_I^+} = \pi/2 \quad \Longrightarrow \quad N = 2 \tag{6.8a}$$

$$(II): \quad \zeta_I(\lambda_I^\star) < 0 \quad \Longrightarrow \quad [\arg\zeta]_{\Gamma_I^+} = -3\pi/2 \quad \Longrightarrow \quad N = 0. \tag{6.8b}$$

With these preliminary observations, we obtain the following instability result for the j-th mode on the range $\mathcal{D}_0 > D_{0,j}^+$.

Proposition 6.2 *Suppose that $\mathcal{D}_0 > D_{0,j}^+$ and that Conjecture 4.4 holds. Then, for the j-th mode with $j = 1, \ldots, K-1$, we have $N = 1$ for all $\tilde{\tau}_j \geq 0$.*

Proof: When $\mathcal{D}_0 > D_{0,j}^+$, we have $b < b_c \equiv 3\eta/(\eta + 3/2)$ and consequently $\mathcal{C}_R(0) > 1/2$ from (III) of (6.4). This yields $\zeta_R(0) > 0$, and thus $\zeta_R(\lambda_I) > 0$ for all $\lambda_I > 0$ using the monotonicity result (6.7), which holds when $\mathcal{F}'_R(\lambda_I) < 0$ for all $\lambda_I > 0$. Therefore $[\arg\zeta]_{\Gamma_I^+} = -\pi/2$ and (6.5) yields $N = 1$ for all $\tilde{\tau}_j > 0$. ∎

Together with the ordering principle $D_{0,j+1}^+ < D_{0,j}^+$ for $j = 1, \ldots, K-2$ from (5.16), this instability result proves, for any $\hat{\tau}_u > 0$, that there are exactly $K-1$ positive real eigenvalues of the NLEP (3.36) when $\mathcal{D}_0 > D_{0,1}^+$.

Proposition 6.3 *Suppose that $\mathcal{D}_0 < D_{0,j}^+$ and that Conjecture 4.4 holds. Then, for the j-th mode with $j = 1, \ldots, K-1$, we have either $N = 0$ or $N = 2$ for all $\tilde{\tau}_j > 0$. Moreover, if $\tilde{\tau}_j \ll 1$ we have $N = 0$.*

Proof: If $\mathcal{D}_0 < D_{0,j}^+$, then $b > 3\eta/(\eta + 3/2)$, and so $\mathcal{C}_R(0) < 1/2$ by (II) of (6.4). Therefore, since $\zeta_R(0) < 0$, $\zeta_R(\infty) > 0$, and $\zeta'_R(\lambda_I) > 0$, which holds when $\mathcal{F}'_R(\lambda_I) < 0$ for all $\lambda_I > 0$, it follows that there is a unique root $\lambda_I^\star$ for which $\zeta_R(\lambda_I^\star) = 0$. From (6.8), we have for all $\hat{\tau}_j > 0$ that either $N = 0$ or $N = 2$ depending on the sign of $\zeta_I(\lambda_I^\star)$.

32

Next, we prove that $N = 0$ if $\tilde{\tau}_j \ll 1$. For $\tilde{\tau}_j \ll 1$, (6.6) yields that

$$\mathcal{C}_R(\lambda_I) \sim \frac{\eta}{b}\left(1 - \frac{3b}{9 + \lambda_I^2}\right),$$

uniformly in λ_I. It follows that $\zeta_R(\lambda_I^\star) = 0$ at some $\lambda_I^\star = \mathcal{O}(1)$ when $\tilde{\tau}_j \ll 1$. However, for $\tilde{\tau}_j \ll 1$, we have from (6.6) that $\mathcal{C}_I(\lambda_I^\star) \sim -\eta\lambda_I/(9 + \lambda_I^2) < 0$. Under Conjecture 4.4 that $\mathcal{F}_I(\lambda_I) > 0$, we conclude that $\zeta_I(\lambda_I^\star) = \mathcal{C}_I(\lambda_I^\star) - \mathcal{F}_I(\lambda_I^\star) < 0$. Therefore, from (6.8b) we conclude that $N = 0$. ∎

This result proves that the j-th mode is linearly stable on the range $\mathcal{D}_0 < D_{0,j}^+$ whenever $\tilde{\tau}_j \ll 1$. The next result determines N for $\tilde{\tau}_j \gg 1$ on the entire range $\mathcal{D}_0 < D_{0,j}^+$.

Proposition 6.4 *Suppose that $D_{0,j}^- < \mathcal{D}_0 < D_{0,j}^+$ and that Conjecture 4.4 holds. Then, for the j-th mode with $j = 1, \ldots, K - 1$, we have $N = 2$ when $\tilde{\tau}_j \gg 1$. In contrast, if $\mathcal{D}_0 < D_{0,j}^-$, then $N = 0$ when $\tilde{\tau}_j \gg 1$.*

<u>Proof:</u> We first observe from (6.4) that $D_{0,j}^- < \mathcal{D}_0 < D_{0,j}^+$ when $b_c < b < 3$ and $\mathcal{D}_0 < D_{0,j}^-$ when $b > 3$. For $\mathcal{D}_0 < D_{0,j}^+$, we have $\zeta_R(0) < 0$ and so there is a unique root $\lambda_I^\star$ to $\zeta_R(\lambda_I^\star) = 0$. For $\tilde{\tau}_j \gg 1$, and for $b > b_c \equiv 3\eta/(\eta + 3/2)$, this unique root of $\zeta_R(\lambda_I)$ occurs for $\lambda_I = \mathcal{O}(\tilde{\tau}_j^{-1/2}) \ll 1$. By setting $\mathcal{C}_R(\lambda_I) = \mathcal{F}_R(\lambda_I)$, and using $\lambda_I = \mathcal{O}(\tilde{\tau}_j^{-1/2}) \ll 1$ together with (6.6) for $\mathcal{C}_R$, we get that

$$\frac{\eta}{b}\left(1 + \frac{b}{9}(\tilde{\tau}_j\lambda_I^2 - 3)\right) \sim \mathcal{F}_R(0) = \frac{1}{2}.$$

In this way, we obtain for $\tilde{\tau}_j \gg 1$ that the unique root $\lambda_I^\star$ of $\zeta_R(\lambda_I) = 0$ occurs when

$$\lambda_I^\star \sim \beta/\tilde{\tau}_j^{1/2}, \qquad \beta \equiv \sqrt{3\left(1 - \frac{3}{b}\right) + \frac{9}{2\eta}}. \tag{6.9}$$

From (6.6) for $\mathcal{C}_I$, we then calculate for $\tilde{\tau}_j \gg 1$ that

$$\mathcal{C}_I(\lambda_I^\star) \sim \frac{\eta\beta}{3b}(3 - b)\tilde{\tau}_j^{1/2} = \mathcal{O}(\tilde{\tau}_j^{1/2}). \tag{6.10}$$

When $b > 3$, corresponding to $\mathcal{D}_0 < D_{0,j}^-$, we have $\mathcal{C}_I(\lambda_I^\star) < 0$. Therefore, with $\mathcal{F}_I(\lambda_I) > 0$ from Conjecture 4.4, we conclude that $\zeta_I(\lambda_I^\star) < 0$. This yields that $N = 0$ from (6.8b). Now suppose that $b_c < b < 3$, corresponding to $D_{0,j}^- < \mathcal{D}_0 < D_{0,j}^+$. Then, since $\mathcal{C}_I(\lambda_I^\star) > 0$, with $\mathcal{C}_I(\lambda_I^\star) = \tilde{\tau}_j^{1/2} \gg 1$ for $\tilde{\tau}_j \gg 1$, while $\mathcal{F}_I(\lambda_I^\star) = \mathcal{O}(1)$, we conclude that $\zeta_I(\lambda_I^\star) > 0$. This yields that $N = 2$ from (6.8a). ∎

On the range $D_{0,j}^- < \mathcal{D}_0 < D_{0,j}^+$, Propositions 6.4 and 6.3 show for the j-th mode that $N = 2$ for $\tilde{\tau}_j \gg 1$ and $N = 0$ for $\tilde{\tau}_j \ll 1$. Therefore, by continuity, there is a Hopf bifurcation value of $\tilde{\tau}_j$ on this range of $\mathcal{D}_0$. Although this proves the existence of a Hopf bifurcation threshold for $\hat{\tau}_u$ on the range $D_{0,j}^- < \mathcal{D}_0 < D_{0,j}^+$ for any mode $j = 1, \ldots, K - 1$, it does not establish uniqueness of this threshold or provide any its qualitative properties. This is done numerically in §6.2.

The remaining issue relates to the range $\mathcal{D}_0 < D_{0,j}^-$, where we have proved that $N = 0$ when either $\tilde{\tau}_j \ll 1$ or $\tilde{\tau}_j \gg 1$. Next, we study for this range of $\mathcal{D}_0$ whether $N = 0$ *for all $\tilde{\tau}_j > 0$*.

To examine this question we will proceed as follows: Suppose that $\mathcal{C}_R(0) < 1/2$ and that $\mathcal{C}_R(\infty) > 1/2$. Then, with Conjecture 4.4 that $\mathcal{F}_R'(\lambda_I) < 0$ for all $\lambda_I > 0$, and with $\mathcal{F}_R(0) = 1/2$, it follows that the unique root $\lambda_I^\star$ to $\zeta_R(\lambda_I) = 0$ satisfies $\lambda_I^\star < \lambda_{Im}$ where λ_{Im} is defined by $C_R(\lambda_{Im}) = 1/2$. If we can then show that $C_I(\lambda_{Im}) < 0$, it follows that $C_I(\lambda_I^\star) < 0$. Then, by Conjecture 4.4 that $\mathcal{F}_I(\lambda_I) > 0$ for all $\lambda_I > 0$, we obtain that $\zeta_I(\lambda_I^\star) < 0$, and consequently $N = 0$ from (6.8b). Therefore, our goal is to determine the range of b, with $b > 3$, for which

$$\mathcal{C}_R(0) < 1/2, \qquad \mathcal{C}_R(\infty) > 1/2, \qquad \text{and} \quad \mathcal{C}_I(\lambda_{Im}) < 0 \quad \text{where} \quad \mathcal{C}_R(\lambda_{Im}) = 1/2. \tag{6.11}$$

33

When $b > b_c$ we have $\mathcal{C}_R(0) < 1/2$, and from property (vi) of Lemma 6.1 we have $\mathcal{C}_R(\infty) > 1/2$ provided that

$$\frac{\eta}{b}\left(1 + \tilde{\tau}_j b\right) > \frac{1}{2}\,. \tag{6.12}$$

Now by using (6.6) for $\mathcal{C}_R$, we obtain that $\mathcal{C}_R(\lambda_{Im}) = 1/2$ when

$$\frac{1 + 3\tilde{\tau}_j}{9 + \lambda_{Im}^2} = \frac{1}{3\eta}\left[\frac{\eta}{b}(1 + \tilde{\tau}_j b) - \frac{1}{2}\right]\,.$$

By using this expression in (6.6) for $\mathcal{C}_I(\lambda_I)$ we get, after some algebra, that

$$\mathcal{C}_I(\lambda_{Im}) = \frac{\eta\lambda_{Im}}{b}\left(\tilde{\tau}_j - \frac{b(1 + 3\tilde{\tau}_j)}{9 + \lambda_{Im}^2}\right) = -\frac{\eta\lambda_{Im}}{3b}\left[\tilde{\tau}_j(b - 3) + 1 - \frac{b}{2\eta}\right]\,.$$

We conclude that $\mathcal{C}_I(\lambda_{Im}) < 0$ when $1 + \tilde{\tau}_j b - b/(2\eta) > 3\tilde{\tau}_j$. Since, from (6.12), we have $\mathcal{C}_R(\infty) > 1/2$ when $1 + \tilde{\tau}_j b - b/(2\eta) > 0$, we conclude that the inequalities in (6.11) hold when

$$b > b_c \equiv \frac{3\eta}{\eta + 3/2} \qquad \text{and} \qquad 1 + \tilde{\tau}_j b - b/(2\eta) > 3\tilde{\tau}_j\,. \tag{6.13}$$

We now determine a range of b, independent of $\tilde{\tau}_j$, for which the inequalities (6.13) hold. A sufficient condition for (6.13) to hold is that $b > 3$ and $b < 2\eta$. If $\eta < 3/2$, there is no such range of b. If $\eta > 9/2$, these inequalities hold on the full range $3 < b < 9/2$ where $\mathcal{D}_0 < D_{0,j}^-$, as given in (I) in (6.4). However, when $3/2 < \eta < 9/2$, the interval $3 < b < 2\eta$ is only a subset of the full range in (I) of (6.4) where $\mathcal{D}_0 < D_{0,j}^-$. By using (6.1) for η, together with (6.2) to relate b to $\mathcal{D}_0$, we summarize our result as follows:

Proposition 6.5 *Suppose that Conjecture 4.4 holds. Then, for the j-th mode with $j = 1, \ldots, K - 1$ we have the following:*

(I) *Suppose $U_0 < 2\omega/q$ and $\mathcal{D}_0 < D_{0,j}^-$. Then $N = 0$ for all $\hat{\tau}_u > 0$.* $\tag{6.14a}$

(II) *Suppose $2\omega/q < U_0 < 3\omega/q$ and $\left(\dfrac{qU_0}{\omega} - 2\right)D_{0,j}^- < \mathcal{D}_0 < D_{0,j}^-$. Then $N = 0$ for all $\hat{\tau}_u > 0$.* $\tag{6.14b}$

This result provides no stability information for the range $\mathcal{D}_0 < D_{0,j}^-$ when $U_0 > 3\omega/q$.

As a result of the ordering principle $D_{0,K-1}^- < D_{0,j}^-$ for $j = 1, \ldots, K - 2$ and $K \geq 3$, we conclude from (I) of Proposition 6.5, upon recalling $\omega = S(\gamma - \alpha) - U_0$, that a K-hotspot pattern is linearly stable for all $\hat{\tau}_u > 0$ on the range $\mathcal{D}_0 < D_{0,K-1}^-$ when $U_0 < 2S(\gamma - \alpha)/(q + 2)$. This result is weaker than that obtained for the explicitly solvable case $q = 3$, In fact, since $\omega = S(\gamma - \alpha) - U_0$, it provides no stability information on $\mathcal{D}_0 < D_{0,j}^-$ when $U_0 > 3(S - \gamma)/(q + 3)$. For $q = 3$, we recall from Proposition 5.1 that for the j-th mode we have $N = 0$ for $\mathcal{D}_0 < D_{0,j}^-$ for all $\hat{\tau}_u > 0$ without any restriction on U_0.

In §6.2 we will investigate numerically the possibility of a Hopf bifurcation for the range $0 < \mathcal{D}_0 < D_{0,j}^-$ when $U_0 > 3\omega/q$, for which Proposition 6.5 does not apply. Our numerical procedure in §6.2 suggests that no Hopf bifurcation exists on the range $0 < \mathcal{D}_0 < D_{0,j}^-$ for any $U_0 < U_{0,\max}$, as qualitatively identical to the second statement proved in Proposition 5.1 for the explicitly solvable case $q = 3$.

To gain some insight into the behavior of the Hopf bifurcation threshold $\tilde{\tau}_j$ for the j-th mode, we now derive a scaling law for it to show that $\tilde{\tau}_j \to \infty$ and $\lambda_I \to 0^+$ as $\mathcal{D}_0 \to D_{0,j}^-$ from above, or equivalently as $b \to 3$ from below. For $b \to 3^-$, we look for a solution to $\zeta(i\lambda_I) = 0$ with $\lambda_I \to 0$, $\tilde{\tau}_j \to \infty$, with the distinguished balance $\lambda_I = \mathcal{O}(\tilde{\tau}_j^{-1/2})$. By setting $\mathcal{C}_R(\lambda_I) = \mathcal{F}_R(\lambda_I)$, and using $\mathcal{F}_R(\lambda_I) \sim 1/2$ together with (6.6) for $\mathcal{C}_R$, we get that

$$\frac{\eta}{b}\left(1 - \frac{b}{9}\left(3 - \tilde{\tau}_j\lambda_I^2\right)\right) \sim \frac{1}{2}\,.$$

By solving for $\tilde{\tau}_j \lambda_I^2$ and letting $b \to 3$, we obtain that $\tilde{\tau}_j \lambda_I^2 = 9/(2\eta) + 3(b-3)/b$. By letting $b \to 3$, we conclude that

$$\lambda_I \sim \sqrt{\frac{9}{2\eta\tilde{\tau}_j}}, \qquad \text{as} \quad \tilde{\tau}_j \to \infty. \tag{6.15}$$

Then, we set $\mathcal{C}_I(\lambda_I) = \mathcal{F}_I(\lambda_I)$, and use (6.6) for $\mathcal{C}_I$, together with the local behavior for $\mathcal{F}_I(\lambda_I)$ as $\lambda_I \to 0$ from (iv) of Proposition 4.3. This yields that

$$\frac{\eta\lambda_I}{b(9 + \lambda_I^2)} \left(3\tilde{\tau}_j(3-b) - b + \tilde{\tau}_j\lambda_I^2\right) \sim \frac{\lambda_I}{4}\left(1 - \frac{1}{q}\right).$$

Upon cancelling the factor of λ_I and using $\tilde{\tau}_j \lambda_I^2 \sim 9/(2\eta)$, we solve for $\tilde{\tau}_j$ in the expression above to get

$$\tilde{\tau}_j \sim \frac{1}{3(3-b)}\left[b - \frac{9}{2\eta} + \frac{9b}{4\eta}\left(1 - \frac{1}{q}\right)\right] \sim \frac{1}{3-b}\left[1 + \frac{3}{4\eta}\left(1 - \frac{3}{q}\right)\right], \qquad \text{as} \quad b \to 3. \tag{6.16}$$

In terms of the original variables $\mathcal{D}_0$, U_0 and $\hat{\tau}_u$ we use (6.1) and (6.2) to get

$$\frac{3}{4\eta} = \frac{qU_0}{6\omega}, \qquad \hat{\tau}_u = \frac{\alpha}{2}\left(\frac{\kappa_q}{\kappa_3}\right)\frac{\mathcal{D}_0}{D_{0,j}^-}\tilde{\tau}_j, \qquad b - 3 \sim 1 - \frac{\mathcal{D}_0}{\mathcal{D}_{0,j}^-} \quad \text{as} \quad \mathcal{D}_0 \to D_{0,j}^-. \tag{6.17}$$

Upon substituting (6.17) into (6.16) and (6.15) we get the limiting Hopf bifurcation threshold

$$\hat{\tau}_{u,H} \sim \frac{\alpha}{2}\left(\frac{\kappa_q}{\kappa_3}\right)\frac{1}{(\mathcal{D}_0/D_{0,j}^- - 1)}\left(1 + \frac{qU_0}{6\omega}\left(1 - \frac{3}{q}\right)\right)^{1/2}, \qquad \lambda_{IH} \sim \sqrt{\frac{\mathcal{D}_0}{D_{0,j}^-} - 1}\left(\frac{qU_0}{\omega}\right)^{1/2}\left[1 + \frac{qU_0}{6\omega}\left(1 - \frac{3}{q}\right)\right]^{-1/2}, \tag{6.18}$$

as $\mathcal{D}_0 \to D_{0,j}^-$. For the special case where $q = 3$, this limiting result for λ_{IH} and $\hat{\tau}_{u,H}$ agrees with that in (5.14) and (5.10), respectively.

Finally, for the j-th mode we will calculate an additional scaling law for the Hopf bifurcation threshold and the Hopf eigenvalue as $b \to b_c \equiv 3\eta/(\eta + 3/2)$ from above, corresponding to the limit $\mathcal{D}_0 \to D_{0,j}^+$ from below. We look for a root $\lambda_I \ll 1$ to $\mathcal{C}_R(\lambda_I) = \mathcal{F}_R(\lambda_I)$ and use

$$\mathcal{F}_R \sim \frac{1}{2} - k_R\lambda_I^2 + \cdots, \qquad \text{as} \quad \lambda_I \to 0, \tag{6.19}$$

for some $k_R > 0$, together with (6.6) for $\mathcal{C}_R(\lambda_I)$, to obtain that

$$\frac{\eta}{b(9 + \lambda_I^2)}\left[9 - 3b + \lambda_I^2(1 + \tilde{\tau}_j b)\right] \sim \frac{1}{2} - k_R\lambda_I^2.$$

Upon isolating λ_I, we get

$$\frac{\eta}{b}(9 - 3b) - \frac{9}{2} = \lambda_I^2\left(\frac{1}{2} - 9\kappa_R - \frac{\eta}{b_c}(1 + \tilde{\tau}_j b_c)\right). \tag{6.20}$$

We then set $\mathcal{C}_I(\lambda_I) = \mathcal{F}_I(\lambda_I)$ as $\lambda_I \to 0$ using the local behavior (i) of Lemma 6.1 for $\mathcal{C}_I(\lambda_I)$ and that in (iv) of Proposition 4.3 for $\mathcal{F}_I(\lambda_I)$. This yields that

$$\frac{\eta}{9b_c}\left(3\tilde{\tau}_j(3 - b_c) - b_c\right) \sim \frac{1}{4}\left(1 - \frac{1}{q}\right).$$

Upon using $b_c = 3\eta/(\eta + 3/2)$, we solve for $\tilde{\tau}_j$ in this expression to obtain

$$\tilde{\tau}_j \sim \frac{2\eta}{9}\left[1 + \frac{9}{4\eta}\left(1 - \frac{1}{q}\right)\right], \qquad \text{as} \quad b \to b_c. \tag{6.21}$$

Upon substituting (6.21) into (6.20) and solving for λ_I we obtain, after some algebra, that $\lambda_I \equiv \lambda_{IH}$ satisfies

$$\lambda_{IH} \sim \sqrt{\frac{27}{2}}\left(\frac{1 - b_c/b}{3 - b_c}\right)^{1/2}\left(9\kappa_R + \frac{\eta}{3} + \frac{2\eta^2}{9} + \frac{\eta}{2}\left(1 - \frac{1}{q}\right)\right)^{-1/2}, \qquad \text{as} \quad b \to b_c. \tag{6.22}$$

35

To write $\tilde{\tau}_j$ in (6.21) in terms of the original variables, we use (6.17), together with $D_{0,j}^+/D_{0,j}^- = 1 + qU_0/\omega$, to obtain

$$\hat{\tau}_{u,H} \sim \frac{\alpha\omega}{2qU_0} \left(\frac{\kappa_q}{\kappa_3}\right) \left(1 + \frac{qU_0}{\omega}\right) \left(1 + \frac{U_0}{2\omega}(q-1)\right), \qquad \text{as} \quad \mathcal{D}_0 \to D_{0,j}^+. \tag{6.23}$$

When $q = 3$, the expression in (6.23) agrees with that obtained in (5.10) for the explicitly solvable case. To determine if (6.22) yields the limiting Hopf eigenvalue given in (5.14) when $q = 3$, we use $\mathcal{F}(i\lambda_I) = 3/[2(3 - i\lambda_I)]$, from (4.1). This yields $\mathcal{F}_R(\lambda_I) \sim 1/2 - \lambda_I^2/18$, which identifies $k_R = 1/18$ in (6.19). With this value for k_R and $q = 3$, the expression in the brackets in (6.22) is a perfect square, and simplifies to

$$\lambda_{IH} \sim \sqrt{\frac{27}{2}} \left(1 - \frac{b_c}{b}\right)^{1/2} \frac{(9/2)^{1/2}}{(3 - b_c)^{1/2}(\eta + 3/2)}.$$

We then use $b_c = 3\eta/(\eta + 3/2)$ together with $\eta = 3\omega/(2U_0)$ when $q = 3$ from (6.1), to get

$$\lambda_{IH} \sim \sqrt{\frac{27}{2}} \sqrt{1 - \frac{b_c}{b}} \left(1 + \frac{\omega}{U_0}\right)^{-1/2}. \tag{6.24}$$

Finally, we use (6.2) for b, $D_{0,j}^+/D_{0,j}^- = 1 + 3U_0/\omega$, and $\eta = 3\omega/(2U_0)$ to calculate

$$\frac{b_c}{b} - 1 = \frac{\eta}{3(\eta + 3/2)} \left(\frac{\mathcal{D}_0}{\mathcal{D}_{0,j}^-} + 2\right) = \left(\frac{\mathcal{D}_0}{D_{0,j}^+} - 1\right) \left(\frac{1 + 3U_0/\omega}{3(1 + U_0/\omega)}\right). \tag{6.25}$$

Upon substituting this expression into (6.24), we recover the result for λ_{IH} given in (5.14) for $\mathcal{D}_0 \to D_{0,j}^+$ from below.

6.2 Parameterization of the Hopf Bifurcation Curve

To compute the Hopf bifurcation threshold numerically for the j-th mode on the range $D_{0,j}^- < \mathcal{D}_0 < D_{0,j}^+$, and to explore the range $\mathcal{D}_0 < D_{0,j}^-$ where Proposition 6.5 only gives partial stability information, we now formulate a convenient parameterization of any Hopf bifurcation curve in the $\hat{\tau}_u$ versus $\mathcal{D}_0$ parameter plane.

We set $\zeta(i\lambda_I) = 0$ in (3.40) to get $\mathcal{C}(i\lambda_I) = \mathcal{F}(i\lambda_I)$, where $\mathcal{C}(i\lambda_I)$ and $\mathcal{F}(i\lambda_I)$ are given in (6.1) and (4.2) respectively. By taking the squared modulus of both sides we get

$$\frac{\eta^2}{b^2} \left(1 + \tilde{\tau}_j^2 \lambda_I^2\right) \left[\frac{(3 - b)^2 + \lambda_I^2}{9 + \lambda_I^2}\right] = |\mathcal{F}(i\lambda_I)|^2,$$

which we solve for $\tilde{\tau}_j^2$ to get

$$\tilde{\tau}_j^2 = \frac{1}{\lambda_I^2} \left[-1 + \frac{b^2}{\eta^2} \left(\frac{9 + \lambda_I^2}{(3 - b)^2 + \lambda_I^2}\right) |\mathcal{F}(i\lambda_I)|^2\right]. \tag{6.26}$$

To derive a second equation for $\tilde{\tau}_j$ we set $\text{Im}[\zeta(i\lambda_I)] = 0$ to get, upon using (6.6) for $\mathcal{C}_I(\lambda_I)$, that

$$\frac{\eta\lambda_I}{b(9 + \lambda_I^2)} \left(3\tilde{\tau}_j(3 - b) - b + \tilde{\tau}_j\lambda_I^2\right) = \mathcal{F}_I(\lambda_I).$$

Upon isolating $\tilde{\tau}_j$ from this expression we obtain that

$$\tilde{\tau}_j = \frac{b}{\eta\lambda_I} \frac{[\eta\lambda_I + \mu\mathcal{F}_I(\lambda_I)]}{\mu - 3b}, \qquad \text{where} \quad \mu \equiv 9 + \lambda_I^2. \tag{6.27}$$

Then, by eliminating $\tilde{\tau}_j$ between (6.26) and (6.27) we obtain, after some algebra, that λ_I must satisfy the nonlinear algebraic problem $\mathcal{M}(\lambda_I) = 0$, defined by

$$\mathcal{M}(\lambda_I) \equiv (\mu + b^2 - 6b) \left[(\eta\lambda_I + \mu\mathcal{F}_I)^2 + \frac{\eta^2}{b^2}(\mu - 3b)^2\right] - \mu(\mu - 3b)^2 |\mathcal{F}|^2, \qquad \text{where} \quad \mu \equiv 9 + \lambda_I^2. \tag{6.28a}$$

36

Here we have labeled $\mathcal{F}_I \equiv \mathcal{F}_I(\lambda_I)$ and $|\mathcal{F}|^2 \equiv |\mathcal{F}(i\lambda_I)|^2 = [\mathcal{F}_R(\lambda_I)]^2 + [\mathcal{F}_I^2(\lambda_I)]^2$. In terms of the original $\hat{\tau}_u$ variable, we have from (6.17) and $\mathcal{D}_0/D_{0,j}^- = 9/b - 2$ that the Hopf bifurcation threshold is

$$\hat{\tau}_{u,H} = \frac{\alpha}{2\eta\lambda_I} \left(\frac{\kappa_q}{\kappa_3}\right)(9 - 2b)\frac{[\eta\lambda_I + \mu\mathcal{F}_I(\lambda_I)]}{\mu - 3b}, \qquad \text{where} \quad \mu \equiv 9 + \lambda_I^2. \tag{6.28b}$$

This parameterization (6.28b) and (6.28a) is used numerically as follows: For a given η and q, we will show numerically that (6.28a) has a unique root $\lambda_I = \lambda_{IH}(b)$ on the range $b_c < b < 3$, where $b_c \equiv 3\eta/(\eta + 3/2)$. This corresponds to the range $D_{0,j}^- < \mathcal{D}_0 < D_{0,j}^+$, via the mapping

$$\mathcal{D}_0 = D_{0,j}^-\left(\frac{9}{b} - 2\right). \tag{6.28c}$$

To compute this root $\lambda_{IH}(b)$ by applying a Newton solver to (6.28a), we must compute the functions $\mathcal{F}_R(\lambda_I)$ and $\mathcal{F}_I(\lambda_I)$, as defined in (4.2), using a BVP solver, for any $\lambda_I > 0$. A key simplifying feature of this parameterization is that the root $\lambda_{IH}(b)$ can be used *for all* of the modes $j = 1, \ldots, K - 1$, as the range of $\mathcal{D}_0$ for the specific mode is only identified at the last step (6.28c). A similar universality feature of the Hopf bifurcation curve was exploited in (5.9) for the explicitly solvable case $q = 3$. We further remark that for the explicitly solvable case $q = 3$ where $\mathcal{F}(i\lambda_I) = 3/[2(3 - i\lambda_I)]$, some lengthy but straightforward algebra shows that the root of (6.28a) is given explicitly by (5.13).

On the range $b_c < b < 3$, for which Proposition 6.4 ensures that a Hopf bifurcation exists, the Hopf threshold $\hat{\tau}_{u,Hj}$ for a specific mode $j = 1, \ldots, K-1$ is given uniquely by simply evaluating (6.28b) at the unique root $\lambda_I = \lambda_{IH}(b)$ of $\mathcal{M}(\lambda_I) = 0$. We remark that on the range $b < 3$ we have $\mu - 3b > 0$ for all $\lambda_I > 0$, so that (6.28b) is well-defined. To establish that (6.28a) has a root on $b_c < b < 3$, we set $\lambda_I = 0$ in (6.28a) and use $\mathcal{F}_I(0) = 0$, $|\mathcal{F}(0)|^2 = 1/4$, and $\mu = 9$, to get that

$$\mathcal{M}(0) = (9 - 3b)^2\left[\frac{\eta^2}{b^2}(b - 3)^2 - \frac{9}{4}\right].$$

From this expression, we conclude that $\mathcal{M}(0) = 0$ at $b = b_c \equiv 3\eta/(\eta + 3/2)$ and $b = 3$, and that $\mathcal{M}(0) < 0$ on the interval $b_c < b < b$. Since $\mathcal{M}(\lambda_I) \to +\infty$ as $\lambda_I \to +\infty$, we conclude that there exists a $\lambda_{IH} > 0$ for which $\mathcal{M}(\lambda_{IH}) = 0$.
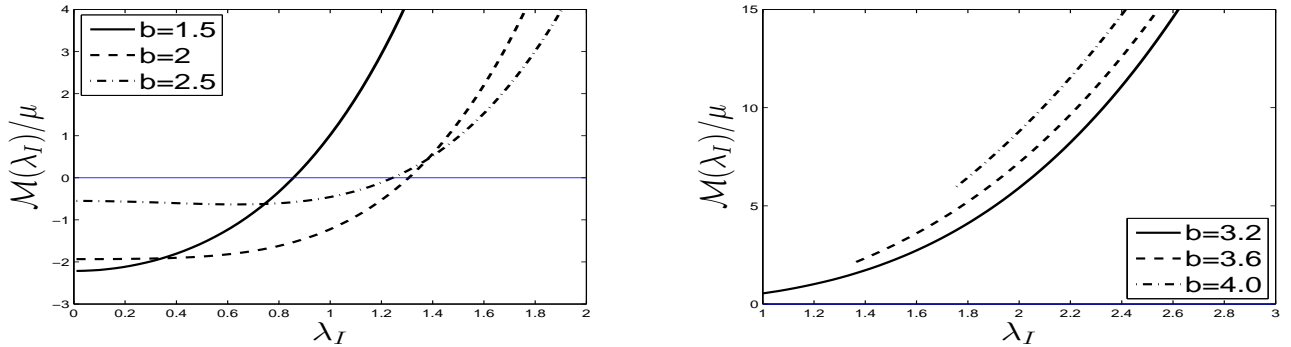

Figure 18: Plots of $\mathcal{M}(\lambda_I)/\mu$, where $\mu \equiv \lambda_I^2 + 9$, versus λ_I for $S = 6$, $\gamma = 2$, $\alpha = 1$, $U_0 = 4$, and $q = 2$. In the left panel, where $b = 1.5, 2.0, 2.5$, which satisfies $b_c < b < 3$, there is a unique root to $\mathcal{M}(\lambda_I) = 0$, yielding the Hopf eigenvalue. In the right panel, where $b = 3.2, 3.6, 4.0$, there is no root to $\mathcal{M}(\lambda_I) = 0$, and hence no Hopf eigenvalue. For our choice $U_0 = 4$, where $U_0 > 3\omega/q$, Proposition 6.5 gives no information regarding Hopf bifurcations on the range $b > 3$.

To examine numerically the uniqueness of the Hopf threshold on the range $b_c < b < 3$, we take the same parameter set $S = 6$, $\gamma = 2$, and $\alpha = 1$, as used in §5 for the $q = 3$ case. We choose $q = 2$ and $U_0 = 4$ for which $\eta \approx 1.286$. For $b = 1.5$, $b = 2.0$, and $b = 2.5$, in the left panel of Fig. 18 we plot $\mathcal{M}(\lambda_I)/\mu$ versus λ_I for $U_0 = 4$ showing numerically the existence of a unique root to $\mathcal{M}(\lambda_I) = 0$, and consequently a unique Hopf bifurcation value of $\hat{\tau}_{uH,j}$ for the j-th mode.

In contrast, suppose that $b > 3$. To investigate whether a Hopf bifurcation is possible for $3 < b < 9/2$, we must determine whether there is a root of $\mathcal{M}(\lambda_I) = 0$ on the range $\mu \equiv 9 + \lambda_I^2 > 3b$ for which $\hat{\tau}_{u,H} > 0$ (see (6.28b)). From (6.28a), we first observe that $\mathcal{M}(\lambda_I) = (b-3)^2 \left(\eta\sqrt{3b-9} + 3b\mathcal{F}_I(3b) \right)^2 > 0$ when $\mu = 3b$ and that $\mathcal{M}(\lambda_I) \to \infty$ as $\lambda_I \to \infty$. Therefore, if such a root exists, $\mathcal{M}(\lambda_I)$ cannot be monotone on $\mu > 3b$. We study this issue numerically in the right panel of Fig. 18 where we plot $\mathcal{M}(\lambda_I)/\mu$ versus λ_I for $b = 3.2$, $b = 3.6$, and $b = 4.0$, on the range $\mu > 3b$, for our parameter set $S = 6$, $\gamma = 2$, $\alpha = 1$, $U_0 = 4$, and $q = 2$. Numerically, we find that there is no root to $\mathcal{M}(\lambda_I) = 0$ when $\mu > 3b$. For $U_0 = 4$ and $q = 2$, we remark that $U_0 > 3\omega/q$, and so Proposition 6.5 gives no information regarding Hopf bifurcations on the range $b > 3$. Further computations (not shown) with $\mathcal{M}(\lambda_I)$ for $b > 3$ suggest that there is never a root to $\mathcal{M}(\lambda_I) = 0$ on $\mu > 3b$ for any $U_0 < U_{0,\max}$. Based on this numerical evidence, we conjecture that no Hopf bifurcations can occur when $\mathcal{D}_0 < D_{0,j}^-$ for any $q > 1$ and $U_0 < U_{0,\max}$.
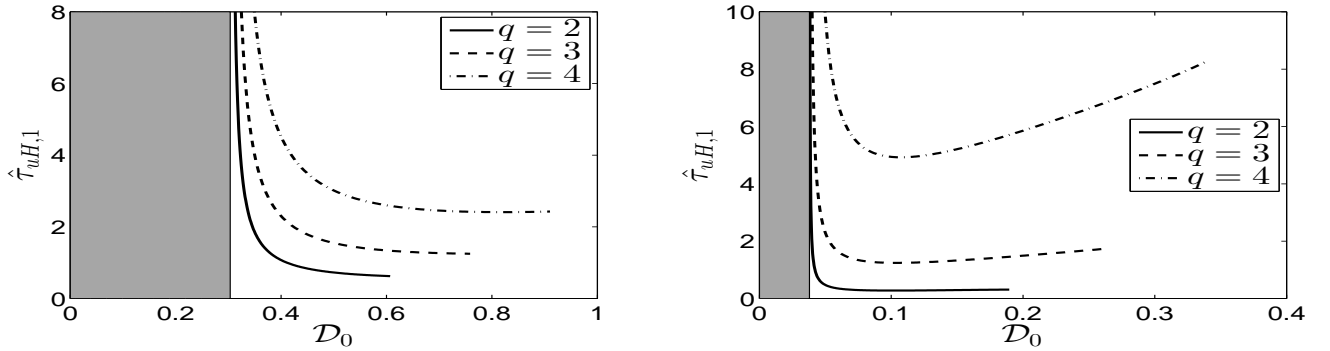

Figure 19: The Hopf bifurcation threshold $\hat{\tau}_{uH_1}$ versus $\mathcal{D}_0$ for $q = 2$ (solid), $q = 3$ (dashed), and $q = 4$ (dot-dashed) on the range $\mathcal{D}_{0,c}/(1 + qU_0/\omega) < \mathcal{D}_0 < \mathcal{D}_{0c}$ for $K = 2$, $S = 6$, $\gamma = 2$, $\alpha = 1$, and with $U_0 = 2$ (left panel) and $U_0 = 4$ (right panel). Here $\mathcal{D}_{0,c}$ is the competition stability threshold defined in (4.9), which depends on q. The lower bound $\mathcal{D}_{0,c}/(1 + qU_0/\omega)$ is independent of q. The two-hotspot steady-state is linearly stable for $\mathcal{D}_0 < \mathcal{D}_{0,c}/(1 + qU_0/\omega)$ (shaded region) as well as under the Hopf bifurcation curve. For $\mathcal{D}_0 > \mathcal{D}_{0,c}$ the hotspot pattern is unstable for all $\hat{\tau}_u$. We observe that the interval in $\mathcal{D}_0$ where an oscillatory instability of the hotspot amplitudes can occur increases with q. The Hopf bifurcation threshold $\hat{\tau}_{uH,1}$ also increases with q.

Next, we use our parameterization to compute the Hopf bifurcation threshold for $\hat{\tau}_u$ on the range $D_{0,j}^- < \mathcal{D}_0 < D_{0,j}^+$, and plot the region of linear stability for $q = 2$ and $q = 4$ in order to compare with our previous results in §5 for $q = 3$.

For our parameter set, and for a two-hotspot solution, in Fig. 19 we plot the linear stability phase diagram in the $\hat{\tau}_u$ versus $\mathcal{D}_0$ plane when either $U_0 = 2$ (left panel) and for $U_0 = 4$ (right panel). In both panels we compare the linear stability thresholds for $q = 2, 3, 4$. In the left and right panels of Fig. 19, the two-hotspot steady-state is linearly stable in the shaded region, which is the same for each q, and in the region below the Hopf bifurcation threshold for the given q. Since the competition instability threshold $\mathcal{D}_{0,c}$ increases with q, as was shown in §4.4, the interval in $\mathcal{D}_0$ where an oscillatory instability of the hotspot amplitudes can occur increases with q. We further observe from Fig. 19 that the Hopf bifurcation threshold value of $\hat{\tau}_u$ increases with q, and when $U_0 = 4$ the Hopf bifurcation threshold is not monotone in $\mathcal{D}_0$ when either $q = 3$ or $q = 4$ (recall the right panel of Fig. 7 for the $q = 3$ case). These results are discussed qualitatively in §6.3.

For a three-hotspot pattern similar results for the linear stability region in the $\hat{\tau}_u$ versus $\mathcal{D}_0$ plane are shown in Fig. 20 for $U_0 = 2$ and in Fig. 21 for $U_0 = 4$. Results for $q = 2, 3, 4$ are shown in the three subpanels of these figures. We observe that the minimal Hopf threshold value for $\hat{\tau}_u$ increases with q, and this increase is more pronounced for $U_0 = 4$ than for $U_0 = 2$. For $U_0 = 4$, we observe from Fig. 21, as similar to that analyzed for the explicitly solvable case $q = 3$ in §5.1, that when $q = 4$ the minimal Hopf threshold value for $\hat{\tau}_u$ switches between two modes at some critical $\mathcal{D}_0$.

Overall, our numerical results for the linear stability region for $q = 2$ and $q = 4$, as computed from our parameterization

(6.28), are qualitatively similar to those obtained from our detailed analysis in §5 for the explicitly solvable case $q = 3$.
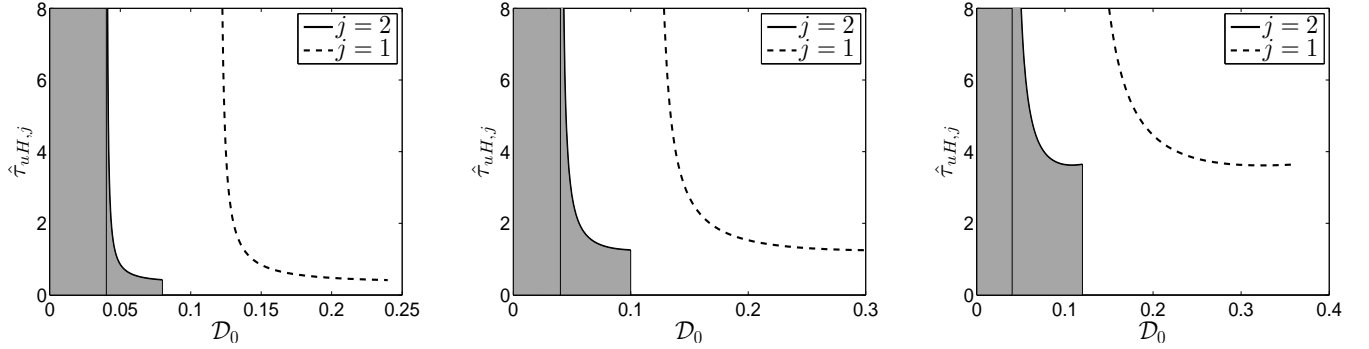

Figure 20: *Linear stability (shaded) region in the $\hat{\tau}_u$ versus $\mathcal{D}_0$ plane for $K = 3$, $S = 6$, $U_0 = 2$, $\gamma = 2$ and $\alpha = 1$, and for $q = 2$ (left panel), $q = 3$ (middle panel), $q = 4$ (right panel). The solid and dashed curves are the Hopf bifurcation boundaries for the (sign-alternating) $j = 2$ mode and the $j = 1$ mode, respectively. In each case, the minimal Hopf boundary threshold for $\hat{\tau}_u$ is determined by the sign-alternating $j = 2$ mode. Observe that $\hat{\tau}_{u,H}$ increases as q increases.*
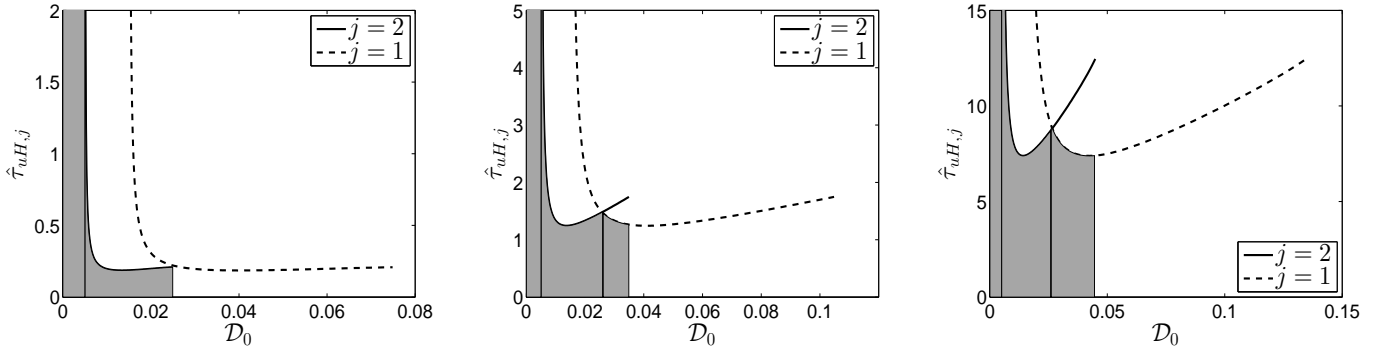

Figure 21: *Same plot and parameters as in Fig. 20 except that $U_0 = 4$: $q = 2$ (left panel), $q = 3$ (middle panel), and $q = 4$ (right panel). The shaded region is the region of linear stability. The solid and dashed curves are the Hopf bifurcation boundaries for the (sign-alternating) $j = 2$ mode and the $j = 1$ mode, respectively. The minimal Hopf bifurcation threshold switches between the two modes only for $q = 3$ and $q = 4$. As q increases the Hopf bifurcation threshold increases significantly (see the different vertical scales in the subfigures). The horizontal edge of the stability region is the competition stability threshold $\mathcal{D}_{0,c}$.*

6.3   Comparison of Linear Stability Theory with PDE Simulations: $q \neq 3$

In this subsection, we validate our linear stability analysis for the "cops-on-the-dots" patrol strategy $q = 2$ by performing full numerical simulations of the RD system (1.4) using the numerical method described in §6.3. When $q = 2$, the police diffusivity has the scaling $D_p = \mathcal{D}_0/(\epsilon\hat{\tau}_u)$ and so our linear stability phase diagrams are plotted in the ϵD_p versus $\mathcal{D}_0$ parameter plane. In all the results below, we use the baseline parameter set $S = 6$, $\gamma = 2$, and $\alpha = 1$.

For a two-hotspot pattern, the phase diagrams in the ϵD_p versus $\mathcal{D}_0$ parameter plane corresponding to the left and right panels of Fig. 19 where $U_0 = 2$ and $U_0 = 4$, respectively, are shown in Fig. 22. At each of the three marked points shown in the left panel of Fig. 22, and with $\epsilon = 0.05$, the full numerical results for the hotspot amplitudes versus time, as shown in the three panels of Fig. 23, are in complete agreement with the predictions of our linear stability theory.

Next, we consider a three-hotspot pattern for $q = 2$ when either $U_0 = 2$ or $U_0 = 4$, where the phase diagrams in the $\hat{\tau}_u$ versus $\mathcal{D}_0$ parameter plane are as shown in the left panels of Fig. 20 and Fig. 21, respectively. The corresponding linear
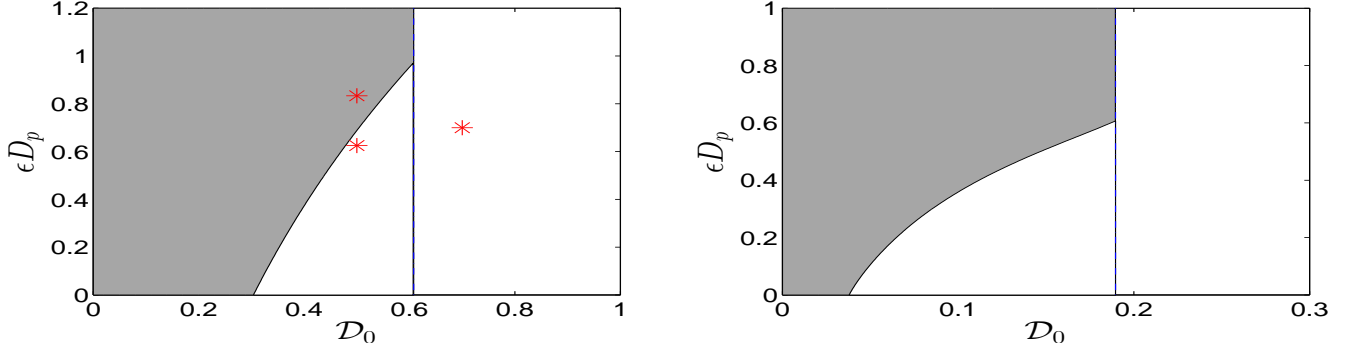
Figure 22: *Linear stability (shaded) region in the ϵD_p versus $\mathcal{D}_0$ plane for a two-spot pattern for the $q = 2$ "cops-on-the-dots" patrol strategy, with $S = 6$, $\gamma = 2$, and $\alpha = 1$, corresponding to Fig. 19. Left panel: $U_0 = 2$. Right panel: $U_0 = 4$. The thin vertical line in each panel is the competition stability $\mathcal{D}_{0,c}$ defined in (4.9). For $\mathcal{D}_0 > \mathcal{D}_{0c}$ the hotspot solution is unstable due to a competition instability, whereas in the small unshaded region for $\mathcal{D}_0 < \mathcal{D}_{0c}$, the hotspot steady-state is unstable to an asynchronous oscillatory instability of the hotspot amplitudes. The full PDE simulations in Fig. 23 are done at the marked points in the left panel.*

stability phase diagrams in the ϵD_p versus $\mathcal{D}_0$ parameter plane are shown in the left and right panels of Fig. 24 for $U_0 = 2$ and $U_0 = 4$, respectively. We now test our linear stability predictions at the marked points in these phase diagrams.
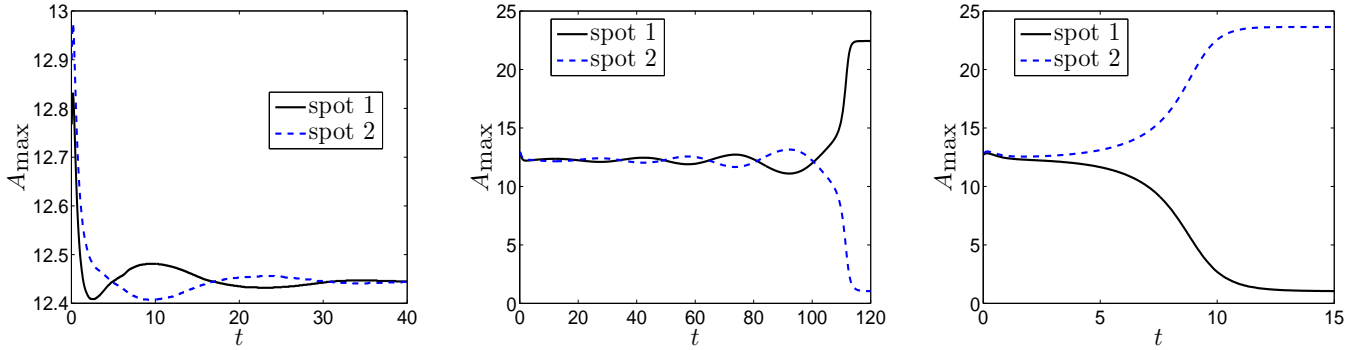

Figure 23: *The spot amplitudes computed numerically from the full PDE system (1.4) for a two-spot pattern for the $q = 2$ "cops-on-the-dots" patrol strategy, and with $S = 6$, $\gamma = 2$, $\alpha = 1$, $U_0 = 2$, and $\epsilon = 0.05$. These simulations at the marked points in the phase diagram in the left panel of Fig. 22 confirm our linear stability theory. Left panel: $\hat{\tau}_u = 0.6$ and $\mathcal{D}_0 = 0.5$, so that $\epsilon D_p \approx 0.833$. The asynchronous spot amplitude oscillations decay in time. Middle panel: $\hat{\tau}_u = 0.8$ and $\mathcal{D}_0 = 0.5$, so that $\epsilon D_p = 0.625$. The asynchronous spot amplitude oscillations grow in time and lead to the collapse of a spot. When $\mathcal{D}_0 = 0.5$, the Hopf bifurcation threshold is $\epsilon D_{p,H} \approx 0.6887$ (see the left panel of Fig. 22). Right panel: $\hat{\tau}_u = 1.0$ and $\mathcal{D}_0 = 0.7$, so that $\epsilon D_p = 0.7$. The competition instability for the spot amplitudes leads to the collapse of a spot.*

We first consider the three marked points shown in the left panel of Fig. 24, where $U_0 = 2$. For $\epsilon = 0.035$, the full numerical results for the hotspot amplitudes versus time, are shown in the three panels of Fig. 25. In the left and middle panels of Fig. 25, which correspond to parameter values either slightly below or slightly above our theoretically predicted Hopf bifurcation threshold, we observe either slowly decaying or growing sign-alternating asynchronous oscillations as predicted by our linear stability theory. These two parameter values correspond to the two closely spaced points in the phase diagram in the left panel of Fig. 24. Moreover, the right panel of Fig. 25 clearly illustrates the competition instability which occurs for the marked point in the left panel of Fig. 24 with $\mathcal{D}_0 > \mathcal{D}_{0,c}$.
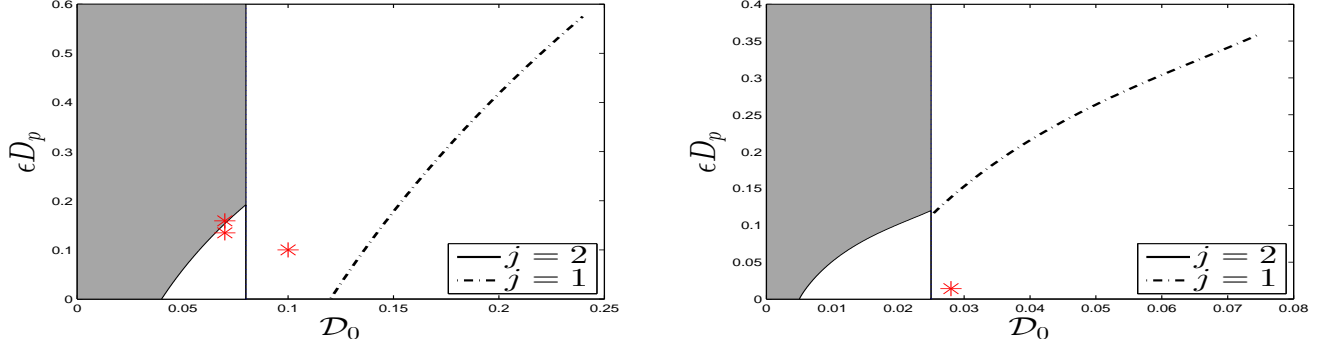
Figure 24: *Linear stability (shaded) region in the ϵD_p versus $\mathcal{D}_0$ plane for a three-spot pattern for the $q = 2$ "cops-on-the-dots" patrol strategy, with $S = 6$, $\gamma = 2$, and $\alpha = 1$ and for $U_0 = 2$ (left panel) and $U_0 = 4$ (right panel). Plots correspond to the left panels of Fig. 20 and Fig. 21. The competition instability threshold is the thin vertical line. The solid and dot-dashed curves are the Hopf bifurcation boundaries for the (sign-alternating) $j = 2$ mode and the $j = 1$ mode, respectively. For both $U_0 = 2$ and $U_0 = 4$, the Hopf boundary for $\mathcal{D}_0 < \mathcal{D}_{0,c}$, marking the boundary of the small unshaded region, is determined by the sign-altering $j = 2$ mode. The full PDE simulations in Fig. 25 and in Fig. 26 are done at the marked point(s) in the left and right panels.*
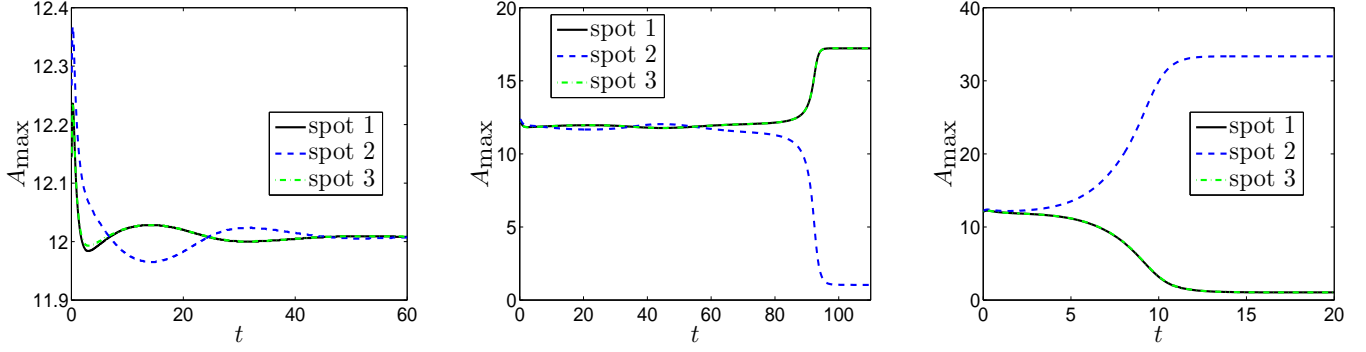

Figure 25: *The spot amplitudes computed numerically from the full PDE system (1.4) for a three-spot pattern for the $q = 2$ "cops-on-the-dots" patrol strategy, and with $S = 6$, $\gamma = 2$, $\alpha = 1$, $U_0 = 2$, and $\epsilon = 0.035$. These simulations at the marked points in the left panel of Fig. 24 confirm our linear stability theory. Left panel: $\hat{\tau}_u = 0.44$ and $\mathcal{D}_0 = 0.07$, so that $\epsilon D_p \approx 0.159$. The asynchronous spot amplitude oscillations decay in time. Middle panel: $\hat{\tau}_u = 0.52$ and $\mathcal{D}_0 = 0.07$, so that $\epsilon D_p = 0.1346$. The asynchronous spot amplitude oscillations grow in time and lead to the collapse of a spot. When $\mathcal{D}_0 = 0.07$, the Hopf bifurcation threshold is $\epsilon D_{p,H} \approx 0.1532$ (see the left panel of Fig. 24). Right panel: $\hat{\tau}_u = 1.0$ and $\mathcal{D}_0 = 0.1$, so that $\epsilon D_p = 0.1$. The competition instability for the spot amplitudes leads to the collapse of a spot.*

Finally, as a more refined test of our linear stability theory, we perform full numerical simulations for the marked point in the phase diagram shown in the right panel of Fig. 24 where $U_0 = 4$. This stability phase diagram predicts that the three-spot pattern is unstable to both a competition instability and a $j = 1$ mode asynchronous oscillatory instability, representing anti-phase oscillations between the first and third hotspots. However, the unstable real eigenvalue associated with the competition instability is rather close to the origin of the spectral plane since $\mathcal{D}_0$ is only slightly above the competition threshold $\mathcal{D}_{0,c}$. As such, we predict that the anti-phase oscillation should be the more dominant of the two instabilities. This anti-phase oscillation is clearly evident from the full PDE simulation shown in Fig. 26 when $\epsilon = 0.035$.

8   Discussion and Outlook

We have used a combination of matched asymptotic expansions and the analysis of nonlocal eigenvalue problems (NLEP) to study the existence and linear stability of localized hotspot steady-state solutions for the three-component RD system
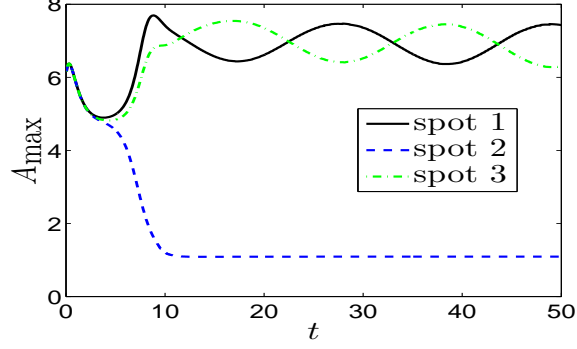
Figure 26: The numerically computed spot amplitudes at the marked point in the right panel of Fig. 24 for $U_0 = 4$, where $\mathcal{D}_0 = 0.028$, $\hat{\tau}_u = 2$, so that $\epsilon D_p \approx 0.014$. The other parameters are $S = 6$, $\gamma = 2$, $\alpha = 1$, and $\epsilon = 0.035$. The phase diagram in the right panel of Fig. 24 predicts that the three-spot pattern is unstable to a competition instability together with a $j = 1$ mode anti-phase oscillatory instability between the first and third spots. Since $\mathcal{D}_0 \approx \mathcal{D}_{0,c}$, the competition instability should be weak, and so the anti-phase oscillation is predicted to be the more dominant of the two instabilities. This is confirmed by the full PDE simulation.

(1.1) in the limit $\epsilon \to 0$ with $D = \mathcal{D}_0/\epsilon^2$ on the 1-D domain $0 \le x \le S$. We have investigated how the multiple hotspot steady-states and their linear stability properties depend on the total police deployment $U_0 > 0$, the patrol focus parameter $q > 1$, and the police diffusivity $D_p \equiv \mathcal{D}_0/\varepsilon^2 \tau_u$, where $\tau_u = \epsilon^{q-3}\hat{\tau}_u$ with $\hat{\tau}_u = \mathcal{O}(1)$.

Our NLEP linear stability analysis has provided phase diagrams in the $\epsilon^{q-1}D_p$ versus $\mathcal{D}_0$ parameter space where multiple hotspot steady-states are linearly stable. We have shown that the hotspot amplitudes are always linearly stable to synchronous perturbations of their amplitudes. Instabilities can only arise from the asynchronous modes, which decrease the amplitudes of certain hotspots at the expense of increasing the intensity of others. For the special case $q = 3$, and for $K \ge 2$, for which the discrete spectrum of the NLEP can be reduced to the study of a family of $K - 1$ quadratic equations in the eigenvalue parameter, stability phase-diagrams in the $\epsilon^2 D_p$ versus $\mathcal{D}_0$ parameter plane were constructed explicitly. For general $q > 1$, the phase diagrams were determined by combining some rigorous spectral results obtained from the argument principle together with numerical results obtained from a parameterization of the Hopf bifurcation threshold.

Our hybrid anayltical-numerical study has shown that steady-state multiple hotspot patterns are unconditionally unstable if $\mathcal{D}_0 > \mathcal{D}_{0,c}$, and are always linearly stable if $0 < \mathcal{D}_0 < \mathcal{D}_{0,c}/(1 + qU_0/\omega)$, where $\omega = S(\gamma - \alpha) - U_0$ and $\mathcal{D}_{0,c}$ is the competition instability threshold given in (4.9). On the intermediate range $\mathcal{D}_{0,c}/(1 + qU_0/\omega) < \mathcal{D}_0 < \mathcal{D}_{0,c}$, we have shown from an analysis of the NLEP that the hotspot amplitudes exhibit an asynchronous oscillatory instability of their amplitudes due to a Hopf bifurcation when the police diffusivity D_p is below a certain threshold, which depends on $\mathcal{D}_0$. Therefore, for this range of $\mathcal{D}_0$, a sufficiently "sluggish" police intervention has the effect of only displacing crime between adjacent hotspots. The specific asynchronous spatial mode for this displacement depends on the level of police deployment U_0. For U_0 small enough, the sign-alternating asynchronous mode was shown to be the dominant oscillatory instability.

We conclude this paper by briefly discussing a few problems that warrant further study.

From a mathematical viewpoint, there are some open theoretical questions for our RD system (1.4). Firstly, for a general $q > 1$, our result in Proposition 6.5 proves that the NLEP (3.36) has no unstable eigenvalues on the entire range $\mathcal{D}_0 < \mathcal{D}_{0,c}/(1 + qU_0/\omega)$, where $\omega = S(\gamma - \alpha) - U_0 > 0$, only when the total police deployment U_0 satisfies $U_0 < 2S(\gamma - \alpha)/(q+1)$. Although our numerical evidence obtained from the Hopf threshold parameterization (6.28) supports a conclusion that the NLEP has no unstable eigenvalues on the entire range $\mathcal{D}_0 < \mathcal{D}_{0,c}/(1 + qU_0/\omega)$ for any $0 < U_0 < U_{0,max}$ and $q > 1$, it would be worthwhile to prove this result rigorously. For the explicitly solvable case $q = 3$, such a rigorous proof was done in §5. Secondly, our analysis of steady-state hotspot patterns and their stability properties is not valid when $q = 1$. Qualitatively,

for $q = 1$, the police are less focused on maxima of A than are the criminals, so that the density of police remains at a significant level near the peripheries of a hotspot region. Such a policing strategy is related to the concept of peripheral interdiction, as discussed in [11]. Mathematically, for $q = 1$, we need to modify our steady-state hotspot construction as well as modify the derivation of the underlying NLEP. This latter fact follows since for $q = 1$ we have $\hat{\tau}_u = \epsilon^2 \tau_u$ from (3.11), so that the ODE for the perturbation η in (3.14) now satisfies $\mathcal{D}_0 \eta_{xx} = \hat{\tau}_u \lambda \eta$. As such, the expression for $\eta(0)$ in (3.19) is no longer valid. As a result, we will obtain a modified NLEP problem, distinct from that in (3.36), which will require a separate analysis. Intuitively, we might expect that a $q = 1$ peripheral-based policing strategy will act to decrease the parameter range where asynchronous temporal instabilities in the hotspot amplitudes can occur. Thirdly, we emphasize that our analysis has been based on using NLEP theory to examine the linear instability mechanisms on an $\mathcal{O}(1)$ time-scale of symmetric steady-state hotspot patterns. As an extension to our NLEP analysis, one should examine the role of the "small" eigenvalues in the spectrum of the linearization that tend to zero $\epsilon \to 0$. Zero-crossings of these small eigenvalues should correspond to bifurcation points where asymmetric hotspot steady-states bifurcate from the steady-state symmetric solution branch. Lastly, it would be interesting to develop a weakly nonlinear analysis to establish whether both the competition instability and the Hopf bifurcation for the asynchronous mode are subcritical. The full PDE numerical simulations shown in §5.2 and in §6.3 support this conjecture in that small-scale asynchronous oscillations appear to trigger a nonlinear process through which one or more hotspots are ultimately annihilated.

Finally, we discuss a few possible extensions of the analysis and the model of police interactions. For the RD system (1.4) it would be interesting to study hotspot patterns for the regime where $D = \mathcal{O}(1)$. For the basic two-component crime model with no police intervention, it was shown in [28] that near a saddle-node bifurcation point for hotspot equilibria there can be a nucleation of new hotspots of criminal activity from an otherwise quiescent, largely crime-free, background. In this direction it would be interesting to investigate whether the police presence can eliminate this "peak-insertion" effect, and more generally how the global bifurcation behavior of multiple hotspot steady-state solutions is modified due to the police. A second open area is to study the existence and linear stability properties of hotspot patterns for our three-component RD system in a 2-D spatial domain in order to determine whether the police intervention can lead to asynchronous temporal oscillations in the hotspot amplitudes, which model the displacement of crime between various localized spatial regions. Finally, it would be interesting to consider a more general model for police intervention whereby the police interaction I on the criminal density is modeled by the "predator-prey" interaction $I(U, \rho) = -U\rho$ rather than simply $I = -U$ as we have done. The NLEP characterizing the linear stability of steady-state symmetric hotspot patterns on an $\mathcal{O}(1)$ time-scale will now have three, instead of two, nonlocal terms, which makes a detailed stability analysis rather challenging. However, the determination of the competition instability threshold, corresponding to the zero-eigenvalue crossing, should be feasible.

A   The Continuum Limit of the Agent-Based Model

Acknowledgments

References

[1] H. Berestycki, J. Wei, M. Winter, *Existence of symmetric and asymmetric spikes for a crime hotspot model*, SIAM J. Math. Anal., **46**(1), (2014), pp. 691–719.

[2] J. G. Blom, R. A. Trompert, J. G. Verwer, *Algorithm 758: VLUGR 2: A vectorizable adaptive grid solver for PDEs in 2D*, ACM Trans, Math. Softw., **22**(3), (1996), pp. 302–328.

[3] A. A. Braga, *The effects of hot spots policing on crime*, Ann. Am. Acad. Polit. S. S., **578**, (2001), pp. 104–125.

[4] P. L. Brantingham, P. J. Brantingham, *Crime patterns*, McMillan, (1987).

[5] A. Camacho, H. R. L. Lee, L. Smith, *Modeling policing strategies for departments with limited resources*, Europ. J. Appl. Math., **27**(3), (2016). pp. 479–501.

[6] R. Cantrell, C. Cosner, R. Manasevich, *Global bifurcation of solutions for crime modeling equations*, SIAM J. Math. Anal., **44**(3), (2012), pp. 1340–1358.

[7] A. Doelman, R. A. Gardner, T. J. Kaper, *Large stable pulse solutions in reaction-diffusion equations*, Indiana U. Math. J., **50**(1), (2001), pp. 443–507.

[8] Y. Gu, Q. Wang, G. Yi, *Stationary patterns and their selection mechanism of urban crime models with heterogeneous near-repeat victimization effect*, Europ. J. Appl. Math., **28**(1), (2017), pp. 141–178.

[9] D. Iron, M. J. Ward, J. Wei, *The stability of spike solutions to the one-dimensional Gierer-Meinhardt model*, Physica D, **150**(1-2), (2001), pp. 25–62.

[10] S. Johnson, K. Bower, *Domestic burglary repeats and space-time clusters: The dimensions of risk*, Europ. J. of Criminology, **2**, (2005), pp. 67–92.

[11] P. A. Jones, P. J. Brantingham, L. Chayes, *Statistical models of criminal behavior: The effect of law enforcement actions*, Math. Models. Meth. Appl. Sci., **20**, Suppl., (2010), pp. 1397–1423.

[12] T. Kolokolnikov, M. J. Ward, J. Wei, *The stability of steady-state hot-spot patterns for a reaction-diffusion model of urban crime*, DCDS-B, **19**(5), (2014), p. 1373–1410.

[13] R. McKay, T. Kolokolnikov, *Stability transitions and dynamics of localized patterns near the shadow limit of reaction-diffusion systems*, DCDS-B, **17**(1), (2012) pp. 191–220.

[14] T. Kolokolnikov, M. J. Ward, J. Wei, *The existence and stability of spike equilibria in the one-dimensional Gray-Scott model: The low feed rate regime*, Studies in Appl. Math, **115**(1), (2005), pp. 21–71.

[15] T. Kolokolnikov, J. Wei, *Stability of spiky solutions in a competition model with cross-diffusion*, SIAM J. Appl. Math., **71**(4), (2011), pp. 1428–1457.

[16] D. J. B. Lloyd, H. O'Farrell, *On localised hotspots of an urban crime model*, Physica D, **253**, (2013), pp. 23–39.

[17] I. Moyles, W.-H. Tse, M. J. Ward, *Explicitly solvable nonlocal eigenvalue problems and the stability of localized stripes in reaction-diffusion systems*, Studies in Appl. Math., **136**(1), (2016), pp. 89–136.

[18] Y. Nec, M. J. Ward, *An explicitly solvable nonlocal eigenvalue problem and the stability of a spike for a class of reaction-diffusion system with sub-diffusion*, Math. Model. of Nat. Phenom., **8**(2), (2013), pp. 55–87.

[19] Y. Nec, M. J. Ward, *The dynamics and stability of spike-type solutions to the Gierer-Meinhardt model with sub-diffusion*, Physica D, **241**(10), (2012), pp. 947–963.

[20] H. van der Ploeg, A. Doelman, *Stability of spatially periodic pulse patterns in a class of singularly perturbed reaction-diffusion equations*, Indiana Univ. Math. J., **54**(5), (2005), pp. 1219–1301

[21] A. B. Pitcher, *Adding police to a mathematical model of burglary*, Europ. J. Appl. Math., **21**(4-5), (2010), pp. 401–419.

[22] L. Ricketson, *A continuum model of residential burglary incorporating law enforcement*, unpublished, (2011). Retrieved from http://cims.nyu.edu/˜lfr224/writeup.pdf.

[23] N. Rodriguez, A. Bertozzi, *Local existence and uniqueness of solutions to a PDE model for criminal behavior*, M3AS (special issue on Mathematics and Complexity in Human and Life Sciences), **20**(1), (2010), pp. 1425–1457.

[24] I. Rozada, S. Ruuth, M. J. Ward, *The stability of localized spot patterns for the Brusselator on the sphere*, SIAM J. Appl. Dyn. Sys., **13**(1), (2014), pp. 564–627.

[25] M. B. Short, M. R. D'Orsogna, V. B. Pasour, G. E. Tita, P. J. Brantingham, A. L. Bertozzi, L. B. Chayes, *A statistical model of criminal behavior*, Math. Models. Meth. Appl. Sci., **18**, Suppl., (2008), pp. 1249–1267.

[26] M. B. Short, A. L. Bertozzi, P. J. Brantingham *Nonlinear patterns in urban crime - hotspots, bifurcations, and suppression*, SIAM J. Appl. Dyn. Sys., **9**(2), (2010), pp. 462–483.

[27] M. B. Short, P. J. Brantingham, A. L. Bertozzi, G. E. Tita (2010), *Dissipation and displacement of hotpsots in reaction-diffusion models of crime*, Proc. Nat. Acad. Sci., **107**(9), pp. 3961-3965.

[28] W.-H. Tse, M. J. Ward, *Hotspot formation and dynamics for a continuum model of urban crime*, Europ. J. Appl. Math., **27**(3), (2016), pp. 583–624.

[29] J. C. Tzou, M. J. Ward, *The stability of localized spikes for the 1-D Brusselator reaction-diffusion model*, Europ. J. Appl. Math., **24**(4), (2013), pp. 515–564.

[30] M. J. Ward, J. Wei, *Hopf bifurcations and oscillatory instabilities of spike solutions for the one-dimensional Gierer-Meinhardt model*, J. Nonlinear Sci., **13**(2), (2003), pp. 209–264.

[31] J. Wei, *Existence and stability of spikes for the Gierer-Meinhardt system*, book chapter in *Handbook of Differential Equations, Stationary Partial Differential Equations*, Vol. 5 (M. Chipot ed.), Elsevier, (2008), pp. 489–581.

[32] J. Q. Wilson, G. L. Kelling, *Broken windows and police and neighborhood safety*, Atlantic Mon., **249**, (1998), pp. 29–38.

[33] J. R. Zipkin, M. B. Short, A. L. Bertozzi, *Cops on the dots in a mathematical model of urban crime and police response*, DCDS-B, **19**(5), (2014), pp. 1479–1506.